PRODUCTION OF SUSTAINABLE THERMOPLASTICS AND THERMOPLASTIC ELASTOMERS THROUGH CONTROLLED CATIONIC POLYMERIZATIONS

A Dissertation
Presented to the Faculty of the Graduate School
of Cornell University
in Partial Fulfillment of the Requirements for the Degree of
Doctor of Philosophy

by
Scott Wesley Spring
August 2022

PRODUCTION OF SUSTAINABLE THERMOPLASTICS AND THERMOPLASTIC ELASTOMERS THROUGH CONTROLLED CATIONIC POLYMERIZATIONS

Scott Wesley Spring, Ph. D.
Cornell University 2022

The design, development, and implementation of sustainable polymers is paramount to the preservation of our planet. Three grand challenges lie before us in this aim: a) generating monomers from renewable resources or waste feedstock, b) the synthesis of robust polymers with material properties comparable to current plastics, and c) the design of end-of-life solutions. The development of economically viable biorenewable plastics is often hindered by the production and availability of chemical feedstocks as well as the efficiency of monomer synthesis. We have identified bioalcohols as an underutilized resource, where they can be efficiently transformed into vinyl ether monomers. Recent advancements in controlled cationic polymerizations have enabled the polymerization of vinyl ethers into sustainable polymers. Specifically, we have demonstrated the synthesis of ABA block copolymers using cationic reversible addition-fragmentation chain-transfer (RAFT) polymerization. The cationic RAFT method used is performed at room temperature, marking an improvement over

previous methods for cationic polymerization that relied on low temperatures to maintain a controlled process. The polymers produced were entirely composed of sustainable vinyl ethers and performed comparably to commercial thermoplastic elastomers. Further improvement of this system led to the discovery of a new, “green” chain transfer agent (CTA) for cationic RAFT polymerizations. We then demonstrated the utility of this CTA in chemical, electrochemical, photochemical, and acid-initiated cationic RAFT polymerizations, where it performed better or comparably to previous CTAs. Another notable development in cationic polymerizations has been the advent of a single-component acid initiator that allows for controlled cationic polymerizations under ambient conditions. We employed this acid initiator in the polymerization of the biorenewable cyclic vinyl ether 2,3-dihydrofuran (DHF). Under inert conditions, we were able to achieve high molecular weights (up to 256 kg/mol) and these samples revealed strong and tough tensile properties. Leveraging PDHF’s susceptibility to oxidative degradation, we developed an accelerated degradation method for reducing PDHF to oligomers over 48 hours. This comprehensive study of PDHF revealed this thermoplastic to be strong, tough, sustainable, and degradable. Combined, the advancements in cationic polymerization methods outlined in this work explicate the opportunity available in producing polyvinyl ethers from bioalcohols to provide robust, sustainable, and degradable plastics to meet the grand challenges of today.

BIOGRAPHICAL SKETCH

Scott Wesley Spring was born in northern California to Douglas and Melanie Spring in the spring of 1994. In his childhood he enjoyed camping, skiing, and getting into trouble. Scott was in poor academic standing early on in high school and finding himself crushed by a self-imposed crisis he could not postpone or evade, he relocated to Kalispell, Montana. It was in Kalispell that he found a new footing in life and managed to scrape through high school and earn his diploma. Leaving high school with no academic aspirations, he began working as a carpenter. He began attending Flathead Valley Community College with the intention of studying cabinetry, but soon found himself in a chemistry class as well. Through the encouragement of an advisor, he continued on with chemistry and made the decision to attend Montana State University. At University he found a community of chemists and academics who showed him how to be successful. After drastically improving his academic prowess during the years at MSU, he was accepted into Cornell University's Chemistry and Chemical Biology PhD program. Here, he found a welcoming community of graduate students and a supportive advisor in the Fors Group. With their assistance, he accomplished the work reported within this thesis and secured a position along with his partner at 3M.

DEDICATION

This work is dedicated to my father, Douglas Wesley Spring, for always encouraging me. Though he only saw my first steps down my current path, I know he would be ecstatic to see this day.

ACKNOWLEDGMENTS

These last five years were not accomplished alone, and I must emphatically thank everyone who has helped me along the way. I would first like to thank my PhD Advisor, Brett Fors. He has been immensely supportive throughout my graduate school studies. When I was deciding what graduate school and advisor to join, I heard nothing but positive things from my advisors as Montana State, our common alma mater, and found their kind words to be true upon meeting Brett at visit weekend. The decision to join his group was easy after I saw the genuine happiness and comradery of his graduate students and the department as a whole. I genuinely consider myself fortunate to have been a part of Brett's group, where I found an environment that fostered creative scientific thought and an enjoyable work environment from day one. My grad school experience and the Cornell Chemistry Department would not be the same without him.

I also must thank my PhD Committee members, Song Lin and Geoffrey Coates. They were both incredible professors during my first year and their classes helped me grow as a student. Geoff's class in particular provided my foundation in polymer chemistry an instilled my love of polymer-noodle analogies. Both provided insightful feedback through A- and B-exam and I hope to remain "unflappable" in my career. In addition, I would like to thank the professors in the Center for Sustainable Polymers I collaborated with, Christopher Ellison, Marc Hillmyer, and Stuart Rowan for their support and insight during our work. In

particular, I greatly appreciated Marc's interest in highlighting my work to the NSF and for providing considerate feedback during my job search.

As mentioned, the Fors group as a whole has provided so much in the way of help and friendship throughout my PhD, and I would like to specifically thank some of them. First, I must thank Jacob Trotta for being a mentor to me my first two years and for serving as my guide in the CSP. I hope that upon reading my thesis he finally concedes that DHF is indeed the "monomer of the future". I must also apologize for never completing that itaconic acid review, but I'm sure it will be published one day. I also thank Dillon Gentekos for always speaking his mind in grad school and for assisting in my career choices at 3M. Although I'm disappointed we won't overlap, I wish you the best in your future career. In my first year, Veronika Kottisch appeared at times to be the polymer savant, with her prolific work effort. As I got to know her, I appreciated her jokes, love of camping, and most importantly, baked goods. Lab 3 never felt the same without Brian Peterson and Mike Supej. They really helped carry the energy throughout long days in lab through good and/or terrible music, brainstorming memes for twitter, and odd lab competitions. Renee Sifri was a constant source of positive energy, through her unwavering excitement in lab, and general optimism, although she may not admit it. In addition, I learned a lot from the post-docs in the Fors group as well. I thank Quentin Michaudel for his constructive critique of both my presentation slides and lab technique. Elizabeth McLoughlin for her friendship and for emphasizing the importance of personal well-being when building one's

career. I would also like to thank Erin Stache (now Professor Stache!) for her insight as a post-doc and for her support and advice as a professor while I was deciding what to do after graduate school.

I would also like to thank some of the grad students who came after me. Thank you to Luis Melecio-Zambrano for always being a great climbing partner, and I am very excited in what lies ahead for you. Thank you Yuting Ma for your hilarious sense of humor and in a world of statues, I hope you are the pigeon every day. Thank you to Shelby Shankel and Jenny Hu, you have been great friends this last year and I appreciate our comradery over climbing, boba, and British panel shows. Jesse Hsu, thank you for always encouraging me to do better and be more sustainable in my chemistry. To paraphrase your words, if we aren't striving to make the perfect sustainable polymer, what's the point? If we aim for Jesse's expectations, we'll land somewhere closer to a sustainable world. You undertook a lot of responsibility, just remember not to carry the world on your shoulders. In addition, I would also like to thank all the other Fors group members not mentioned by name. It feels like I have handed off the proverbial torch to the younger generation of grad students and I have no doubts y'all will continue to accomplish great things, while fostering a healthy, creative, and welcoming lab environment. Thank you as well to all my other friends in grad school I've made over the years! In particular, thank you Mike, Cara, and Joe for convincing me to complete the Syracuse half-ironman with you, I will cherish that memory forever. I'll also always appreciate the F1 watch parties of Peter, Cheyenne, Michael, Greg,

and sometimes Lejla and Shelby. Thanks Jesse, Ananya, and Grace for many great nights out.

In addition to the grad students and post-docs, I have been very fortunate to work with incredible undergraduate students as well. Red Smith-Sweetser was an absolute pleasure to work with, he was very hard-working and was always enthusiastic in lab. I also couldn't have accomplished what I did this last year without the diligent work of Chloe Cerione. Chloe was a wonderful independent researcher who embraced the projects we worked on, and I'm very excited to see her pursue a PhD in polymer chemistry at Caltech.

I also must thank all those who helped me reach grad school, as I would not have made it here without them. Thanks to Jessica Ennist, for being an inspiration and friend through my undergraduate education at MSU, I will always cherish our friendship. I also thank Axl, Anna, Tacey, Kori, Jessie, and Devin for being such a great study group, carrying me through many classes and for giving me the confidence I needed going to grad school. Thank you to the BYP, as well as Jaffe, Josh, Silas, Trevor and Zack for keeping me sane and encouraging me to enjoy the mountains. I also would have never pursued a degree in chemistry without my community college professor, David Long, who sparked my passion for chemistry and science. I owe a lot to Flathead Valley Community College and the professors there who were all passionate about teaching and encouraging students. I also could not have accomplished any of this without the support and mentorship of Tim Harmon, an exceptional person who has repeatedly inspired me over the last

10 years to become the person I am today.

In addition, I would like to thank all my family for encouraging me along the way. My mom and dad for bringing me up in a great home, and my sister for always believing in me and showing me how to have a kind heart. Thank you, Roger, for being there for me throughout my life, and for always listening.

Finally, my heart goes out to my incredible partner Stephanie Rosenbloom, who has been there through my entire PhD. She has always been a great friend and has always reminded me to take care of myself. We have grown a lot together over the last four years, and I'm so excited for us to begin this next phase of life together in Minnesota. In addition, you have always been an extraordinary caretaker of our little family and life wouldn't be complete without Petrie and Jenson.

TABLE OF CONTENT

LIST OF FIGURES

LIST OF TABLES

LIST OF ABBREVIATIONS

TPE_____ Thermoplastic elastomer

RAFT _____ Reversable addition-fragmentation chain-transfer

PS_____ Polystyrene

LDPE _____ High-density polyethylene

HEX _____ Hexagonally packed cylinders

LAM _____ Lamellae

mw_____ Molecular weight

rt_____ Room temperature

$CDCl_3$ _____ Deuterated chloroform

THF _____ Tetrahydrofuran

GPC_____ Gel-permeation chromatography

SEC _____ Size-exlcusion chromatography

rpm _____ revolutions per minute

BHT _____ Butylated hydroxytoluene

MeOH _____ Methanol

MeCN _____ Acetonitrile

DCM _____ Dichloromethane

EtOAc _____ Ethyl acetate

PET_____ Poly(ethylene terethalate)

DMA_____ Dynamic mechanical analysis

SAXS _____ Small-angle X-ray scattering

CTA _____ Chain transfer agent

MA _____ Methyl acrylate

AIBN _____ Azobisisobutyronitrile

LS _____ Light scattering

RI _____ Refractive index

VE _____ Vinyl ether

PVE _____ Poly(vinyl ether)

IBVE _____ Isobutyl vinyl ether

PIBVE _____ Poly(isobutyl vinyl ether)

MOS _____ *p*-methoxystyrene

PMOS _____ Poly(*p*-methoxystyrene)

EVE _____ ethyl vinyl ether

PEVE _____ Poly(ethyl vinyl ether)

NBVE _____ n-butyl vinyl ether

PNBVE _____ Poly(n-butyl vinyl ether)

AdVE _____ 2-adamantyl vinyl ether

PAdVE _____ Poly(2-adamantyl vinyl ether)

TCDVE _____ tricyclodecyl vinyl ether

PTCDVE _____ Poly(tricyclodecyl vinyl ether)

Cl-EVE _____ chloroethyl vinyl ether

PCl-EVE _____ Poly(chloroethyl vinyl ether)

DHF _____ 2,3-dihydrofuran

PDHF_____ Poly(2,3-dihydrofuran)

PC _____Poly(bisphenyl A carbonate)

$FcBF_4$_____ Ferrocenium tetrafluoroborate

FTIR _____Fourier transform infrared

NMR _____Nuclear magnetic resonance

AE_____Atom Economy

PMI _____ Process Mass Index

PCCP_____ pentacarbomethoxycyclopentadiene

PMP_____ 2,4,6-tris(4-methoxyphenyl)pyrylium tetrafluoroborate

HBD_____Hydrogen bond donor

CPME _____cyclopentyl methyl ether

LIST OF SYMBOLS

$Đ$ _____ Disperisty

M_n _____ Number-average molar mass

T_g _____ Glass-transition temperature

σ_B _____ Tensile strength at break

ε_B _____ Tensile strength at break

E _____ Young's modulus

η^* _____ Complex viscosity

G' _____ Storage modulus

G" _____ Loss modulus

G_N^0 _____ Loss modulus

f_{HB} _____ Volume fraction of hard block

M_e _____ Entanglement molecular weight

T_d _____ Degradation temperature

°C _____ Degrees Celcius

q _____ Scattering vector

λ _____ Wavelength

ρ _____ Density

δ _____ Chemical shift

Chapter 1

Sustainability Advancements in Controlled Cationic Polymerizations

1.1 Introduction

In 2009, Aoshima and Kanaoka wrote "A Renaissance in Living Cationic Polymerization", detailing methods available and some of the polymers enabled by these methods.[1] Since this time, several new controlled cationic polymerization methods have been reported, enabling new materials, and improving sustainability. The attention of the polymer science community has turned to focus on polymer sustainability as the plastic problem grows. Hillmyer and coworkers outline three grand challenges in producing the next generation of plastics: "(a) the efficient and sustainable conversion of biomass to polymer ingredients, (b) the design and development of high-performance sustainable plastics, elastomers, and thermosets, and (c) advances in sustainable polymer degradation, chemical recycling, and compatibilization".[2] Sustainability advancements in the field of cationic polymerizations have aimed to meet these challenges using energy efficient methods to generate thermoplastics and thermoplastic elastomers using renewable monomers.

1.2 Synthesis of Renewable Monomers for Cationic Polymerization

A significant hurdle in the production of sustainable polymers is the sourcing

of monomers from biorenewable feedstocks. Currently, over 90% of overall plastic production comes from virgin petroleum feedstock and it is projected that by 2050 plastic production will account for 20% of global oil consumption. Therefore, the decoupling of plastic production from petroleum feedstock is paramount to the development of a sustainable plastics economy. Bioalcohols represent a largely untapped resource in the production of biorenewable monomers. Several alcohols are already produced on large scale from biomass for use as transportation fuel. In 2019 the United States produced 15.7 billion gallons of bioethanol and 1 million gallons of bio-isobutanol for use as transportation fuel. Recently, Novamont and Genomatica built the first plant dedicated to production of 1,4-butanediol from biomass, in the aim of incorporating the diol into renewable plastics such as poly(butylene terethalate).[3,4] There have now been several reports for the efficient transformation of these alcohols into vinyl ethers (Figure 1.1). Matsubara and coworkers reported the vinylation of alkyl alcohols to vinyl ethers using calcium carbide as a sustainable source of acetylene.[5] Alkyl vinyl ethers, and specifically isobutyl vinyl ether (IBVE), have been bellwether monomers in development of new controlled cationic polymerization methods.[6,7] However, these alkyl vinyl ethers produce polymers with low glass transition temperatures (T_gs) on their own, leading to poor material properties. Therefore, groups have explored the sustainable generation of other vinyl ethers and compatible monomers from renewable feedstocks.

Most notably, Liete and coworkers reported on the catalytic cyclization of 1,4 butanediol to produce 2,3-dihydrofuran (DHF) in high yield.[8] DHF is a cyclic vinyl ether that has been demonstrated to produce a high T_g polymer through cationic polymerization.[9,10] In addition, Fors and coworkers developed a pathway for generating *p*-methoxystyrene (MOS) from *p*-coumaric acid in a two-step, one-pot synthesis.[11] *p*-coumaric acid can be sourced from sugarcane bagasse, the inedible byproduct of sugar production.[12,13] MOS has been implemented in many cationic polymerization methods and yields a polymer with a higher T_g than its petroleum counterpart, polystyrene (113 and 100 °C, respectively). While MOS is not sourced as efficiently from bioalcohols as vinyl ethers, its high T_g and compatibility with vinyl ether polymerizations improves material properties and adds value to poly(vinyl ethers) (PVEs). With vinyl ethers being only one step from bioalcohols already produced on plant scale, their cationic polymerization proves an efficient method for transforming bioalcohols into sustainable thermoplastics and thermoplastic elastomers.

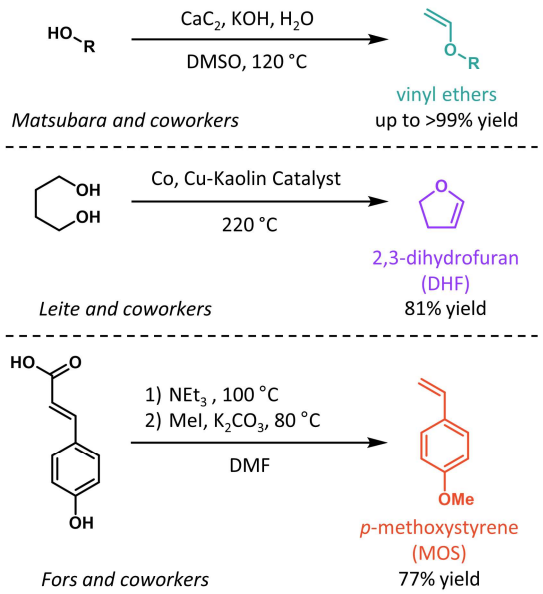

Figure 1.1: Synthesis of monomers from renewable feedstock

1.3 Polymerization Methods

Previously, the bulk of cationic polymerizations were performed with Lewis acids such as metal halides.[1] These Lewis acids can be used in conjunction with additives to produce living polymerization of vinyl ethers. Work done by Aoshima and Higashimura have shown a typical system of a $EtAlCl_2$, an acid adduct of IBVE, and an added ether or ester affords a living polymerization of vinyl ethers (Figure 1.2).[14,15] However, typically this system requires low reaction temperatures (0 °C) to achieve controlled polymerization. This system has been widely explored to polymerize homopolymers[1,10,15], ABA block copolymers[16–18], and even star polymers[17,19]. While this system has been highly effective, the low reaction temperatures limit the utility of this system to produce polymer materials on large scale.

Recent work by Fors and coworkers has demonstrated the ability to perform

controlled cationic polymerizations at room temperature using reversable addition-fragmentation chain transfer (RAFT) chemistry. Cationic RAFT was first demonstrated by Kamigaito and coworkers using dithiocarbamate and trithiocarbonate chain transfer agents (CTAs) and ppm amounts of triflic acid as an initiator.[6] This system suffered similar issues to the lewis acid method, requiring a low reaction temperature (−78 °C). Fors and coworkers hypothesized that rather than using an acid initiator, they could perform an oxidation of the CTA to initiate polymerization. This was subsequently demonstrated with chemical[20], photochemical[7,21,22], and electrochemical[23,24] oxidation methods, all of which were performed at room temperature. This represents a marked improvement I reaction energy efficiency over Lewis acid cationic polymerizations.

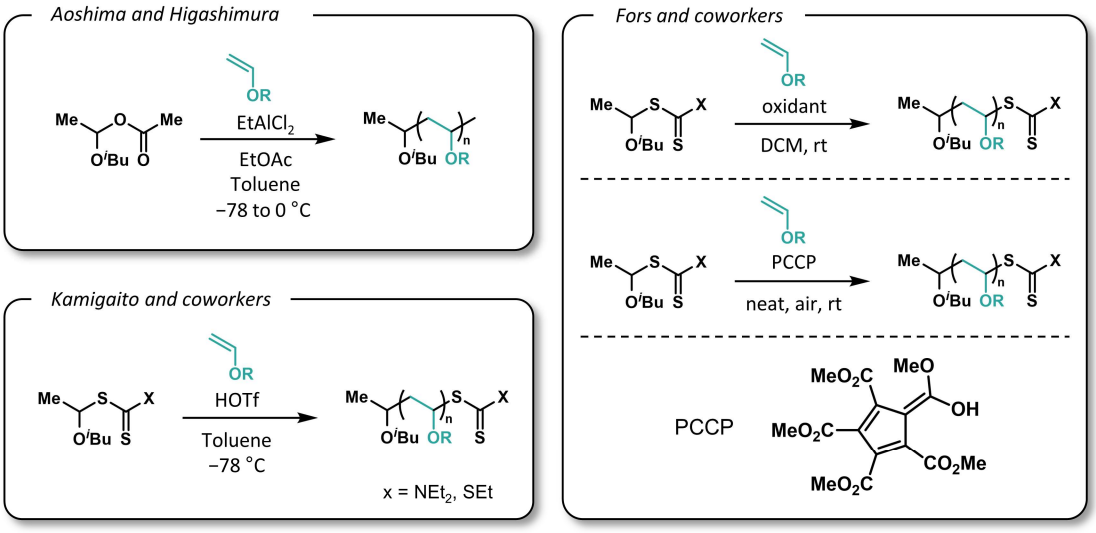

Figure 1.2: Controlled cationic polymerization methods

One disadvantage to RAFT chemistry and particularly cationic RAFT chemistry is the synthesis of the CTAs. Previous methods involved multiple steps at reduced temperatures to afford a CTA that was a viscus yellow oil that required solvent

intense column chromatography.[6,7] Fors and coworkers implemented an aqueous, room temperature synthesis to afford a solid, white CTA, CTA-1 (Figure 1.3a). The crystalline nature of the CTA allows for recrystallization for purification, reducing cost and increasing sustainability. This CTA was then demonstrated to perform controlled cationic RAFT polymerization with all previously studied oxidation initiators as well as acid initiators (Figure 1.3b). This new CTA enables facile preparation of reagents for cationic RAFT polymerizations, decreasing the barrier for future work and implementation in industry.

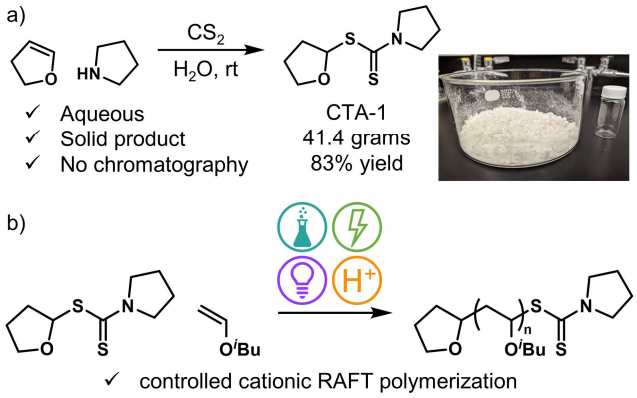

Figure 1.3: Green chain transfer agent for cationic RAFT polymerizations

Additional advancements made by Fors and coworkers has afforded a controlled cationic polymerization under ambient conditions. They demonstrated that pentakis-(methoxycarbonyl)cyclopentadiene (PCCP) could initiate controlled polymerization of vinyl ethers.[25] The reactions were caried out without drying or distillation of monomer, without solvent, and under an atmosphere of air at room temperature. It was hypothesized the strong coordination of the cyclopentadienyl anion to the propagating oxocarbenium chain end directed monomer addition and prevented termination from adventitious nucleophiles.

The ambient conditions, removal of solvent, and elimination of monomer distillation represent further sustainability and utility improvements. This system was then further developed to reduce chain transfer events and increase the molecular weight of the polymers. Fors and coworkers found that the addition of a hydrogen bond donor (HBD) allowed greater M_n to be reached under ambient, solvent free conditions.[26] In addition, they found that HBD catalyst allowed the polymerization to be carried out in cyclopentyl methyl ether (CPME), a "green" solvent currently being developed for process chemistry applications (Figure 1.4).[27–30] Therefore, the PCCP and HBD system for cationic polymerization affords controlled cationic polymerization of vinyl ethers under ambient conditions and allows for the use of "green" solvents.

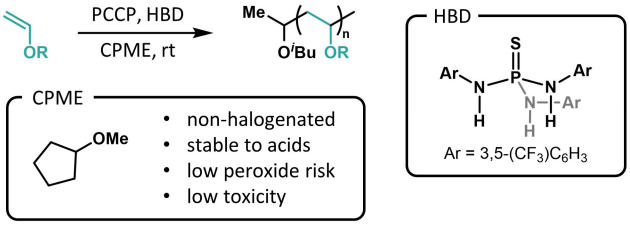

Figure 1.4: Hydrogen bond donor enables use of green solvent

1.4 Poly(2,3-dihydrofuran) as a strong, sustainable, and degradable thermoplastic

While most PVEs have low T_gs, and therefore make poor thermoplastics, there are a few notable exceptions. Most notably, PDHF has captured recent interest due to its favorable properties. Sanda and Matsumoto implemented a lewis acid initiator to obtain a controlled polymerization at −78 °C and characterized the relationship between PDHF diastereoselectivity and T_g.[9] Aoshima and coworkers

more recently published a base-stabilized polymerization that gave a controlled polymerization at 0 °C.[10]Improving upon these cationic polymerizations, Fors and coworkers demonstrated the controlled polymerization of DHF at room temperature.[25] This work was then extended to generate high molecular weight (M_n) PDHF, displaying impressive tensile strength and toughness (1.4Figure 1.5). This method employs the organic acid initiator, PCCP, in a metal-free, single-component system. Additionally, they showed the toxic solvent DCM could be replaced with CPME when HBD was used. Under these conditions, the polymerization affords an atactic polymer with ~65% *trans*-content. The high M_n PDHF demonstrated high tensile strength (≤ 70 MPa) and moderate toughness (≤ 14 MPa), comparable to commercial poly(bispheol A carbonate). Additionally, the gas and water vapor transmission properties of PDHF films were low, promising for food packaging applications. Finally, this study investigated the degradation of PDHF, as this is a vital consideration for bringing any next generation plastic. Previously, Sanda and Matsumoto reported the degradation in air at high temperatures resulted in reduced molecular weights.[31] In addition, several patents reference decomposition of PDHF-based materials in the presence of air oxygen.[32–34] The Fors group thus hypothesized this could be accelerated through use of a strong chemical oxidant. They successfully demonstrated the accelerated degradation of PDHF over 48 hours using a combination of H_2O_2 and Fe(II), commonly referred to as Fenton's reagent. This comprehensive study demonstrated that PDHF is a promising sustainable thermoplastic, sourced

efficiently from bioalcohol and can be degraded after use.

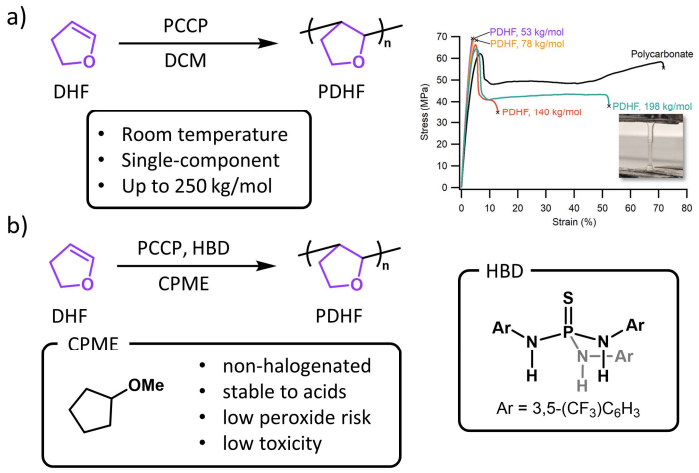

Figure 1.5: Polymerization of DHF to produce a strong and tough thermoplastic

1.5 Thermoplastic Elastomers

The incorporation of renewable alkyl vinyl ethers into TPEs is an effective way to add value to typically poor performing PVEs. TPEs are typically composed of a low T_g midblock bookended by two high T_g endblocks. The rubbery midblock makes up the large majority of polymer mass, and thus makes effective use of cheap low T_g polymers that perform poorly on their own. Thus, this area has been explored previously with Lewis acid living cationic polymerizations, where Hashimoto and coworkers successfully synthesized PVE ABA copolymers with poly(tricyclodecyl vinyl ether) (PTCDVE) end blocks and poly(*n*-butyl vinyl ether) (PNBVE) mid block (PTCDVE-NBVE-PTCDVE).[18] They followed up this work with the synthesis of ABA copolymers composed of poly(2-adamantyl vinyl ether) (PAdVE) hard blocks with the same PNBVE rubbery block (PAdVE-PNBVE-PAdVE, Table 1.1).[17] In this study, they reported tensile properties for both materials and found moderate tensile strength (≤ 5.55 MPa) and elongation (≤ 355%) for their

ABA copolymers.

Motivated by these results, Fors and coworkers sought to apply their cationic RAFT polymerization to the generation of TPEs from vinyl ethers.[11] For this study, Fors and coworkers sought to utilize isobutyl vinyl ether (IBVE) as the rubbery mid block and DHF as the hard end block. In addition, they employed MOS as a styrenic hard block amenable to cationic polymerization. To generate ABA block copolymers, they employed a chemical oxidant, ferrocenium tetrafluoroborate ($FcBF_4$), to oxidize a difunctional chain transfer agent (CTA) and initiate polymerization. They successfully produced ABA copolymers composed of a rubbery PIBVE mid block and either PDHF or PMOS hardblocks through a single sequential addition (Figure 1.6). The PDHF-PIBVE-PDHF TPEs showed a significant improvement over other PVE ABA copolymers, with an elongation of up to 570%. This work is being continued by the group to investigate PDHF-PIBVE AB-star copolymers for further improvement of material properties.

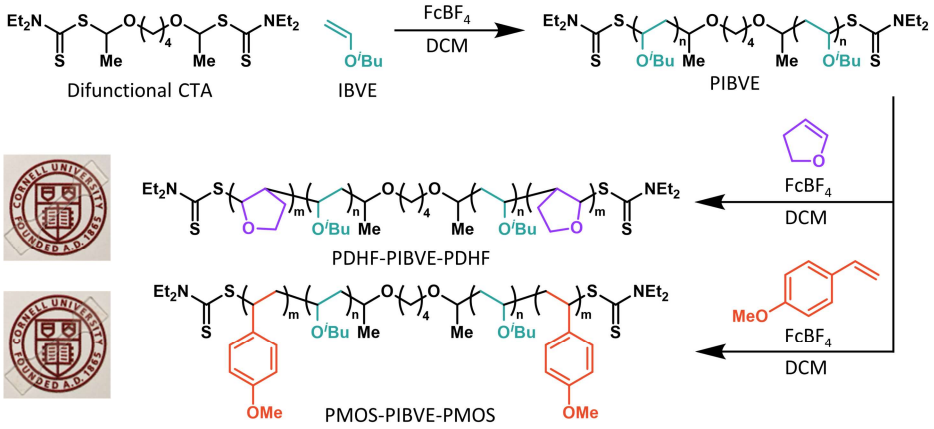

Figure 1.6: ABA copolymers produced via cationic RAFT polymerization

Table 1.1: Comparison of material properties for PVE ABA copolymer TPEs

Entry	Polymer	f_{HB} [a]	M_n, total (kg/mol) [b]	Tensile Strength at Break (MPa) [c]	Elongation at Break (%)
1 [d]	PAdVE-PNBVE-PAdVE	0.25	106	1.52	355
2 [d]	PAdVE-PNBVE-PAdVE	0.48	110	5.55	245
3	PMOS-PIBVE-PMOS	0.21	66	1.4	405
4	PMOS-PIBVE-PMOS	0.23	75	3.1	340
5	PMOS-PIBVE-PMOS	0.32	71	3.3	126
6	PMOS-PIBVE-PMOS	0.38	68	7.2	152
7	PDHF-PIBVE-PDHF	0.23	68	4.3	570
8	PDHF-PIBVE-PDHF	0.31	69	3.4	335

[a] f_{HB} = volume fraction hard block. [b] M_n determined from light scattering data. [c] Tensile data is the average of at least 3 samples. [d] Data from Hashimoto and coworkers[13]

1.6 Conclusion

New methods for controlled cationic polymerizations have not only improved the sustainability of the procedures, but they have also enabled the production of new sustainable materials. The cationic polymerization of vinyl ethers allows us to utilize cheap and abundant bioalcohol feedstock in the production of next generation plastics. The development of room temperature cationic RAFT polymerization has reduced the energy cost of generating these polymers. Further advancements with the PCCP acid initiator have enabled ambient conditions and the polymerization of PDHF to high molecular weights. PDHF has demonstrated to be a promising thermoplastic with high strength, while also being degradable. Incorporation of the alkyl vinyl ethers and PDHF into PDHF-PIBVE-PDHF provided a TPE with improved physical properties over previous PVE TPEs. These demonstrations reveal that the recent advances in cationic polymerizations provide a steppingstone from abundant bioalcohols to robust, sustainable, and

degradable plastics.

1.7 References

(1) Aoshima, S.; Kanaoka, S. A Renaissance in Living Cationic Polymerization. *Chem. Rev.* **2009**, *109* (11), 5245–5287.

(2) Haque, F. M.; Ishibashi, J. S. A. A.; Lidston, C. A. L. L.; Shao, H.; Bates, F. S.; Chang, A. B.; Coates, G. W.; Cramer, C. J.; Dauenhauer, P. J.; Dichtel, W. R.; et al. Defining the Macromolecules of Tomorrow through Synergistic Sustainable Polymer Research. *Chem. Rev.* **2022**, *122* (6), 6322–6373.

(3) Bomgardner, M. M. Novamont Opens Bio-BDO Plant. *C&EN* **2016**, *94* (40).

(4) *U.S. Fuel Ethanol Plant Production Capacity*; 2020.

(5) Matake, R.; Adachi, Y.; Matsubara, H. Synthesis of Vinyl Ethers of Alcohols Using Calcium Carbide under Superbasic Catalytic Conditions (KOH/DMSO). *Green Chem.* **2016**, *18* (9), 2614–2618.

(6) Uchiyama, M.; Satoh, K.; Kamigaito, M. Cationic RAFT Polymerization Using Ppm Concentrations of Organic Acid. *Angew. Chemie Int. Ed.* **2015**, *54* (6), 1924–1928.

(7) Kottisch, V.; Michaudel, Q.; Fors, B. P. Cationic Polymerization of Vinyl Ethers Controlled by Visible Light. *J. Am. Chem. Soc.* **2016**, *138* (48), 15535–15538.

(8) Ludmila, L.; Stonkus, V.; Edolfa, K.; Ilieva, L.; Plyasova, L.; Zaikovskii, V. Copper-Promoted Cobalt Catalysts for 2,3-Dihydrofuran Synthesis. *Appl. Catal. A Gen.* **2006**, *311*, 86–93.

(9) Sanda, F.; Matsumoto, M. Cationic Polymerization of 2,3-Dihydrofuran. Study on the Relationship between Glass Transition Temperature and Tacticity of the Polymer. *Macromolecules* **1995**, *28* (20), 6911–6914.

(10) Yonezumi, M.; Kanaoka, S.; Aoshima, S. Living Cationic Polymerization of Dihydrofuran and Its Derivatives. *J. Polym. Sci. Part A Polym. Chem.* **2008**, *46* (13), 4495–4504.

(11) Spring, S. W.; Smith-Sweetser, R. O.; Rosenbloom, S. I.; Sifri, R. J.; Fors, B. P. Sustainable Thermoplastic Elastomers Produced via Cationic RAFT Polymerization. *Polym. Chem.* **2021**, *12*, 1097–1104.

(12) Ou, S. Y.; Luo, Y. L.; Huang, C. H.; Jackson, M. Production of Coumaric Acid from Sugarcane Bagasse. *Innov. Food Sci. Emerg. Technol.* **2009**, *10* (2), 253–259.

(13) Li, M.; Jia, Z.; Wan, G.; Wang, S.; Min, D. Enhancing Isolation of P-Coumaric and Ferulic Acids from Sugarcane Bagasse by Sequential Hydrolysis. *Chem. Pap.* **2020**, *74* (2), 499–507.

(14) Ogawa, Y.; Sawamoto, M.; Higashimura, T. Living Cationic Polymerization of Cyclic Unsaturated Ethers. *Polym. J.* **1984**, *16* (5), 415–422.

(15) Higashimura, T.; Aoshima, S.; Higashimura, T. Living Cationic Polymerization of Vinyl Monomers by Organoaluminum Halides. 3. Living Polymerization of Isobutyl Vinyl Ether by Ethyldichloroaluminum in the Presence of Ester Additives. *Macromolecules* **1989**, *22* (3), 1009–1013.

(16) Hashimoto, T.; Imaeda, T.; Irie, S.; Urushisaki, M.; Sakaguchi, T. Synthesis

of Poly(Vinyl Ether)-Based, ABA Triblock-Type Thermoplastic Elastomers with Functionalized Soft Segments and Their Gas Permeability. *J. Polym. Sci. Part A Polym. Chem.* **2015**, *53* (9), 1114–1124.

(17) Imaeda, T.; Hashimoto, T.; Irie, S.; Urushisaki, M.; Sakaguchi, T. Synthesis of ABA-Triblock and Star-Diblock Copolymers with Poly(2-Adamantyl Vinyl Ether) and Poly(n-Butyl Vinyl Ether) Segments: New Thermoplastic Elastomers Composed Solely of Poly(Vinyl Ether) Backbones. *J. Polym. Sci. Part A Polym. Chem.* **2013**, *51* (8), 1796–1807.

(18) Hashimoto, T.; Namikoshi, T.; Irie, S.; Urushisaki, M.; Sakaguchi, T.; Nemoto, T.; Isoda, S. Synthesis and Microphase-Separated Structure of Poly(Tricyclodecyl Vinyl Ether)-Block-Poly(n-Butyl Vinyl Ether)-Block-Poly(Tricyclodecyl Vinyl Ether): New Triblock Copolymer as Thermoplastic Elastomer Composed Solely of Poly(Vinyl Ether) Backbones. *J. Polym. Sci. Part A Polym. Chem.* **2008**, *46* (5), 1902–1906.

(19) Shibata, T.; Kanaoka, S.; Aoshima, S. Quantitative Synthesis of Star-Shaped Poly(Vinyl Ether)s with a Narrow Molecular Weight Distribution by Living Cationic Polymerization. *J. Am. Chem. Soc.* **2006**, *128* (23), 7497–7504.

(20) Peterson, B. M.; Kottisch, V.; Supej, M. J.; Fors, B. P. On Demand Switching of Polymerization Mechanism and Monomer Selectivity with Orthogonal Stimuli. *ACS Cent. Sci.* **2018**, *4* (9), 1228–1234.

(21) Michaudel, Q.; Chauviré, T.; Kottisch, V.; Supej, M. J.; Stawiasz, K. J.; Shen, L.; Zipfel, W. R.; Abruña, H. D.; Freed, J. H.; Fors, B. P. Mechanistic Insight

into the Photocontrolled Cationic Polymerization of Vinyl Ethers. *J. Am. Chem. Soc.* **2017**, *139* (43), 15530–15538.

(22) Kottisch, V.; Supej, M. J.; Fors, B. P. Enhancing Temporal Control and Enabling Chain-End Modification in Photoregulated Cationic Polymerizations by Using Iridium-Based Catalysts. *Angew. Chemie Int. Ed.* **2018**, *57* (27), 8260–8264.

(23) Supej, M. J.; Peterson, B. M.; Fors, B. P. Dual Stimuli Switching: Interconverting Cationic and Radical Polymerizations with Electricity and Light. *Chem* **2020**, *6* (7), 1794–1803.

(24) Peterson, B. M.; Lin, S.; Fors, B. P. Electrochemically Controlled Cationic Polymerization of Vinyl Ethers. *J. Am. Chem. Soc.* **2018**, *140* (6), 2076–2079.

(25) Kottisch, V.; O'Leary, J.; Michaudel, Q.; Stache, E. E.; Lambert, T. H.; Fors, B. P. Controlled Cationic Polymerization: Single-Component Initiation under Ambient Conditions. *J. Am. Chem. Soc.* **2019**, *141* (27), 10605–10609.

(26) Kottisch, V.; Jermaks, J.; Mak, J.-Y.; Woltornist, R. A.; Lambert, T. H.; Fors, B. P. Hydrogen Bond Donor Catalyzed Cationic Polymerization of Vinyl Ethers. *Angew. Chemie Int. Ed.* **2021**, *60* (9), 4535–4539.

(27) Watanabe, K.; Yamagiwa, N.; Torisawa, Y. Cyclopentyl Methyl Ether as a New and Alternative Process Solvent. *Org. Process Res. Dev.* **2007**, *11* (2), 251–258.

(28) Azzena, U.; Carraro, M.; Pisano, L.; Monticelli, S.; Bartolotta, R.; Pace, V. Cyclopentyl Methyl Ether: An Elective Ecofriendly Ethereal Solvent in Classical and Modern Organic Chemistry. *ChemSusChem* **2019**, *12* (1), 40–70.

(29) Watanabe, K. The Toxicological Assessment of Cyclopentyl Methyl Ether (CPME) as a Green Solvent. *Molecules* . 2013.

(30) de Gonzalo, G.; Alcántara, A. R.; Domínguez de María, P. Cyclopentyl Methyl Ether (CPME): A Versatile Eco-Friendly Solvent for Applications in Biotechnology and Biorefineries. *ChemSusChem* **2019**, *12* (10), 2083–2097.

(31) Sanda, F.; Matsumoto, M. Degradation Behavior of Poly(2,3-Dihydrofuran). *J. Appl. Polym. Sci.* **1996**, *59* (2), 295–299.

(32) Matsumoto, M. Sanda, F. Disposable Molding Compositions Containing THF Skeleton-Containing Polymers and Phenolic Compounds and/or Plasticizers. JP03146509A, 1991.

(33) Matsumoto, M.; Sanda, F.; Sasaki, S.; Okazaki, M. Disposable Moldings and Polymer Compositions for Their Production. Google Patents June 16, 1992.

(34) Ootake, Y.; Asabe, H. Biodegradable Polymer Compositions., August 9, 1994.

Chapter 2

Sustainable Thermoplastic Elastomers Produced *via* Cationic RAFT Polymerization [ϕ]

2.1 Abstract

Plastic production continually increases its share of global oil consumption. Thermoplastic elastomers (TPEs) are a necessary component of many industries, from automotive and construction to healthcare and medical devices. To reduce the environmental burden of TPE production on the world, we developed two new ABA triblock copolymers synthesized through cationic reversable addition-fragmentation chain transfer (RAFT) polymerization from renewable monomers. Using poly(isobutyl vinyl ether) (PIBVE) as the soft block and either poly(*p*-methoxystyrene) (PMOS) or poly(2,3-dihydrofuran) (PDHF) as the hard blocks, we produced triblock copolymers with varying volume fractions and characterized their material properties. PDHF-PIBVE-PDHF is sourced almost entirely from simple alcohols and exhibits mechanical properties comparable to those of

[ϕ] This chapter was reproduced from Spring, S. W., *et al. Polym. Chem.* **2021**, *12*, 1097–1104. with permission from the Royal Society of Chemistry.

commercial TPEs. This effort demonstrates the utility of cationic RAFT for the production of sustainable TPEs.

2.2 Introduction

Increasing attention in the scientific community has turned to the creation of a renewable plastic economy less reliant on fossil fuels. Currently, over 90% of overall plastic production comes from virgin petroleum feedstock and it is projected that by 2050 plastic production will account for 20% of global oil consumption.[1] Significantly, thermoplastic elastomers (TPEs) represent a 5 million metric ton per year market of such petroleum-based materials.[2] TPEs possess the elastomeric properties of rubbers and the processability and recyclability of thermoplastics and are commonly used in the automotive, construction, and footwear industries. The decoupling of advanced materials from petroleum feedstock remains a challenge in creating a sustainable plastics economy and requires the development of new renewably sourced polymers that match the physical performance of current TPEs.

TPEs are typified by their ABA copolymer structure composed of a rubbery B-block and glassy A-blocks. At sufficiently low volume fractions of the A-block, microphase separation leads to physical crosslinks formed by discrete glassy domains contained within a continuous phase of the rubbery segment, which affords TPEs their high elongation at break (ε_B) and tensile strength at break (σ_B).[3] Much of the work to attain TPE properties with renewable ABA copolymers has focused on ring opening polymerizations of lactones or condensation reactions of

carboxylic acids with diols.[4] Hillmyer and coworkers have developed aliphatic polyester block copolymers, with ε_B values in excess of 1000% strain and σ_B values over 30 MPa, comparable with commercial TPEs.[5–8] Although these polyester-based TPEs exhibit physical properties similar to commercial materials, they are thermally and hydrolytically unstable, leading to desired degradability, but limiting their application. Furthermore, ring opening polymerizations are mostly limited to polyesters and the lactone monomers employed are often several synthetic steps from biomass-derived chemicals. We posited that development of cationic polymerization for production of ABA copolymers would enable renewably sourced vinyl ethers to be incorporated in sustainable TPEs (Figure 2.1).

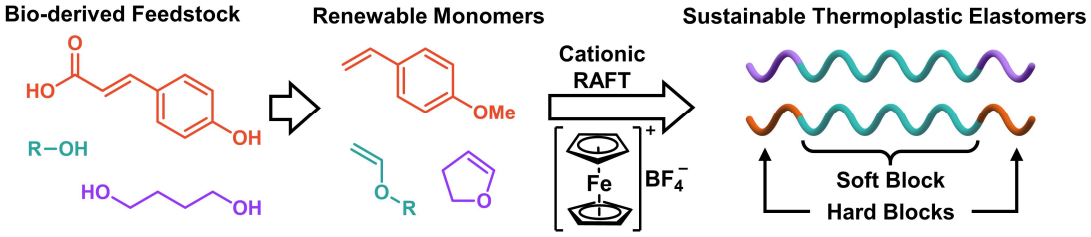

Figure 2.1: Synthesis of sustainable TPEs through cationic RAFT polymerization initiated by a chemical oxidant.

Cationic reversable addition-fragmentation chain-transfer (RAFT) polymerization is an alluring method for producing TPEs, as this method has emerged as an effective technique for polymerizing vinyl ethers in a controlled manner. Cationic RAFT polymerization was first reported by Kamigaito, where the use of chain transfer agents (CTAs) achieves control through a degenerate chain-transfer mechanism.[9] Recently, our group developed several methods for

reversibly oxidizing CTAs using photocatalysts[10–13], electrochemical mediators[14,15], or chemical oxidants[16] to gain temporal control over cationic polymerizations. Our methods enabled the synthesis of multiblock copolymers; however, they did not possess glassy blocks and, therefore, lacked the aforementioned physical crosslinks that would lead to a TPE. Furthermore, this method only produced block copolymers up to 19 kg/mol. Consequently, we set out to identify renewable monomers that could be controllably polymerized *via* a cationic mechanism to produce rubbery and glassy polymers.

Vinyl ethers represent an exciting prospect for renewable polymers because they can be synthesized from widely available bio-derived alcohols. Matsubara and coworkers have demonstrated that calcium carbide is an effective, safe, and renewable alternative to acetylene for the vinylation of alcohols, which we envisaged we could use to make entirely renewable vinyl ether monomers.[17] Importantly, most polyvinyl ethers (PVEs) have low glass transition temperatures (T_gs) making them suitable for use in the rubbery midblock but not the glassy end blocks of TPEs.[18] Hashimoto and coworkers achieved PVE TPEs using poly(2-adamanyl vinyl ether) as the glassy A-blocks; however, because the 2-adamantyl vinyl ether was an expensive and petroleum-derived monomer, we sought other readily available and renewable high T_g polymers accessible by cationic polymerization.[19,20] We initially identified the cyclic vinyl ether 2,3-dihydrofuran (DHF), because its respective polymer from cationic polymerization possesses a rigid backbone leading to a high T_g of ~140 °C.[21–23] As such, DHF has historically

been considered an alluring monomer for glassy polymers.[24,25] Additionally, DHF can be synthesized with industrially relevant efficiency from biosourced 1,4-butanediol using a heterogeneous catalysis making it an ideal choice for renewable TPEs.[26,27]

In our initial planning stage of this study, we were aware that the controlled polymerization of DHF has previously been a challenge. We anticipated that the cationic polymerization methodology recently developed in our lab could address this challenge; however, we also wanted to pursue other renewable monomers that could undergo cationic polymerization to yield glassy end blocks. To this end, poly(*p*-methoxystyrene) (PMOS) was identified as a candidate which has been used to make PVE-PMOS diblock copolymers.[28] Because this monomer is typically derived from petroleum feedstocks, we envisaged an efficient pathway to MOS from renewable coumaric acid, which can be found in many food sources, most notably sugar bagasse, the inedible byproduct of sugar production.[29,30]

Herein, we disclose our synthesis of renewable ABA block copolymers produced through cationic RAFT polymerization. Our method enables the use of a PVE as the rubbery B-block and either PDHF or PMOS as the glassy A-blocks. All the monomers we employ can be obtained from renewable feedstocks due in part to our development of a two-step synthesis of MOS from coumaric acid. ABA copolymers with high molar masses (70 kg/mol) are produced utilizing cationic RAFT initiated by a chemical oxidant. In addition, we characterize the mechanical properties and compare them to other renewably sourced TPEs. To this end, we

show how cationic polymerization of vinyl ethers enable sustainable TPEs sourced entirely from bio-derived alcohols.

2.3 Results and Discussion

2.3.1 Synthesis of p-methoxystyrene from renewable p-coumaric acid

Styrenic block copolymers are the most common TPE and contain glassy polystyrene A-blocks and usually polybutadiene or polyisoprene as the rubbery B-block. To match the material properties of commercial TPEs with sustainable polymers, we posited using a renewable analogue of styrene would provide a starting point for our investigation. We set out to produce MOS, which has been shown to polymerize controllably under cationic conditions and provides a polymer with a high T_g, from coumaric acid.[31–34] Recently, Kamigaito and coworkers showed that they can decarboxylate ferulic and coumaric acid, which are derived from lignin, using triethylamine and subsequently protect the phenol, enabling controlled radical polymerization.[35,36] Using a similar strategy, we sought to decarboxylate *p*-coumaric acid and methylate the phenol to produce MOS in a sustainable manner (Figure 2.2). It was also necessary for us to develop a one-pot synthesis from *p*-coumaric acid to avoid the spontaneous polymerization of the *p*-hydroxystyrene.

We first optimized the decarboxylation of coumaric acid to *p*-hydroxystyrene, which has been reported with conventional heating in alkaline aqueous solution and more recently microwave heating with catalytic triethylamine.[37,38] We found that conventional heating to 80 °C with 2 equivalents of triethylamine achieved

high yields when a small amount of butylated hydroxytoluene (BHT) radical inhibitor was added to prevent radical polymerization of the product, *p*-hydroxystyrene (Figure 2.2, entry 1). The use of lower molar equivalents of triethylamine or other bases led to lower yields (Figure 2.2, entries 2-6). Addition of methyl iodide after decarboxylation using the optimized conditions did not give any desired MOS, likely due to triethylamine serving as a favorable nucleophile itself (Figure 2.2, entry 7). To circumvent this, triethylamine was removed via rotary evaporation before the addition of a different base and methyl iodide. The transformation was attempted with pyridine as a less nucleophilic base, but led to no conversion (Figure 2.2, entry 8). We found that non-nucleophilic bases such as potassium carbonate and potassium phosphate were required for efficient methylation of *p*-hydroxystyrene (Figure 2.2, entry 9 and 10). The reaction was then performed in a single pot on 25g scale with triethylamine and K_2CO_3 in steps 1 and 2, respectively, affording MOS in 77% overall isolated yield.

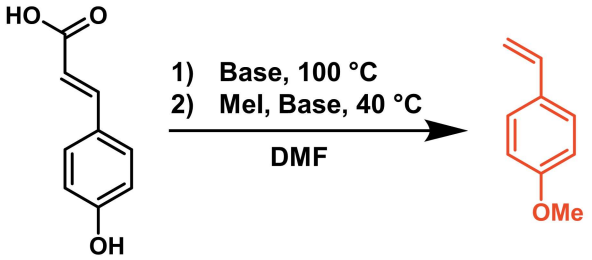

Entry	Base	[Base]/ [*p*-coumaric acid]	Yield (%)
	Step 1		
1	NEt_3	2	95
2	NEt_3	1	60
3	NEt_3	0.5	35
4	K_2CO_3	0.5	7
5	K_3PO_4	0.5	11
6	Pyridine	0.5	16
	Step 2		
7	NEt_3	1	0
8	Pyridine	1	0
9	K_2CO_3	1	96
10	K_3PO_4	1	94

Figure 2.2: Synthesis of MOS from p-coumaric acid, a sugarcane byproduct, in a two-step, one pot procedure.

2.3.2 Synthesis of Triblock Copolymers

To produce sustainable ABA copolymers from vinyl ethers and MOS, we employed a cationic RAFT polymerization procedure recently developed in our lab.[16] In contrast to the traditional monofunctional CTA used in these polymerizations, we synthesized a difunctional CTA from 1,4-butanediol divinyl ether enabling the production of ABA copolymers in two steps. *Iso*-butyl vinyl ether (IBVE) was polymerized using the difunctional CTA and ferrocenium tetrafluoroborate ($FcBF_4$) as a catalytic chemical oxidant (Figure 2.3) to afford telechelic rubbery PIBVE blocks with various molecular weights and narrow dispersity (*Đ*) values (See Supporting Information, Figure 2.11). We selected IBVE as our midblock monomer due to its precedent in controlled cationic

polymerizations and its renewability. Isobutanol is produced renewably on plant scale under the trade name Butamax®. This bio-derived isobutanol can undergo vinylation with calcium carbide using the method the described vinylation by Matsubara and coworkers to generate IBVE.[17] Notably, the use of $FcBF_4$ as a chemical oxidant and cationogen allows for the polymerization to proceed at room temperature, improving gelation issues and decreasing the energy demands associated with Lewis or Brønsted acid-initiated polymerizations performed at low temperatures.[19,20,28,39]

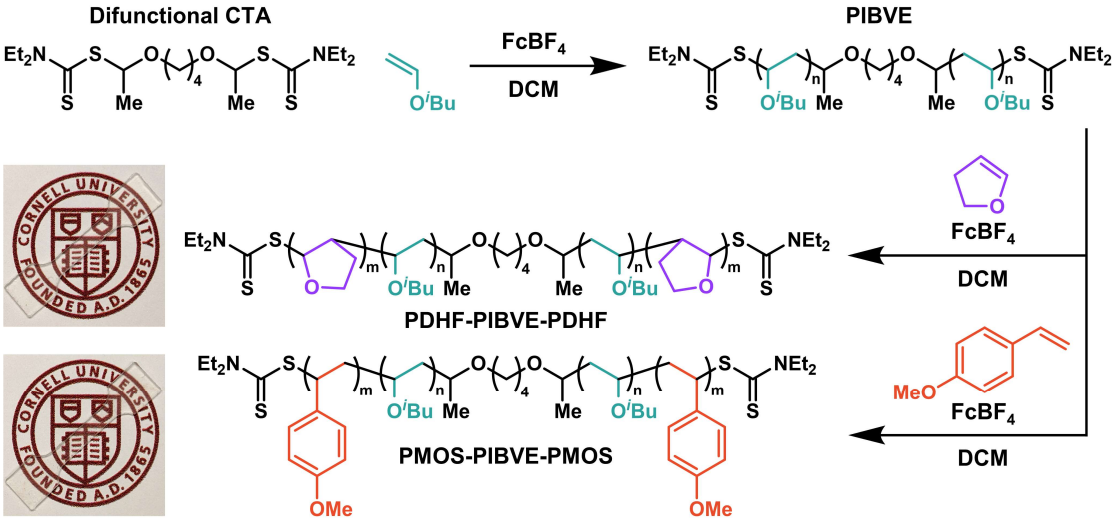

Figure 2.3: Synthesis of ABA triblock copolymers from a difunctional CTA using cationic RAFT initiated by $FcBF_4$ as a chemical oxidant. Picture insets show clear and colourless polymers after processing into dogbones.

Without isolation of the midblock, telechelic PIBVE was then chain extended with either MOS or DHF to yield PMOS-PIBVE-PMOS or PDHF-PIBVE-PDHF, respectively. The polymerization of a PMOS-PIBVE-PMOS copolymer was monitored over time to elucidate the behavior of the chain extension. We

observed a linear increase in M_n with respect to monomer conversion over the course of the reaction for both IBVE and MOS (Figure 2.4a), which illustrates the "living" character of the polymerization. Figure 2.4b shows the gradual shift to higher molecular weight for each block, providing further evidence of the chain extension.

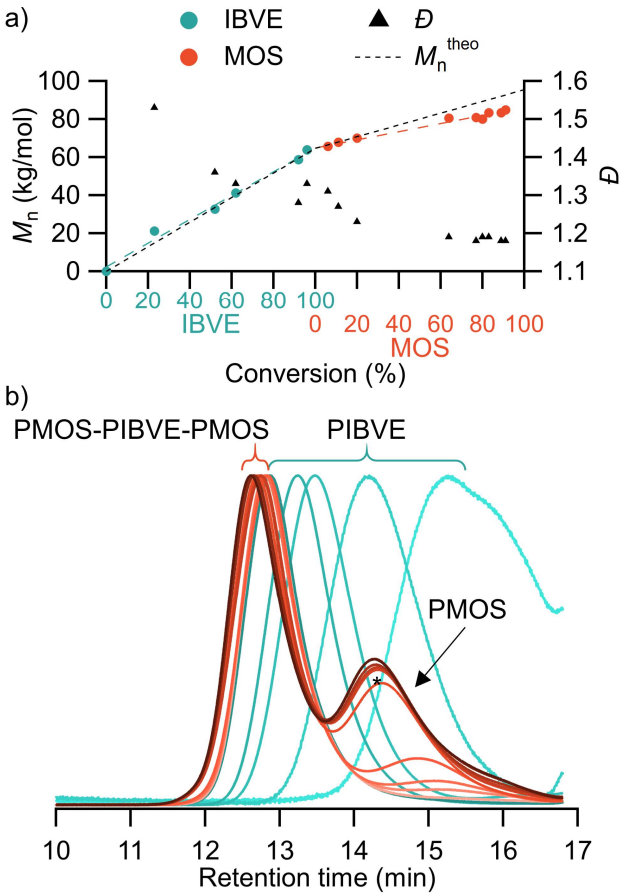

Figure 2.4: Polymerization progress in PMOS-PIBVE-PMOS monitored via (a) monomer conversion relative to Mn and Đ and (b) SEC traces showing chain extension and PMOS homopolymer. *Indicates 64% conversion of MOS.

In addition to the chain extension, there emerged a low molecular weight peak we attributed to PMOS homopolymer. We hypothesize that this homopolymer is

a result of direct oxidation of the monomer to initiate new chains, a known competitive pathway for cationic RAFT polymerizations.[12,16] With the IBVE depleted, any new polymer chains must be PMOS. Due to the increased viscosity upon chain extension, the reaction was diluted and additional $FcBF_4$ was added to compensate the decreased rate of polymerization (See Experimental Section of Supporting Information). However, the additional $FcBF_4$ also increases the favorability of adventitious monomer oxidation. We aimed to terminate the polymerizations at 70% conversion of MOS to limit PMOS homopolymer in the final material. This homopolymer could not be fractionally precipitated or otherwise separated from the copolymer.

The volume fraction of hard block (f_{HB}) in each sample was determined by integration of the respective polymer peaks in ^{1}H NMR (Figure 2.24–Figure 2.29). Therefore, it should be noted that a portion of the f_{HB} is from homopolymer of PMOS or PDHF in their respective samples. Previous studies of styrenic block copolymers have indicated that added homopolymer of polymer A in an ABA copolymer will evenly distribute within the microphase will not form independent microdomains unless the M_n of homopolymer exceeds that of the midblock.[40,41] As such, we anticipate that any PMOS or PDHF homopolymer will reside within the discrete glassy domains formed by the end blocks and will not significantly contribute to the mechanical properties of the materials.

Table 2.1: ABA copolymer composition and material properties

Entry	Polymer	f_{HB}[a]	M_n[b],PIBVE (kg/mol)	M_n[b], total (kg/mol)	σ_B (MPa)	ε_B (%)	E (MPa)	Morphology[c]
1	PMOS-0.21	0.21	54.1	66	1.4 ± 0.1	405 ± 30	1.2 ± 0.2	HEX
2	PMOS-0.23	0.23	50.0	75	3.1 ± 0.2	340 ± 50	1.2 ± 0.2	HEX
3	PMOS-0.32	0.32	52.5	71	3.3 ± 0.8	126 ± 30	6.3 ± 1	LAM
4	PMOS-0.38	0.38	44.8	68	7.2 ± 0.8	152 ± 9	18 ± 6	LAM
5	PDHF-0.23	0.23	53.0	68	4.3 ± 0.2	570 ± 70	1.3 ± 0.2	HEX
6	PDHF-0.31	0.31	52.0	69	3.4 ± 0.3	335 ± 50	1.9 ± 0.1	HEX

[a] Total volume fraction of the hard block calculated from NMR integration, which includes homopolymer. [b] Determined by SEC against polystyrene standards. Peaks were defined as seen in Figure 1.9, where the reported Mn omits the homopolymer peak. [c] Determined from the ratios of scattering peaks relative to the principal scattering wavevector, q*, where HEX = hexagonally packed cylinders and LAM = lamellae.

We produced a series of each triblock copolymer targeting the same total molecular weight (*c.a.* 70 kg/mol) and varying f_{HB} of hard block (Table 2.1). The samples are referenced by their hard block polymer and composition as PMOS-f_{HB} or PDHF-f_{HB}. These polymers were easily processed into dogbone-shaped tensile bars using a heated press. Interestingly, unlike most polymers produced from RAFT initiators, our ABA triblock copolymers are clear and colorless (Figure 2.3, picture insets). We attribute this to dithiocarbamates being less colored than the dithiobenzoates and trithiocarbonates used in radical RAFT and the high M_n of the polymers reducing dithiocabamate concentration.[42]

2.3.3 Material Properties

TPEs are typically composed of a two-phase system, where glassy domains are dispersed in a continuous rubbery phase. To determine the morphologies of our samples, small angle X-ray scattering (SAXS) was performed (Figure 2.12) and each sample displayed enough scattering peaks to assign a morphology (Table 2.1).[43] Low f_{HB} samples PMOS-0.21 and PMOS-0.23 display continuous hexagonally packed cylinders (HEX) morphology while PMOS-0.32 and PMOS-

0.38 adopt a lamellae (LAM) morphology. For the PDHF-PIBVE-PDHF, we only targeted low f_{HB} to achieve HEX morphology, which is well known to give superior TPE properties.[3,44] Indeed, both samples, PDHF-0.23 and PDHF-0.31, were assigned HEX morphology from their SAXS peaks.

In addition to the assigned morphologies from SAXS, we confirmed phase separation with differential scanning calorimetry (DSC) and dynamic mechanical thermal analysis (DMTA). For sample PMOS-0.38, two T_gs were observed by DSC (−10 °C corresponding to the PIBVE phase and 105 °C corresponding to the PMOS phase), thus confirming the phase separated microstructure (Figure 2.5). Similarly, we observed two T_gs for PDHF-0.31; −10 and 126 °C, corresponding to the PIBVE and PDHF phases, respectively. We then attempted to corroborate the high T_gs with temperature sweeps in DMTA. The samples were first subjected to oscillatory strain sweeps from 0.1 to 100% strain at an angular frequency of 1 Hz to establish the linear viscoelastic region (Figure 2.13 and Figure 2.14). An oscillatory strain of 0.1% was then applied as the temperature was increased at a rate of 5 °C min^{-1}. A tan δ peak at 111 °C was observed in PMOS-0.38, indicative of the PMOS T_g and aligning with our DSC observations (Figure 2.17). No tan δ peak was observed for PDHF-0.31 from 120–170 °C, attributable to the low f_{HB} (Figure 2.18).

We next examined the thermal decomposition of our ABA copolymers using thermal gravimetric analysis. Both PMOS-PIBVE-PMOS and PDHF-PIBVE-PDHF containing polymers showed similar decomposition temperatures (T_ds, at 5%

weight loss) of 346 and 353 °C, respectively (Figure 2.19). These observed T_ds show remarkable thermal stability compared to other renewable TPEs such as polyesters (T_d = 260 °C) and TPEs derived from acrylates or terpenes (T_d ~ 300 °C).[7,45,46] Thermal decomposition of PMOS-PIBVE-PMOS and PDHF-PIBVE-PDHF also occurs well above their upper T_gs (105 and 126 °C), leading to a large melt-processing window.

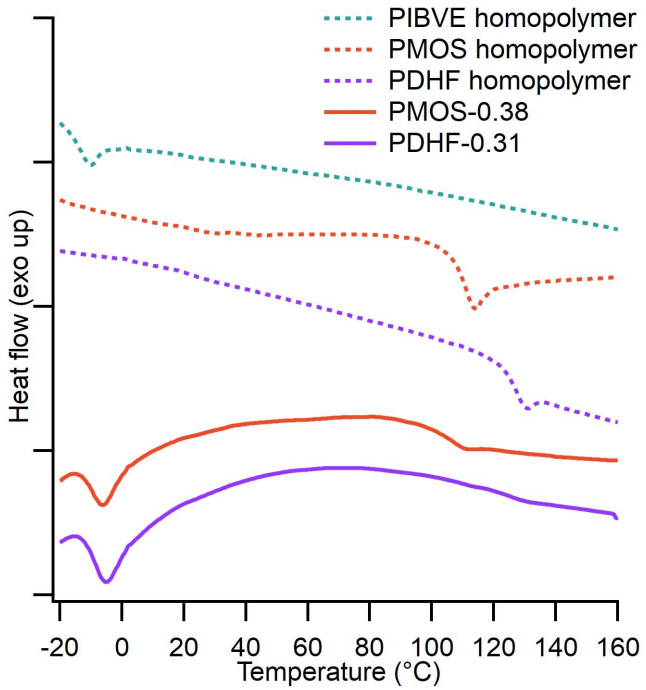

Figure 2.5: DSC reveals two T_gs for each ABA copolymer which were consistent with the respective homopolymer T_gs.

To characterize the performance of our ABA copolymers as TPEs, we investigated their material properties under tensile strain. The dogbone tensile bars were stretched to break at a strain rate of 0.07 s^{-1}. We first examined the tensile properties of copolymers containing PMOS end blocks (Figure 2.6a). Samples PMOS-0.21 and PMOS-0.23 exhibited moderate elongation-at-break

(ε_B); 405 ± 30% and 340 ± 50%, respectively. Notably, the stress-at-break (σ_B) for PMOS-0.23 (3.1 MPa) is twice as large as σ_B of PMOS-0.21 (1.4 MPa). For all samples, as f_{HB} increases we observe increased values of tensile strength and Young's modulus (E). The observed elongation is drastically reduced for PMOS-0.32 and PMOS-0.38 (126 ± 30% and 152 ± 9%, respectively). Whereas the increase in tensile strength and E is consistent with an increase in f_{HB}, the lower ε_B is consistent with the difference in morphological assignments, from PMOS-0.23 with a continuous phase of rubbery PIBVE (HEX), to PMOS-0.32 discontinuous LAM morphology.[3]

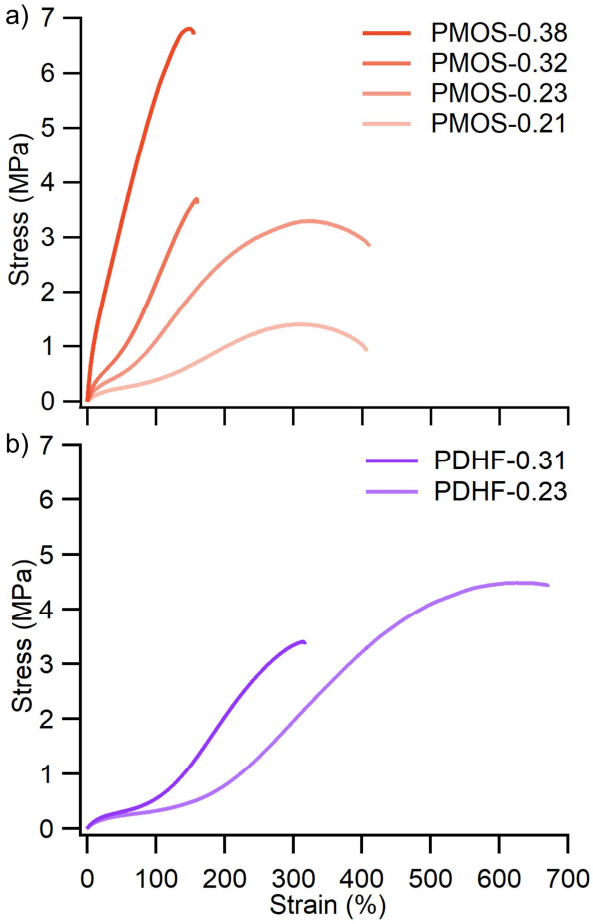

Figure 2.6: Representative stress-strain curves of (a) PMOS-PIBVE-PMOS and (b) PDHF-PIBVE-PDHF extended to break.

Polymers with PDHF end blocks were synthesized with f_{HB} of 0.23 and 0.31 to examine their elastic behavior. It was observed that both PDHF-0.23 and PDHF-0.31 displayed superior material properties compared to the PMOS samples, achieving higher ε_B and σ_B (Figure 2.6b). Remarkably, PDHF-0.23 had an observed ε_B of 570 ± 70%, higher than any previously reported PVE TPE.[19,20,39] In addition to increased elongation, PDHF-0.23 shows greater σ_B than PMOS-0.23; 4.3 ± 0.2 MPa compared to 3.1 ± 0.2 MPa, respectively.

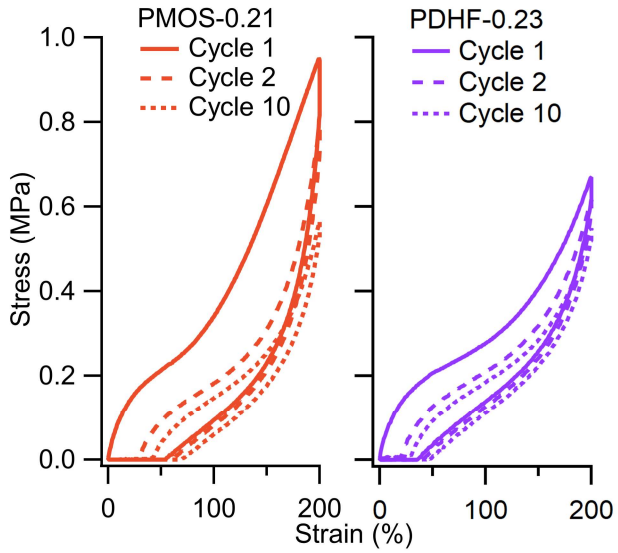

Figure 2.7: Cyclic loading and unloading of sustainable TPEs containing a) PMOS and b) PDHF end blocks.

A defining characteristic of TPEs is their reversable deformation, which we examined in our elastomeric (high ε_B) samples of PMOS-0.21 and PDHF-0.23 using cyclic tensile strains to 200% elongation (Figure 2.7). Hysteresis energy is described as the energy difference between the loading and unloading of a polymer and gives insight into the microstructural changes that occur under tension. Both samples show significant energy loss from cycle 1 to 2, but the hysteresis energy stays relatively consistent from cycle 2 to cycle 10. This is likely due initial breakup and reorientation of the glassy domains during the first cycle and the formation of a preferred microstructure and orientation that remains consistent for the remainder of the cycles.[47–50] PDHF-0.23 displayed lower hysteresis energy and less energy loss over 10 cycles when compared to PMOS-0.21. Over cycles 2-10, PMOS-0.21 shows a 24% reduction in toughness while PDHF only decreases 13%, where toughness is measured as the total area under

the loading curve. Lower energy loss observed for PDHF-0.23 compared to PMOS-0.21 indicates PDHF-PIBVE-PDHF copolymers retain more of their physical properties over repetitive cyclic loads, demonstrating greater recovery after deformation.

2.3.4 Green Metrics

Green metrics were evaluated for the synthesis of MOS and the polymerizations of ABA copolymers. Reported in Table 2.3 are the calculated isolated yields, atom economies (AEs), process mass intensities (PMI), and renewability index (RI). AE evaluates the percent molecular weight of the desired product compared to the molecular weight of all reactants.[51] For an account of all resources required in a process, the PMI was calculated as the mass of product divided by the mass of all reagents, solvents, and catalysts used in the reaction, workup, and purification.[52,53] We found that while our MOS synthesis provides a renewable route this monomer, it scored low in green metrics due to both steps being quite mass intense. AE was only 44% due to the mass loss from decarboxylation and the loss of iodine in the methylation. The PMI, was high as well, 33 kg kg^{-1}, above other reported PMIs for renewable monomers, such as itaconic acid derivatives.[54] While this synthesis is not well-optimized in relation to green metrics, it does demonstrate the ability to source MOS, a common monomer in cationic RAFT polymerizations, from biomass.

The polymerizations of PMOS-PIBVE-PMOS and PDHF-PIBVE-PDHF are both ideal in AE, at 100%. This combined with high isolated yields (>70%), highlights

the efficiency of our cationic polymerization in producing ABA copolymers. While the PMI for each polymerization is high (>900 kg kg^{-1}), this comes from the amount of methanol used to crash out the polymer for purification. However, the only byproducts left over are unreacted monomer, solvent, and ferrocene. The unreacted monomer and solvent can be removed under vacuum and, depending on the application of the polymer, the removal of ferrocene (0.07 wt%) would not be required, reducing the PMI by over 200% (<5 kg kg^{-1}).

2.4 Conclusions

We developed a new method for the synthesis of ABA copolymers from sustainable monomers as an avenue toward renewable TPEs. A sustainable, one pot synthetic protocol for MOS from *p*-coumaric acid, a renewable feedstock, was discovered, producing MOS in high yield (77%). Cationic RAFT initiated from a difunctional CTA was employed to first generate well-controlled telechelic PIBVE. Sequential addition of MOS or DHF afforded ABA copolymers of PMOS-PIBVE-PMOS and PDHF-PIBVE-PDHF, respectively. Polymer microphase separation was revealed with DSC and SAXS, the latter enabling assignment of morphology. TGA revealed thermal stability up to 346 °C with both PMOS and PDHF compositions. Tensile characterization revealed that while low f_{HB} polymers of both PDHF-PIBVE-PDHF and PMOS-PIBVE-PMOS behave as TPEs, PDHF-IBVE-PDHF possesses superior strength, elongation, and recovery. Specifically, PDHF-0.23 exhibited the highest elongation observed in a PVE TPE (570 ± 70%). This study demonstrates a significant advance in the cationic RAFT polymerization of vinyl

ethers, enabling the production of ABA copolymers with tensile properties well-suited for use as sustainable TPEs.

2.5 Conflicts of Interest

There are no conflicts to declare.

2.6 Acknowledgements

This material is based upon work supported by the National Science Foundation Graduate Research Fellowship Program under Grant No. DGE-1650441. Any opinions, findings, and conclusions or recommendations expressed in this material are those of the author(s) and do not necessarily reflect the views of the National Science Foundation. This work was supported by the National Science Foundation Center for Sustainable Polymers at the University of Minnesota, a Center for Chemical Innovation (CHE-1901635). This work made use of the Cornell Center for Materials Research Shared Facilities that are supported through the NSF MRSEC program (DMR- 1120296). This work made use of the NMR Facility at Cornell University that is supported, in part, by the NSF under the award number CHE-1531632. This work is based upon research conducted at the Materials Solutions Network at CHESS (MSN-C) which is supported by the Air Force Research Laboratory under award FA8650-19-2-5220.

2.7 Notes and References

(1) Ellen MacArthur Foundation. *The New Plastics Economy: Rethinking the Future of Plastics and Catalysing Action*; 2017.

(2) Drobny, J. G. Handbook of Thermoplastic Elastomers. In *Plastics Design*

Library; Drobny, J. G. B. T.-H. of T. E., Ed.; William Andrew Publishing: Norwich, NY, 2007; pp 1–8.

(3) Holden, G.; Kricheldorf, H. R.; Quirk, R. P. *Thermoplastic Elastomers*, 3rd ed.; Hanser, 2004.

(4) Zhu, Y.; Romain, C.; Williams, C. K. Sustainable Polymers from Renewable Resources. *Nature* **2016**, *540*, 354–362.

(5) Hillmyer, M. A.; Tolman, W. B. Aliphatic Polyester Block Polymers: Renewable, Degradable, and Sustainable. *Acc. Chem. Res.* **2014**, *47* (8), 2390–2396.

(6) Shin, J.; Lee, Y.; Tolman, W. B.; Hillmyer, M. A. Thermoplastic Elastomers Derived from Menthide and Tulipalin A. *Biomacromolecules* **2012**, *13* (11), 3833–3840.

(7) Watts, A.; Kurokawa, N.; Hillmyer, M. A. Strong, Resilient, and Sustainable Aliphatic Polyester Thermoplastic Elastomers. *Biomacromolecules* **2017**, *18*, 1845–1854.

(8) Watts, A.; Hillmyer, M. A. Aliphatic Polyester Thermoplastic Elastomers Containing Hydrogen-Bonding Ureidopyrimidinone Endgroups. *Biomacromolecules* **2019**, *20* (7), 2598–2609.

(9) Uchiyama, M.; Satoh, K.; Kamigaito, M. Cationic RAFT Polymerization Using Ppm Concentrations of Organic Acid. *Angew. Chemie Int. Ed.* **2015**, *54* (6), 1924–1928.

(10) Kottisch, V.; Supej, M. J.; Fors, B. P. Enhancing Temporal Control and

Enabling Chain-End Modification in Photoregulated Cationic Polymerizations by Using Iridium-Based Catalysts. *Angew. Chemie Int. Ed.* **2018**, *57* (27), 8260–8264.

(11) Kottisch, V.; Michaudel, Q.; Fors, B. P. Photocontrolled Interconversion of Cationic and Radical Polymerizations. *J. Am. Chem. Soc.* **2017**, *139* (31), 10665–10668.

(12) Kottisch, V.; Michaudel, Q.; Fors, B. P. Cationic Polymerization of Vinyl Ethers Controlled by Visible Light. *J. Am. Chem. Soc.* **2016**, *138* (48), 15535–15538.

(13) Michaudel, Q.; Chauviré, T.; Kottisch, V.; Supej, M. J.; Stawiasz, K. J.; Shen, L.; Zipfel, W. R.; Abruña, H. D.; Freed, J. H.; Fors, B. P. Mechanistic Insight into the Photocontrolled Cationic Polymerization of Vinyl Ethers. *J. Am. Chem. Soc.* **2017**, *139* (43), 15530–15538.

(14) Peterson, B. M.; Lin, S.; Fors, B. P. Electrochemically Controlled Cationic Polymerization of Vinyl Ethers. *J. Am. Chem. Soc.* **2018**, *140* (6), 2076–2079.

(15) Supej, M. J.; Peterson, B. M.; Fors, B. P. Dual Stimuli Switching: Interconverting Cationic and Radical Polymerizations with Electricity and Light. *Chem* **2020**, *6* (7), 1794–1803.

(16) Peterson, B. M.; Kottisch, V.; Supej, M. J.; Fors, B. P. On Demand Switching of Polymerization Mechanism and Monomer Selectivity with Orthogonal Stimuli. *ACS Cent. Sci.* **2018**, *4* (9), 1228–1234.

(17) Matake, R.; Adachi, Y.; Matsubara, H. Synthesis of Vinyl Ethers of Alcohols

Using Calcium Carbide under Superbasic Catalytic Conditions (KOH/DMSO). *Green Chem.* **2016**, *18* (9), 2614–2618.

(18) Hashimoto, T.; Namikoshi, T.; Irie, S.; Urushisaki, M.; Sakaguchi, T.; Nemoto, T.; Isoda, S. Synthesis and Microphase-Separated Structure of Poly(Tricyclodecyl Vinyl Ether)-Block-Poly(n-Butyl Vinyl Ether)-Block-Poly(Tricyclodecyl Vinyl Ether): New Triblock Copolymer as Thermoplastic Elastomer Composed Solely of Poly(Vinyl Ether) Backbones. *J. Polym. Sci. Part A Polym. Chem.* **2008**, *46* (5), 1902–1906.

(19) Imaeda, T.; Hashimoto, T.; Irie, S.; Urushisaki, M.; Sakaguchi, T. Synthesis of ABA-Triblock and Star-Diblock Copolymers with Poly(2-Adamantyl Vinyl Ether) and Poly(n-Butyl Vinyl Ether) Segments: New Thermoplastic Elastomers Composed Solely of Poly(Vinyl Ether) Backbones. *J. Polym. Sci. Part A Polym. Chem.* **2013**, *51* (8), 1796–1807.

(20) Hashimoto, T.; Imaeda, T.; Irie, S.; Urushisaki, M.; Sakaguchi, T. Synthesis of Poly(Vinyl Ether)-Based, ABA Triblock-Type Thermoplastic Elastomers with Functionalized Soft Segments and Their Gas Permeability. *J. Polym. Sci. Part A Polym. Chem.* **2015**, *53* (9), 1114–1124.

(21) Kim, J.-B.; Cho, I. Synthesis and Cationic Polymerization of Substituted 2,3-Dihydrofurans. *J. Polym. Sci. Part A Polym. Chem.* **1989**, *27* (11), 3733–3744.

(22) Ogawa, Y.; Sawamoto, M.; Higashimura, T. Living Cationic Polymerization of Cyclic Unsaturated Ethers. *Polym. J.* **1984**, *16* (5), 415–422.

(23) Sanda, F.; Matsumoto, M. Cationic Polymerization of 2,3-Dihydrofuran.

Study on the Relationship between Glass Transition Temperature and Tacticity of the Polymer. *Macromolecules* **1995**, *28* (20), 6911–6914.

(24) Nuyken, O.; Braun, H. 2,3-Dihydrofuran: A Special Vinyl Ether for Cationic Photopolymerization. In *Photoinitiated Polymerization*; ACS Symposium Series; American Chemical Society, 2003; Vol. 847, pp 18–213.

(25) Sanda, F.; Matsumoto, M. Degradation Behavior of Poly(2,3-Dihydrofuran). *J. Appl. Polym. Sci.* **1996**, *59* (2), 295–299.

(26) Stonkus, V.; Edolfa, K.; Leite, L.; Sobczak, J. W.; Plyasova, L.; Petrova, P. Palladium-Promoted Co–SiO2 Catalysts for 1,4-Butanediol Cyclization. *Appl. Catal. A Gen.* **2009**, *362* (1), 147–154.

(27) Ludmila, L.; Stonkus, V.; Edolfa, K.; Ilieva, L.; Plyasova, L.; Zaikovskii, V. Copper-Promoted Cobalt Catalysts for 2,3-Dihydrofuran Synthesis. *Appl. Catal. A Gen.* **2006**, *311*, 86–93.

(28) Higashimura, T.; Mitsuhashi, M.; Sawamoto, M. Synthesis of P-Methoxystyrene-Isobutyl Vinyl Ether Block Copolymers by Living Cationic Polymerization with Iodine. *Macromolecules* **1979**, *12* (2), 178–182.

(29) Li, M.; Jia, Z.; Wan, G.; Wang, S.; Min, D. Enhancing Isolation of P-Coumaric and Ferulic Acids from Sugarcane Bagasse by Sequential Hydrolysis. *Chem. Pap.* **2020**, *74* (2), 499–507.

(30) Ou, S. Y.; Luo, Y. L.; Huang, C. H.; Jackson, M. Production of Coumaric Acid from Sugarcane Bagasse. *Innov. Food Sci. Emerg. Technol.* **2009**, *10* (2), 253–259.

(31) Heublein, G.; Spange, S.; Sawamoto, M.; Higashimura, T. Cationic Polymerization of P-Methoxystyrene by the Triphenylmethyl Bromide/Iodine Initiating System: Formation of Long-Lived Polymers in Polar Solvent. *Polym. J.* **1985**, *17* (10), 1085–1090.

(32) Sugihara, S.; Okubo, S.; Maeda, Y. Metal-Free RAFT Cationic Polymerization of p-Methoxystyrene with HCl·Et2O Using a Xanthate-Type RAFT Cationogen. *Polym. Chem.* **2016**, *7* (44), 6854–6863.

(33) Perkowski, A. J.; You, W.; Nicewicz, D. A. Visible Light Photoinitiated Metal-Free Living Cationic Polymerization of 4-Methoxystyrene. *J. Am. Chem. Soc.* **2015**, *137* (24), 7580–7583.

(34) Kanazawa, A.; Shibutani, S.; Yoshinari, N.; Konno, T.; Kanaoka, S.; Aoshima, S. Structure Effects of Lewis Acids on the Living Cationic Polymerization of P-Methoxystyrene: Distinct Difference in Polymerization Behavior from Vinyl Ethers. *Macromolecules* **2012**, *45* (19), 7749–7757.

(35) Takeshima, H.; Satoh, K.; Kamigaito, M. Bio-Based Functional Styrene Monomers Derived from Naturally Occurring Ferulic Acid for Poly(Vinylcatechol) and Poly(Vinylguaiacol) via Controlled Radical Polymerization. *Macromolecules* **2017**, *50* (11), 4206–4216.

(36) Takeshima, H.; Satoh, K.; Kamigaito, M. Bio-Based Vinylphenol Family: Synthesis via Decarboxylation of Naturally Occurring Cinnamic Acids and Living Radical Polymerization for Functionalized Polystyrenes. *J. Polym. Sci.* **2020**, *58* (1), 91–100.

(37) Cohen, L. A.; Jones, W. M. A Study of PH Dependence in the Decarboxylation of P-Hydroxycinnamic Acid. *J. Am. Chem. Soc.* **1960**, *82* (8), 1907–1911.

(38) Nomura, E.; Hosoda, A.; Mori, H.; Taniguchi, H. Rapid Base-Catalyzed Decarboxylation and Amide-Forming Reaction of Substituted Cinnamic Acids via Microwave Heating. *Green Chem.* **2005**, *7* (12), 863–866.

(39) Mizuno, N.; Satoh, K.; Kamigaito, M.; Okamoto, Y. Living Cationic Polymerization of a Novel Bicyclic Conjugated Diene Monomer, Tetrahydroindene, and Its Block Copolymers with Vinyl Ether. *Macromolecules* **2006**, *39* (16), 5280–5285.

(40) Quan, X.; Gancarz, I.; Koberstein, J. T.; Wignall, G. D. Effect of Homopolymer Molecular Weight on the Morphology of Block Copolymer/Homopolymer Blends. *Macromolecules* **1987**, *20* (6), 1431–1434.

(41) Kimishima, K.; Hashimoto, T.; Han, C. D. Spatial Distribution of Added Homopolymer within the Microdomains of a Mixture Consisting of an ABA-Type Triblock Copolymer and a Homopolymer. *Macromolecules* **1995**, *28* (11), 3842–3853.

(42) Perrier, S. 50th Anniversary Perspective: RAFT Polymerization—A User Guide. *Macromolecules* **2017**, *50* (19), 7433–7447.

(43) Matsen, M. W.; Thompson, R. B. Equilibrium Behavior of Symmetric ABA Triblock Copolymer Melts. *J. Chem. Phys.* **1999**, *111* (15), 7139–7146.

(44) Holden, G.; Bishop, E. T.; Legge, N. R. Thermoplastic Elastomers. *J. Polym. Sci. Part C Polym. Symp.* **1969**, *26* (1), 37–57.

(45) Shin, J.; Lee, Y.; Tolman, W. B.; Hillmyer, M. A. Thermoplastic Elastomers Derived from Menthide and Tulipalin A. *Biomacromolecules* **2012**, *13*, 3833–3840.

(46) Bolton, J. M.; Hillmyer, M. A.; Hoye, T. R. Sustainable Thermoplastic Elastomers from Terpene-Derived Monomers. *ACS Macro Lett.* **2014**, *3* (8), 717–720.

(47) Pakula, T.; Saijo, K.; Kawai, H.; Hashimoto, T. Deformation Behavior of Styrene-Butadiene-Styrene Triblock Copolymer with Cylindrical Morphology. *Macromolecules* **1985**, *18* (6), 1294–1302.

(48) Honeker, C. C.; Thomas, E. L.; Albalak, R. J.; Hajduk, D. A.; Gruner, S. M.; Capel, M. C. Perpendicular Deformation of a Near-Single-Crystal Triblock Copolymer with a Cylindrical Morphology. 1. Synchrotron SAXS. *Macromolecules* **2000**, *33* (25), 9395–9406.

(49) Frick, E. M.; Zalusky, A. S.; Hillmyer, M. A. Characterization of Polylactide-b-Polyisoprene-b-Polylactide Thermoplastic Elastomers. *Biomacromolecules* **2003**, *4* (2), 216–223.

(50) Beecher, J. F.; Marker, L.; Bradford, R. D.; Aggarwal, S. L. Morphology and Mechanical Behavior of Block Polymers. *J. Polym. Sci. Part C Polym. Symp.* **1969**, *26* (1), 117–134.

(51) Tobiszewski, M.; Marć, M.; Gałuszka, A.; Namieśnik, J. Green Chemistry Metrics with Special Reference to Green Analytical Chemistry. *Molecules* **2015**, *20* (6), 10928–10946.

(52) Jimenez-Gonzalez, C.; Ponder, C. S.; Broxterman, Q. B.; Manley, J. B. Using the Right Green Yardstick: Why Process Mass Intensity Is Used in the Pharmaceutical Industry To Drive More Sustainable Processes. *Org. Process Res. Dev.* **2011**, *15* (4), 912–917.

(53) Jiménez-González, C.; Constable, D. J. C.; Ponder, C. S. Evaluating the "Greenness" of Chemical Processes and Products in the Pharmaceutical Industry—a Green Metrics Primer. *Chem. Soc. Rev.* **2012**, *41* (4), 1485–1498.

(54) Trotta, J.; Watts, A.; Wong, A.; LaPointe, A. M.; Hillmyer, M. A.; Fors, B. P. Renewable Thermosets and Thermoplastics from Itaconic Acid. *ACS Sustain. Chem. Eng.* **2019**, *7*, 2691–2701.

2.8 Experimental Section

2.8.1 Materials

Isobutyl vinyl ether (IBVE) (99%, TCI), 1,4-butanediol divinyl ether (98%, Millipore Sigma), *p*-methoxystyrene (MOS) (from synthesis or purchased; 98%, TCI) and 2,3-dihydrofuran (DHF) (99%, TCI) were dried over calcium hydride (CaH_2) (ACROS organics, 93% extra pure, 0–2 mm grain size) for 12 hours, distilled under vacuum, and degassed by three freeze-pump-thaw cycles. Ferrocenium tetrafluoroborate ($FcBF_4$) (97%, Millipore Sigma), HCl in Et_2O (2.0 M, Millipore Sigma), *p*-coumaric acid (98%, TCI), butylated hydroxytoluene (BHT) (99%, Millipore Sigma), triethylamine (anhydrous, 99.5%, Millipore Sigma), potassium carbonate (anhydrous, 99%, Millipore Sigma), and methyl iodide (98%, Alfa Aesar) were used as received. Sodium N,N-diethyldithiocarbamate trihydrate (98%, Alfa Aesar) was azeotropically dried with benzene. Dichloromethane (DCM), diethylether (Et_2O), and toluene were purchased from J.T. Baker and were purified by purging with argon for 1 hour, followed by passing through two packed columns of neutral alumina under argon pressure. Hexanes and ethyl acetate were purchased from Fischer scientific and used as received.

2.8.2 General Measurements

All polymer samples were analyzed using a Tosoh EcoSec HLC 8320 GPC system with two SuperHM-M columns in series at a flow rate of 0.350 mL/min. THF was used as the eluent and number-average molecular weights (M_n), weight-average molecular weights (M_w), and dispersities ($Đ$) for PIBVE were determined

by light scattering using a Wyatt miniDawn Treos multi-angle light scattering detector and a calculated dn/dc value of 0.0381 mL g^{-1}. The reported M_ns for triblock copolymers were calculated from refractive index chromatograms against TSKgel polystyrene standards. Nuclear magnetic resonance (NMR) spectra were recorded on a Varian 400 MHz, a Varian 600 MHz, or a Bruker 500 MHz instrument.

2.8.3 Synthesis of *p*-methoxystyrene

p-Coumaric acid (25g, 0.15 mol) and BHT (150 mg, 0.5 wt%) were added to an oven dried flask equipped with a reflux condenser and were dissolved in 70 mL of DMF under nitrogen. Triethylamine (43 mL, 0.31 mol) was added and the reaction mixture was heated to 100 °C and stirred for 6 hours. Triethylamine was then removed *via* rotary evaporation and K_2CO_3 (21g, 0.15 mol) was added, followed by addition of methyl iodide (12.2 mL, 0.20 mol). The reaction mixture was heated to 40 °C and stirred overnight. The reaction was quenched with NaOH (15 mL, 3M) and diluted with H_2O (80 mL). The organic layer was separated, and the aqueous layer extracted with ethyl acetate (3 x 20 mL). The combined organic layers were then washed with H_2O (10 x 20mL), followed by brine, then dried over $MgSO_4$ before being filtered and concentrated in vacuo to yield a dark brown liquid. Fractional distillation at 60 °C under ~300 mtorr vacuum gave a 44 °C vapor that condensed to yield 15.7g (77% yield) of clear, colorless *p*-methoxystyrene. This was dried over CaH_2 and distilled again before use. ^1H and ^{13}C NMR were consistent with previous literature reports.[1]

^{1}H NMR (500 MHz, $CDCl_3$, δ, ppm): 7.36 (m, 2H), 6.87 (m,2H), 6.68 (dd, *J* = 17.6, 10.9 Hz, 1H), 5.62 (d, *J* = 17.6 Hz, 1H), 5.14 (d, *J* = 10.7 Hz, 1H), 3.82 (s, 3H). ^{13}C NMR (126 MHz, $CDCl_3$, δ, ppm) 159.52, 136.37, 130.59, 127.52, 114.05, 111.71, 55.43.

2.8.4 Synthesis of difunctional CTA

1,4-butanediol divinyl ether (0.64 mL, 4 mmol) was added dropwise to a flame-dried flask containing a stirring solution of HCl in diethyl ether (4.4 mL, 8.8 mmol) cooled to −78 °C under nitrogen. This solution was warmed to 0 °C and stirred for 2 hours to produce the chloroether adduct of the oxocabenium ion. In a separate flame-dried flask, sodium *N,N*-diethyl dithiocarbamate (2.1 g, 12 mmol) was dissolved in Et_2O (11 mL) and cooled to 0 °C under nitrogen. The chloroether solution was then added dropwise to the *N,N*-diethyl dithiocarbamate solution over 10 min. The reaction mixture was stirred at 0 °C for 2 hours before being warmed to room temperature and stirred an additional 3 hours. The reaction mixture was then diluted with sat. sodium bicarbonate and extracted with Et_2O (3 x 10 mL). The combined organic layers were then washed with brine and dried over $MgSO_4$ before being filtered and concentrated *via* rotary evaporation. The crude product was a dark red to yellow viscus oil. The product was purified by column chromatography using SiO_2 treated with 3% NEt_3 in hexanes. The column of treated SiO_2 was washed with 200 mL of the mobile phase (14% EtOAc in hexanes) before loading the crude oil. 666 mg (38% yield) of the pale-yellow product was isolated (r.f. = 0.33 in 14% EtOAc in hexanes).

^{1}H NMR (500 MHz, $CDCl_3$, δ, ppm): 5.90 (q, *J* = 6.3 Hz, 2H), 4.02 (q, *J* = 7.1 Hz, 4H), 3.82 – 3.67 (m, 6H), 3.62 – 3.52 (m, 2H), 1.72 (d, *J* = 6.2 Hz, 6H), 1.63 (hept, *J* = 2.5 Hz, 4H), 1.28 (dt, *J* = 9.4, 7.1 Hz, 12H). ^{13}C NMR (125 MHz, $CDCl_3$, δ, ppm): 195.00, 91.38, 91.36, 69.11, 69.06, 48.98, 46.99, 29.97, 26.33, 26.30, 23.61, 12.74, 11.79. ESI-MS (DART): [C18H36N2O2S4+Na^+] calc.: 463.15518, obs.: 463.15491.

2.8.5 Polymerization of PMOS-PIBVE-PMOS

All polymerizations were set up in a nitrogen glovebox. A solution of difunctional CTA in DCM (0.60 mL, 22 mg/mL, 0.03 mmol) and IBVE (2.60 mL, 20 mmol) were added to a 20 mL scintillation vial containing a stir bar. The polymerization was initiated by addition of $FcBF_4$ in DCM (1.1 mL, 1 mg/mL, 0.02 mol% relative to CTA) and the reaction mixture was stirred until IBVE reached >95% conversion by NMR, typically 6 hours. The solution was then diluted with DCM before adding *p*-methoxystyrene and additional $FcBF_4$ (1.1 mL, 1mg/mL, 0.02 mol% relative to CTA) to achieve a total volume of 9 mL. This mixture was then stirred for 20 hours, or until *p*-methoxystyrene conversion reached ~60% conversion. The polymerization was then terminated with sodium *N,N*-diethyl dithiocarbamate (2 equiv relative to CTA) and diluted with DCM. The polymer was precipitated in 1.5 L of stirring MeOH twice before vacuum drying at 80 °C for 48 hours. f_{HB} was calculated from integration of peaks 6.89 – 6.18 and 0.90 ppm in accordance with Equation S1 and S2. ^{1}H NMR (500 MHz, $CDCl_3$, δ, ppm): 6.89 – 6.18 (m, 4H PMOS), 3.84 – 3.66 (m, 3H PMOS), 3.66 – 3.33 (m, 1H PIBVE), 3.33 –

3.03 (m, 2H PIBVE), 2.06 – 1.10 (m, 2H PIBVE, 3H PMOS), 0.90 (m, 6H PIBVE).

Equation S1:

$$x_{PMOS} = \frac{\frac{1}{4} i(6.89 - 6.18\, ppm, PMOS)}{\frac{1}{4} i(6.89 - 6.18\, ppm, PMOS) + \frac{1}{6} i(0.90\, ppm, PIBVE)}$$

Equation S2:

$$f_{HB} = \frac{x_{PMOS} \frac{mw_{MOS}}{\rho_{PMOS}}}{\left[x_{PMOS} \frac{mw_{MOS}}{\rho_{PMOS}} + (1 - x_{PMOS}) \frac{mw_{IBVE}}{\rho_{PIBVE}}\right]}$$

Where x_{PMOS} is the mole fraction of PMOS, mw_{MOS} is the molecular weight of MOS (134.18 g/mol), ρ_{PMOS} is the density of PMOS (0.962 g/mL), mw_{IBVE} is the molecular weight of IBVE (100.16 g/mol), and ρ_{PIBVE} is the density of PIBVE (0.920 g/mL).

2.8.6 Polymerization of PDHF-PIBVE-PDHF

All polymerizations were set up in a nitrogen glovebox. A solution of difunctional CTA in DCM (0.60 mL, 22 mg/mL, 0.03 mmol) and IBVE (2.60 mL, 20 mmol) were added to a 20 mL scintillation vial containing a stir bar. The polymerization was initiated by addition of $FcBF_4$ in DCM (1.1 mL, 1 mg/mL, 0.02 mol% relative to CTA) and the reaction mixture was stirred until IBVE reached >95% conversion by NMR, typically 6 hours. The solution was then diluted with DCM before adding DHF and additional $FcBF_4$ (1.1 mL, 1mg/mL, 0.02 mol% relative to CTA) to achieve a total volume of 8 mL. This was then stirred for an

additional 20 hours, or until full conversion of DHF was reached. The polymerization was then terminated with sodium *N,N*-diethyl dithiocarbamate (2 equiv relative to CTA) and diluted with DCM. The polymer was precipitated in MeOH twice before vacuum drying at 80 °C for 48 hours. f_{HB} was calculated from integration of peaks 4.21 – 2.93 and 0.90 ppm in accordance with Equation S3 and S4. ^{1}H NMR (500 MHz, $CDCl_3$, δ, ppm): 4.21 – 2.93 (m, 3H PDHF, 3H PIBVE), 2.49 – 1.30 (m, 3H PDHF, 3H PIBVE), 0.90 (m, 6H PIBVE).

Equation S3:

$$x_{PDHF} = \frac{i(4.21 - 2.93\ ppm, PIBVE\ and\ PDHF) - \frac{1}{2} i(0.90\ ppm, PIBVE)}{i(4.21 - 2.93\ ppm, PIBVE\ and\ PDHF)}$$

Equation S4:

$$f_{HB} = \frac{x_{PDHF} \frac{mw_{DHF}}{\rho_{PDHF}}}{\left[x_{PDHF} \frac{mw_{DHF}}{\rho_{PDHF}} + (1 - x_{PDHF}) \frac{mw_{IBVE}}{\rho_{PIBVE}}\right]}$$

Where x_{PMOS} is the mole fraction of PDHF, mw_{DHF} is the molecular weight of DHF (70.09 g/mol), ρ_{PDHF} is the density of PDHF (1.04 g/mL), mw_{IBVE} is the molecular weight of IBVE (100.16 g/mol), and ρ_{PIBVE} is the density of PIBVE (0.920 g/mL).

2.9 Material Characterization

Triblock copolymers were pressed into dog-bone-shaped tensile bars using a 4120 Hydraulic Unit Carver heated press. The polymer samples were placed in the mold between two sheets of PTFE protective lining. PMOS-PIBVE-PMOS samples were pressed at 120 °C and 3,000 psi for 1 min. PDHF-PIBVE-PDHF

samples were pressed at 160 °C and 3,000 psi for 1 min. The press was water cooled to room temperature before releasing pressure. Excess material was trimmed away with scissors to obtain dog-bone-shaped tensile bars with approximate gauge dimensions of 16 x 2.5 x 0.7 mm.

Tensile properties of the prepared samples were examined using a Zwick/Roell Z010 testing system equipped with pneumatic grips. Samples were stretched to break at an extension rate of 75 mm min^{-1}. Values reported are an average calculated from three samples. To study the hysteresis behavior of select elastic polymers, a cyclic loading of 300% strain at 50 mm min^{-1} was applied for 10 cycles.

For determination of thermal transitions, differential scanning calorimetry (DSC) was performed using a TA Instruments Q1000. Samples were placed in aluminum crucibles and heated to 200 °C at 20 °C min^{-1} to erase thermal history, cooled to −70 °C and held at this temperature for 10 min to equilibrate. A second heat cycle was performed to 200 °C at 20 °C min^{-1} during which the thermal data was collected. Thermogravimetric analysis (TGA) was performed using a TA Instruments Q500 where samples were heated at a rate of 20 °C min^{-1} from 25 °C to 500 °C.

Rheological tests were performed on a TA Instruments DHR3 rheometer using an 8mm parallel plate in a temperature controlled environmental test chamber under a nitrogen atmosphere. The sample was loaded onto the bottom parallel plate at 170°C and the top plate was lowered to a trim gap of 1050µm. Excess

polymer material was trimmed and then the plate was lowered to a gap of 1000μm. Strain sweeps (0.1–100%) at 170°C were first performed at 6.3 rad/s (1 Hz) to determine the linear viscoelastic region. A 1% strain was selected as it consistently lied within the linear viscoelastic region for the preceding range of frequencies. Before each frequency sweep, the sample was equilibrated at 170 °C for 5 min to ensure uniform sample temperature.

All small-angle X-ray scattering (SAXS) experiments were carried out at the Functional Materials Beamline (FMB) at the Cornell High Energy Synchrotron Source (CHESS). To prepare samples for SAXS, polymers were pressed into the center of stainless-steel washers (4.42 mm I.D., 9.53 mm O.D., 0.79 mm thickness) using a heated press. PMOS-PIBVE-PMOS samples were pressed under 3,000 psi of pressure at 120 °C for 1 min and PDHF-PIBVE-PDHF samples were pressed under 3,000 psi of pressure at 160 °C for 1 min. The washers were sealed between Kapton tape and annealed under vacuum at 140 °C for 48 h, followed by cooling to room temperature under vacuum. The Kapton tape-sealed washers containing the annealed samples were mounted directly onto the sample stage at CHESS for SAXS data acquisition. The X-ray energy of 15.89 keV was selected using a diamond (220) side bounce monochromator[2], and the beam size (0.3 x 0.3 mm^2, ca. 1 m upstream from the sample) was set using slits. SAXS data were collected using a Pilatus 300K detector (pixel size of 0.172 x 0.172 mm^2) positioned approximately 240 cm downstream of the sample. The SAXS flight path was helium-filled, and a beamstop photodiode was used to monitor transmitted

intensity. SAXS data were collected using a 3 s exposure time. Acquired 2D SAXS data was reduced using the Nika and Irena macros[3,4] in Igor Pro 7 (WaveMetrics, Inc.). 1D data was generated from azimuthal integration of the 2D data using silver behenate as the calibration standard. Following this data reduction, intensities were normalized by the diode count, and from this was subtracted the diode count-normalized background intensity. Polymer morphology was determined from the ratios of scattering peaks relative to the principal scattering peak.

2.9.1 Conversion and Molecular Weight Data for Synthesis of PMOS-PIBVE-PMOS

Table 2.2: Data collected during the synthesis of PMOS-PIBVE-PMOS.

Entry	Reaction time (h)	IBVE conv. (%)	MOS conv. (%)	M_n^{theo} (kg/mol)	M_n^{RI} (kg/mol)	$Đ$ [d]	M_n^{LS} (kg/mol)	M_n ABA [e] (kg/mol)
0	0	0	0	0	0	-	0	-
1 [a]	0.17	9	0	5.8	-	-	-	-
2 [a]	0.55	9	0	5.8	1.4	1.4	-	-
3	0.7	23	0	14.8	10.2	1.53	21.1	-
4	0.93	52	0	33.5	24.8	1.36	32.6	-
5	1.07	62	0	40.4	32.2	1.33	41.1	-
6	1.5	92	0	59.2	42.8	1.28	58.6	-
7 [b, c]	2	100	0	64.6	45.7	1.33	59.2	-
8	3	96	0	66.1	46.9	1.33	63.8	63.8
9	4.63	100	6	66.5	48.8	1.31	-	65.7
10	6.05	100	11	68	50.9	1.27	-	67.8
11	8.05	100	20	70.8	53.1	1.23	-	70
12	20.7	100	64	84.4	63.6	1.19	-	80.5
13	25.83	100	77	88.4	63.9	1.18	-	80.8
14	27.77	100	80	89.3	63.1	1.19	-	80
15	32.3	100	83	90.2	66.5	1.19	-	83.4
16	46.07	100	89	92.1	66.4	1.18	-	83.3
17	64.9	100	91	92.7	68	1.18	-	84.9

[a] No light scattering data available, not included in plot (Figure 1.4). [b] ^{1}H NMR showed no IBVE, however, due to IBVE being present in entry 8 ^{1}H NMR, it was assumed the IBVE must have evaporated from this sample and it was not included in the plot (Figure 1.4). [c] MOS was added after 2 hours, just after entry 7. [d] $Đ$ was determined from the SEC trace. [e] M_n was calculated as shown in Equation S5.

Equation S5:

$$M_{\mathrm{n}}\ \mathrm{ABA} = M_{\mathrm{n}}^{\mathrm{RI}} Entry\ n - M_{\mathrm{n}}^{\mathrm{RI}}\ Entry\ 8 + M_{\mathrm{n}}^{\mathrm{LS}}\ Entry\ 8$$

The PMOS homopolymer peak in the GPC prevented proper determination of the refractive index increment (dn/dc) and thus the M_ns reported for the ABA copolymers are calculated from refractive index traces in SEC to polystyrene standards as illustrated in Figure 2.9.

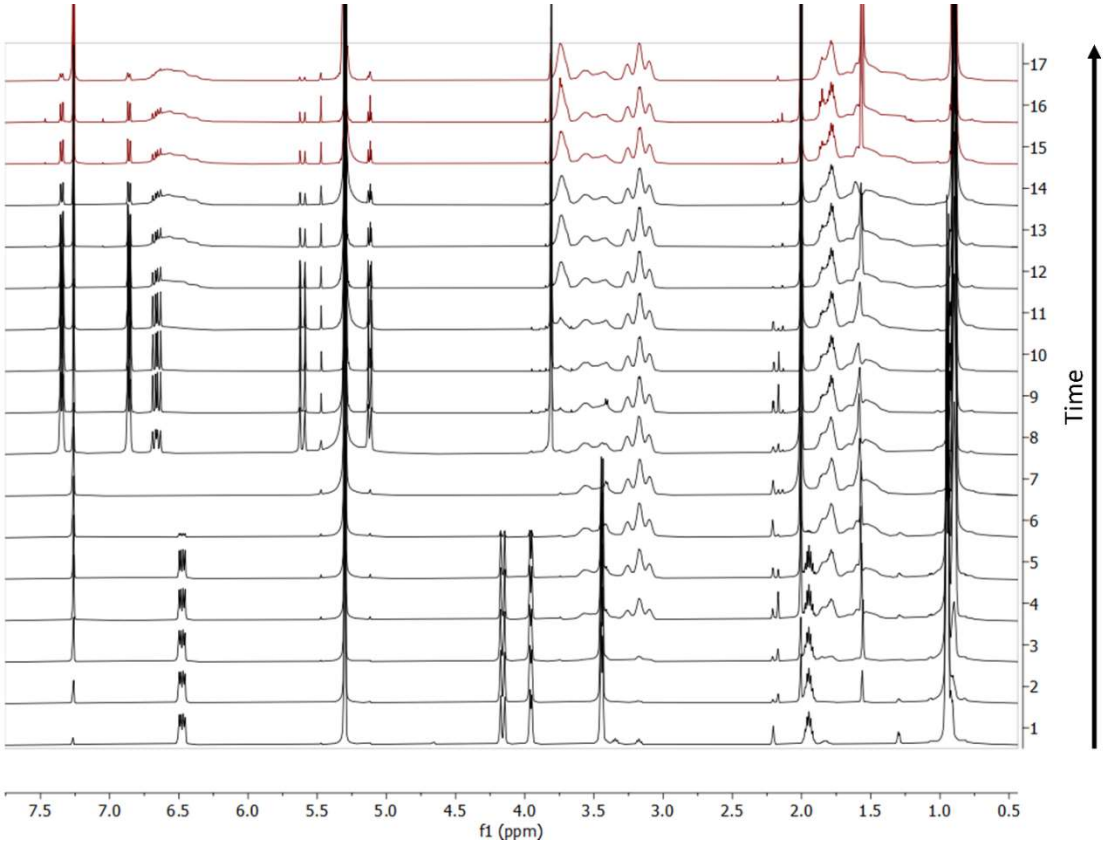

Figure 2.8: Quantitative 1H NMR in CDCl3 of aliquots from PMOS-PIBVE-PMOS reaction over time, reported in Table S1.

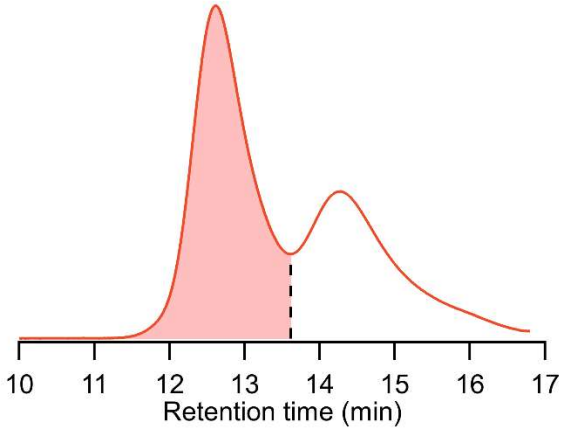

2.9.2 Material Characterization

Figure 2.9: SEC trace of PMOS-PIBVE-PMOS illustrating how the peak for ABA copolymers were selected for M_n and $Đ$ calculations against polystyrene standards.

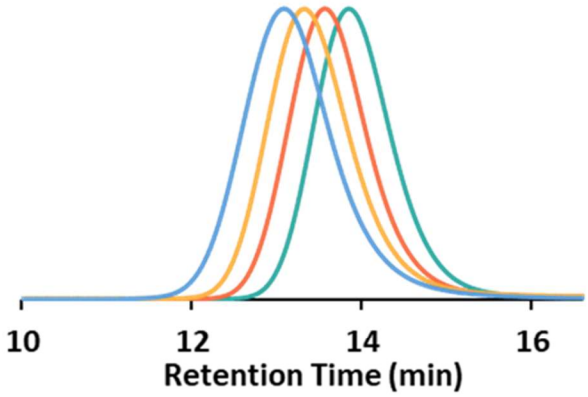

Entry	[IBVE]/ [CTA]	NMR Conv.	M_n (theo) (kg/mol)	M_n (exp) (kg/mol)	$Đ$
1	200	100%	20	23	1.32
2	300	100%	30	33	1.28
3	400	100%	40	41	1.25
4	500	100%	50	53	1.34

Figure 2.10: Polymerizations of telechelic PIBVE from a difunctional CTA.

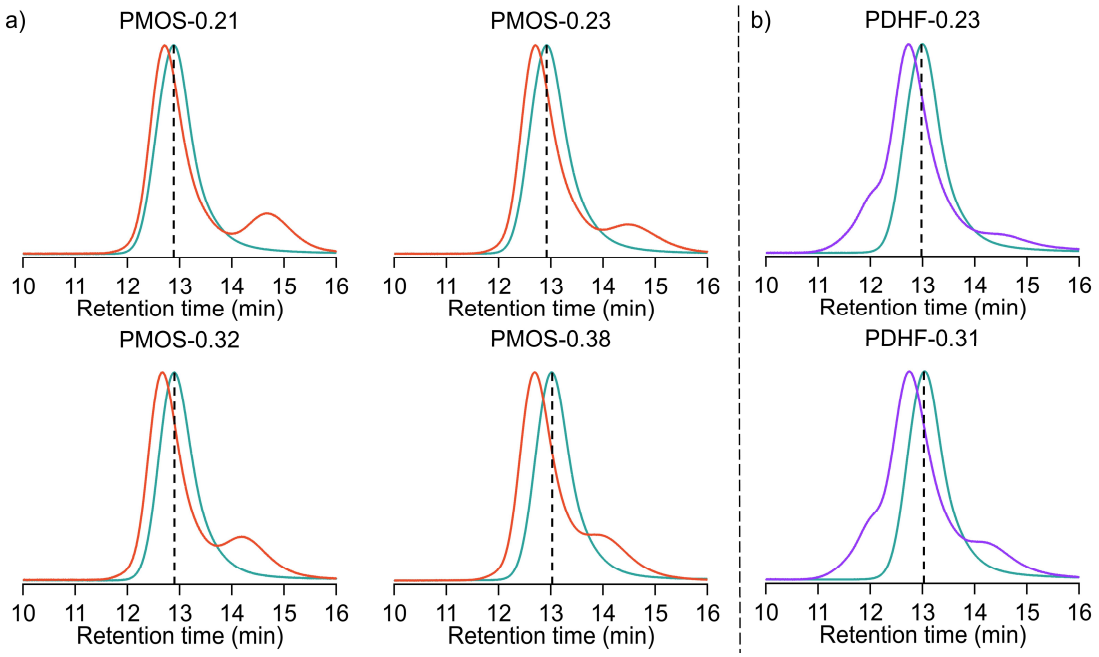

Figure 2.11: SEC traces of a) PMOS-PIBVE-PMOS (red) and b) PDHF-PIBVE-PDHF (blue) copolymers showing the chain extension from telechelic PIBVE (teal).

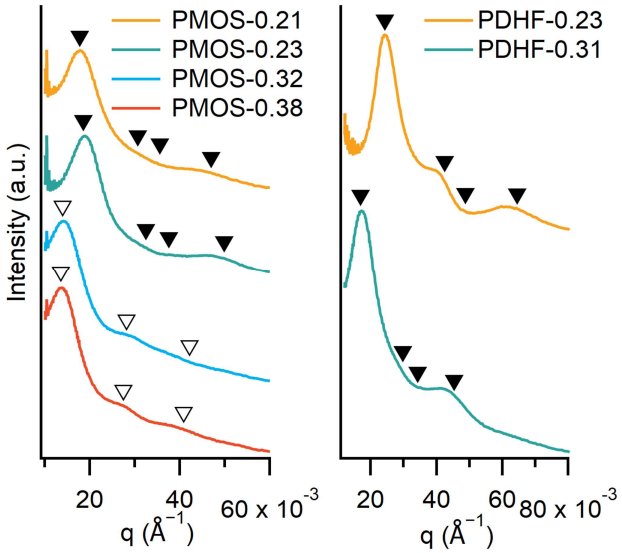

Figure 2.12: SAXS data obtained for each polymer sample. Braggs reflections for hexagonally packed cylinders (filled triangles) and lamellar (open triangles) morphologies are indicated, relative the first indicated peak, defined as q*.

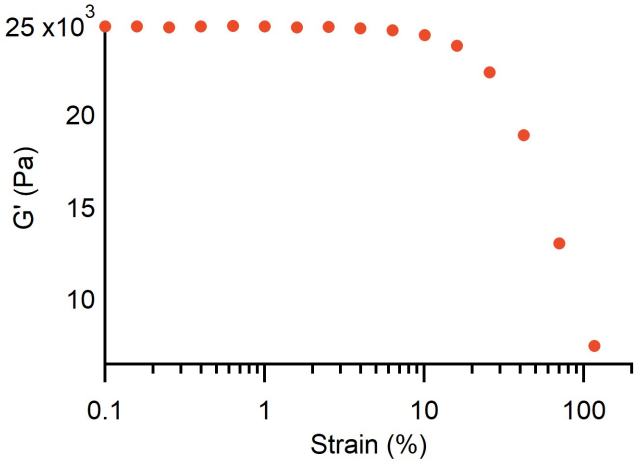

Figure 2.13: Strain sweep of PMOS-PIBVE-PMOS, from 0.1 to 100% strain, 1 Hz, 150 °C.

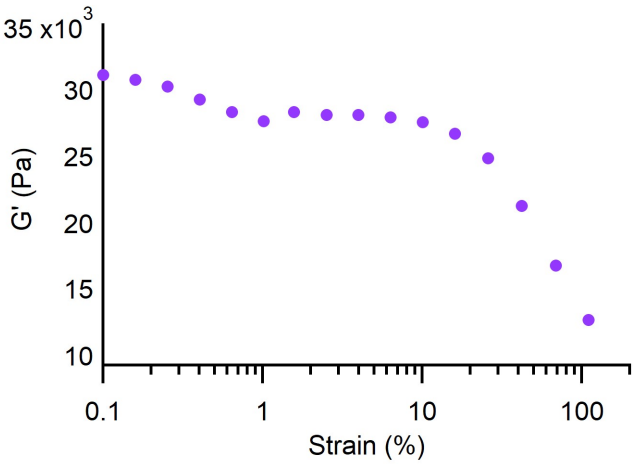

Figure 2.14: Strain sweep of PDHF-PIBVE-PDHF, from 0.1 to 100% strain, 1 Hz, 170 °C.

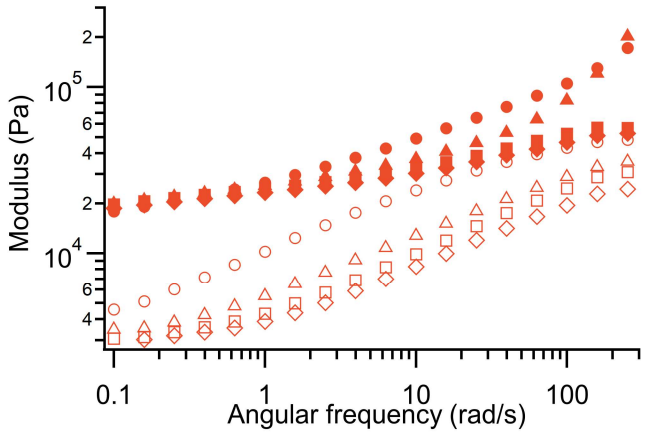

Figure 2.15: Frequency sweep of PMOS-0.21 (circles), PMOS-0.23 (triangles), PMOS-0.32 (squares), and PMOS-0.38 (diamonds) at 170 ºC. Filled markers correspond to G' and open markers correspond to G"

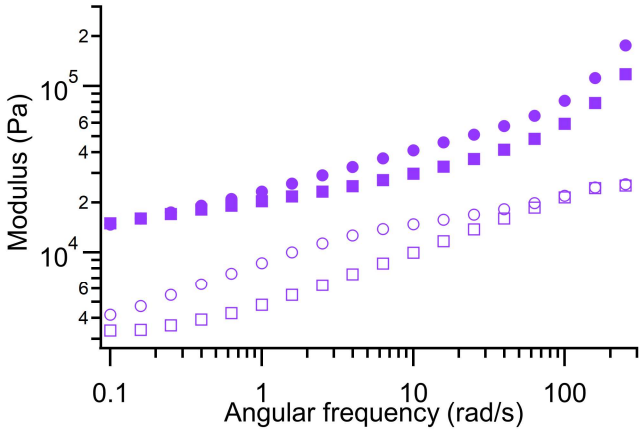

Figure 2.16: Frequency sweep of PDHF-0.23 (circles) and PDHF-0.31 (squares) at 170 ºC. Filled markers correspond to G' and open markers correspond to G".

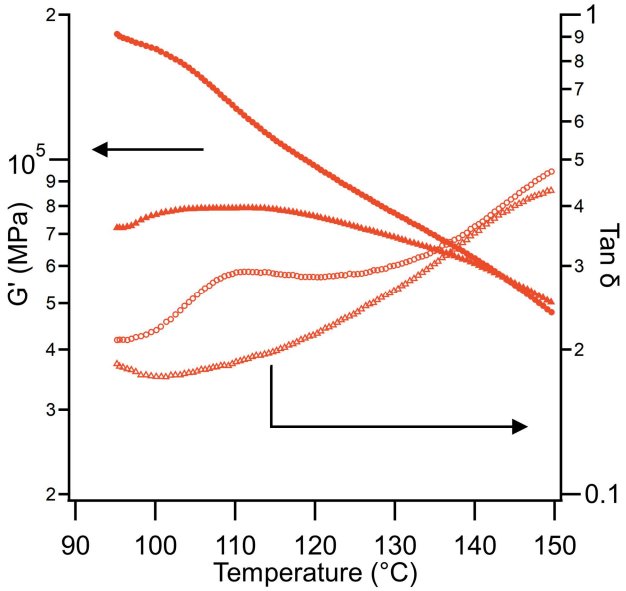

Figure 2.17: Temperature sweep of PMOS-0.38 (circles) and PMOS-0.32 (squares). Filled markers correspond to G' and open markers correspond to tan δ. The tan δ peak at 111 °C corresponds to the T_g of PMOS.

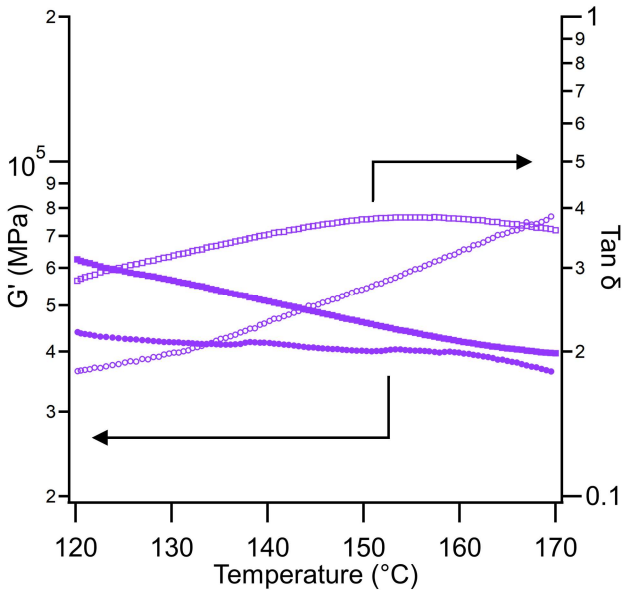

Figure 2.18: Temperature sweep of PDHF-0.31 (circles) and PDHF-0.23 (squares). Filled markers correspond to G' and open markers correspond to tan δ. No tan δ peak is observed due to the low volume fraction of PDHF.

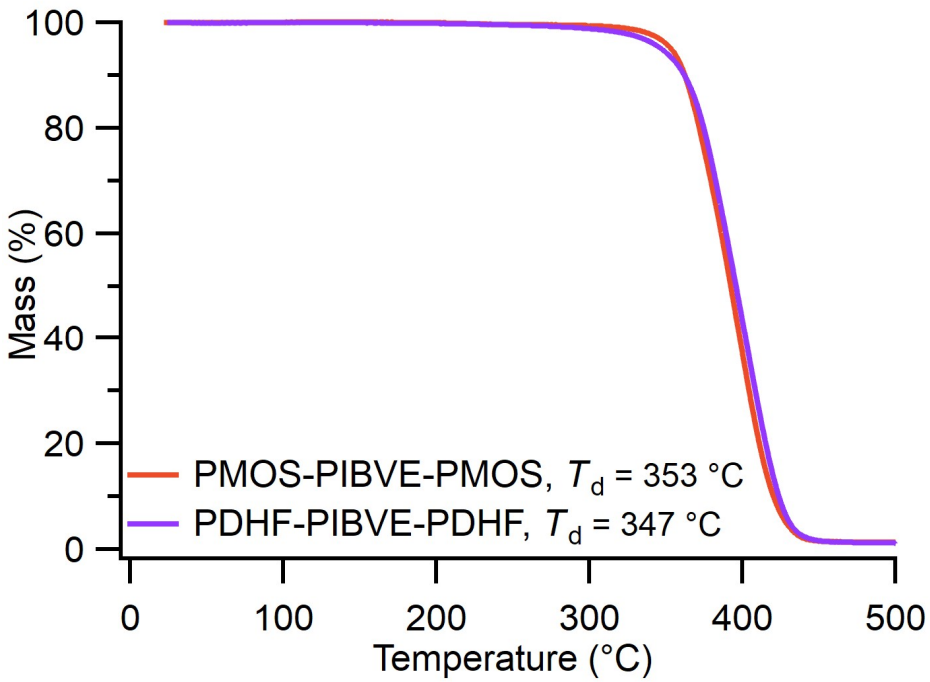

Figure 2.19: Thermal gravimetric analysis of mass vs. temperature (increased 10 °C/min) traces of each ABA copolymer. Degradation temperatures reported at 5% mass loss.

2.9.3 NMR Spectra:

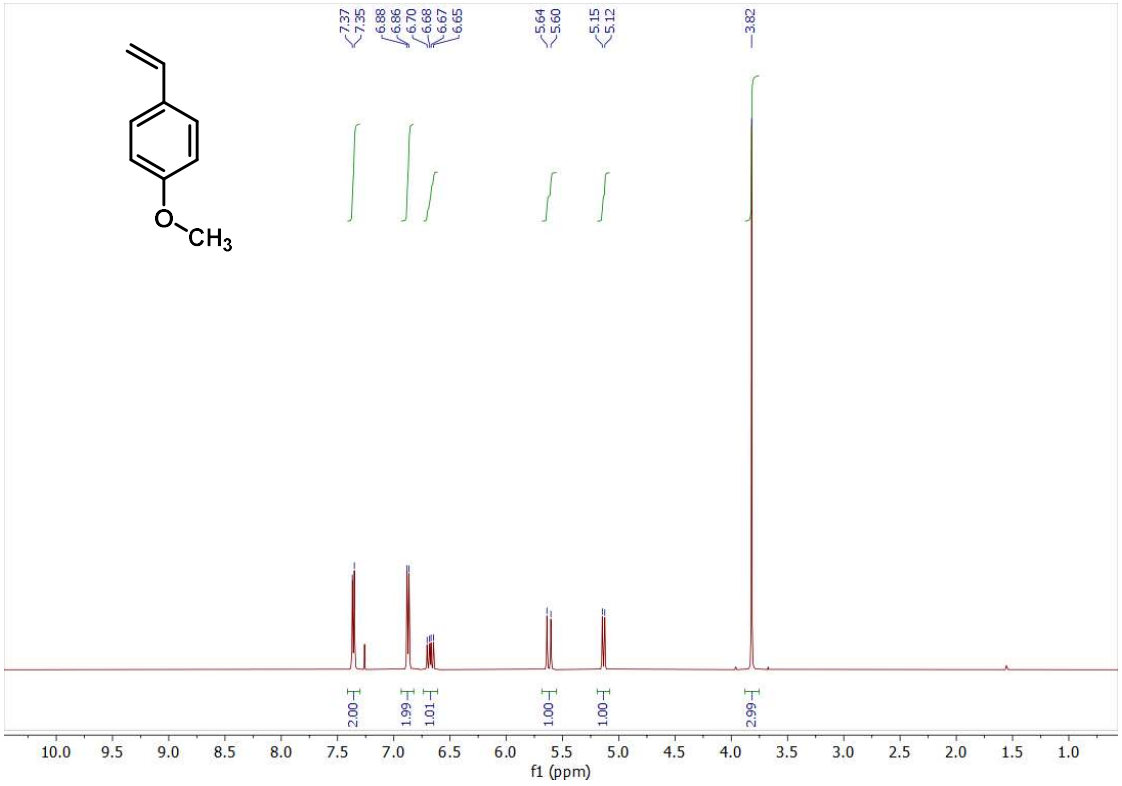

Figure 2.20: Quantitative ^{1}H NMR of *p*-methoxystyrene in $CDCl_3$

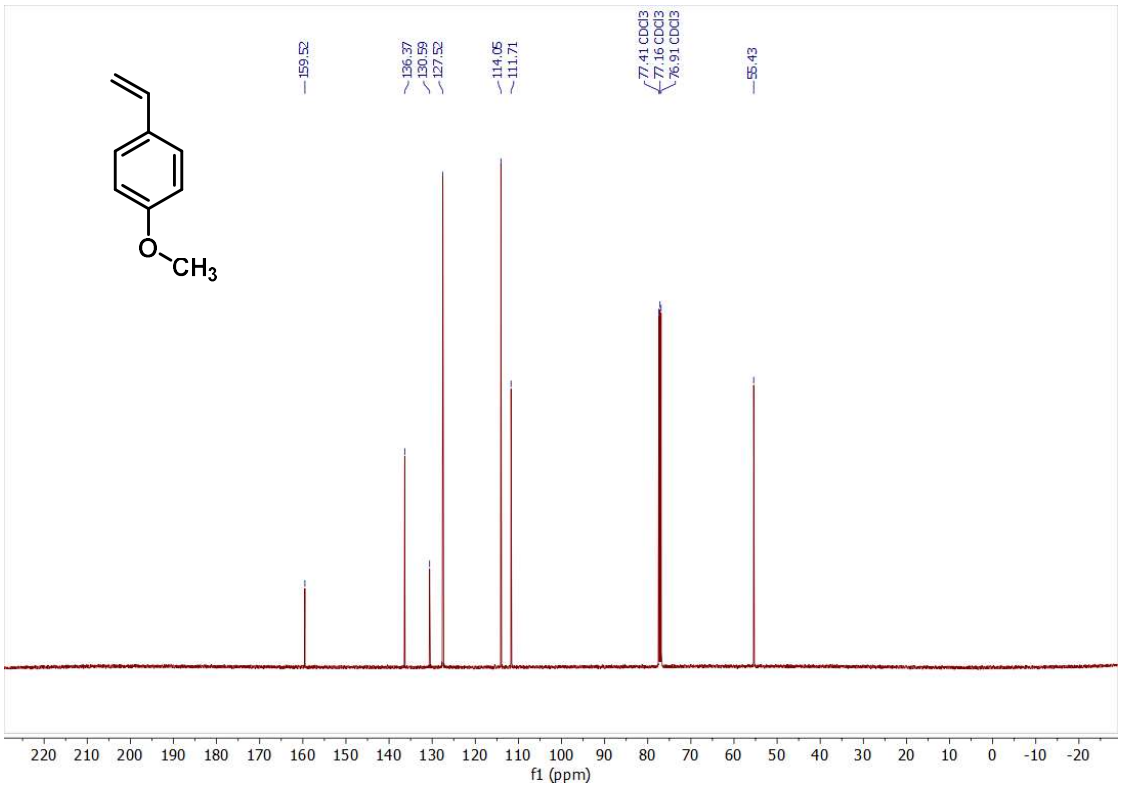

Figure 2.21: ^{13}C NMR of *p*-methoxystyrene in $CDCl_3$

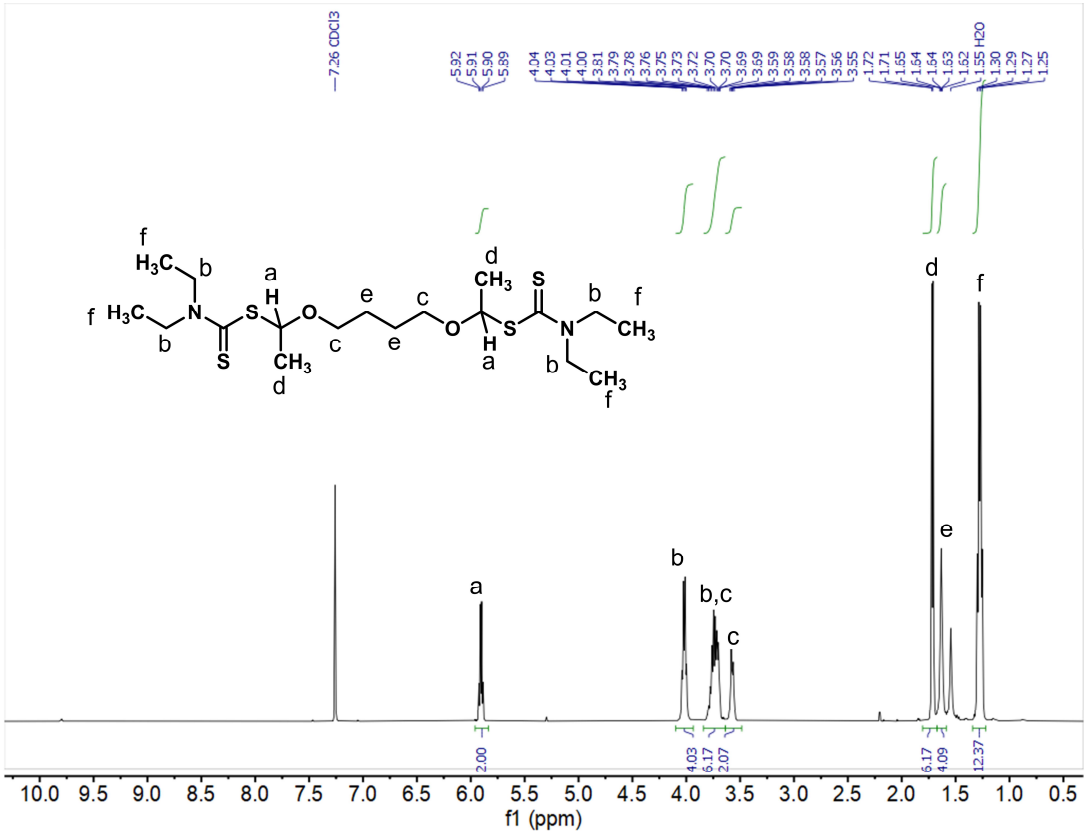

Figure 2.22: Quantitative ^{1}H NMR of difunctional CTA in $CDCl_3$

Figure 2.23: ^{13}C NMR of Difunctional CTA in $CDCl_3$

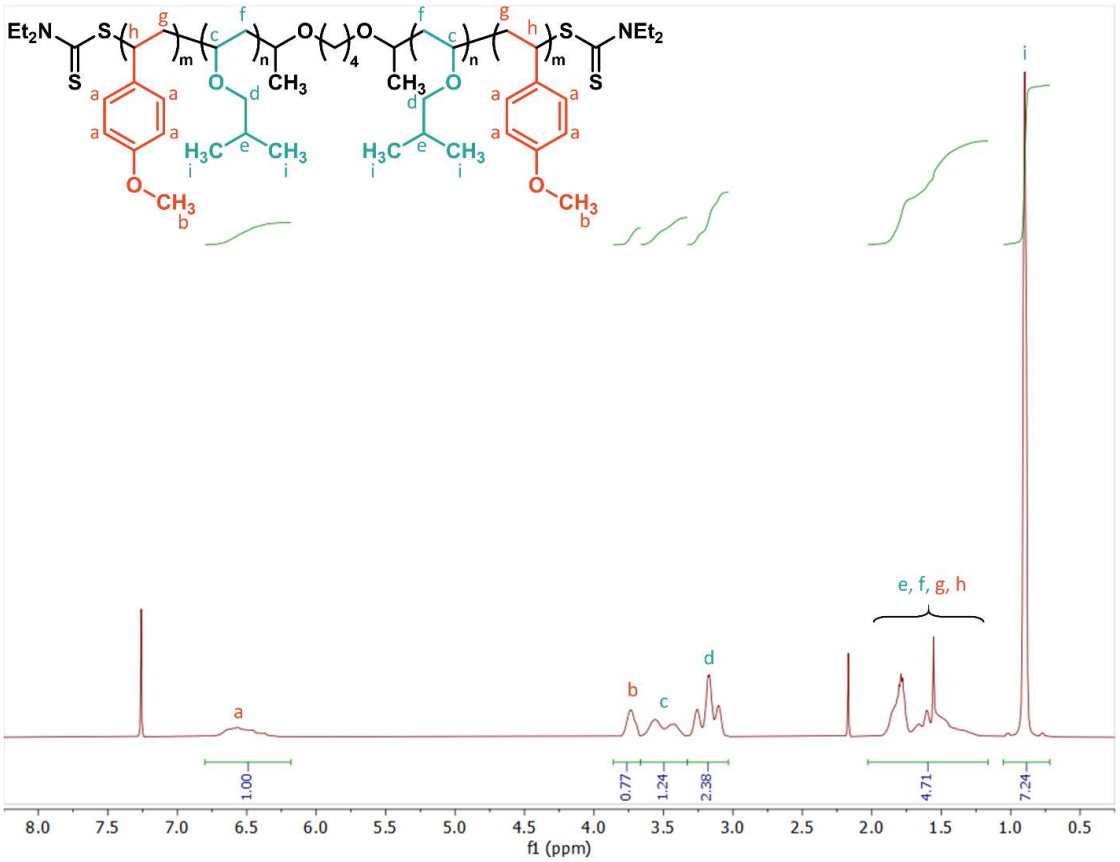

Figure 2.24: Quantitative ^{1}H NMR of PMOS-0.21 in $CDCl_3$

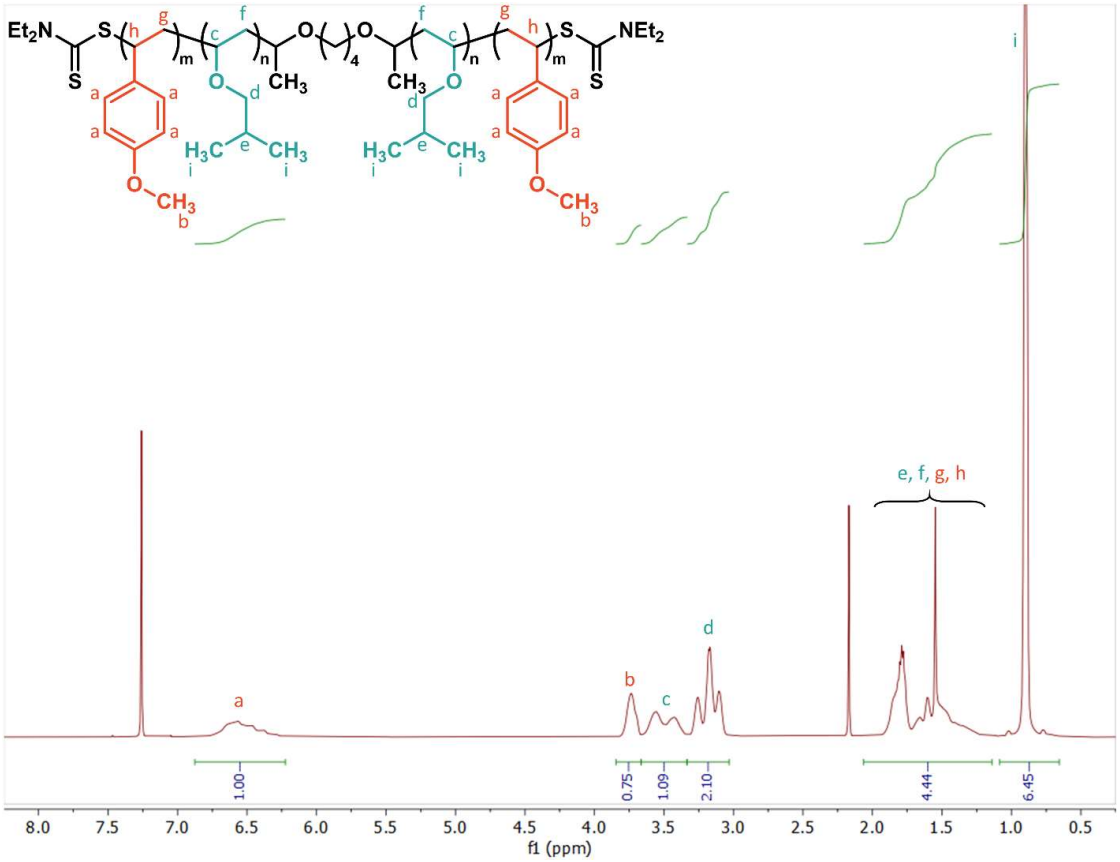

Figure 2.25: Quantitative ^{1}H NMR of PMOS-0.23 in $CDCl_3$

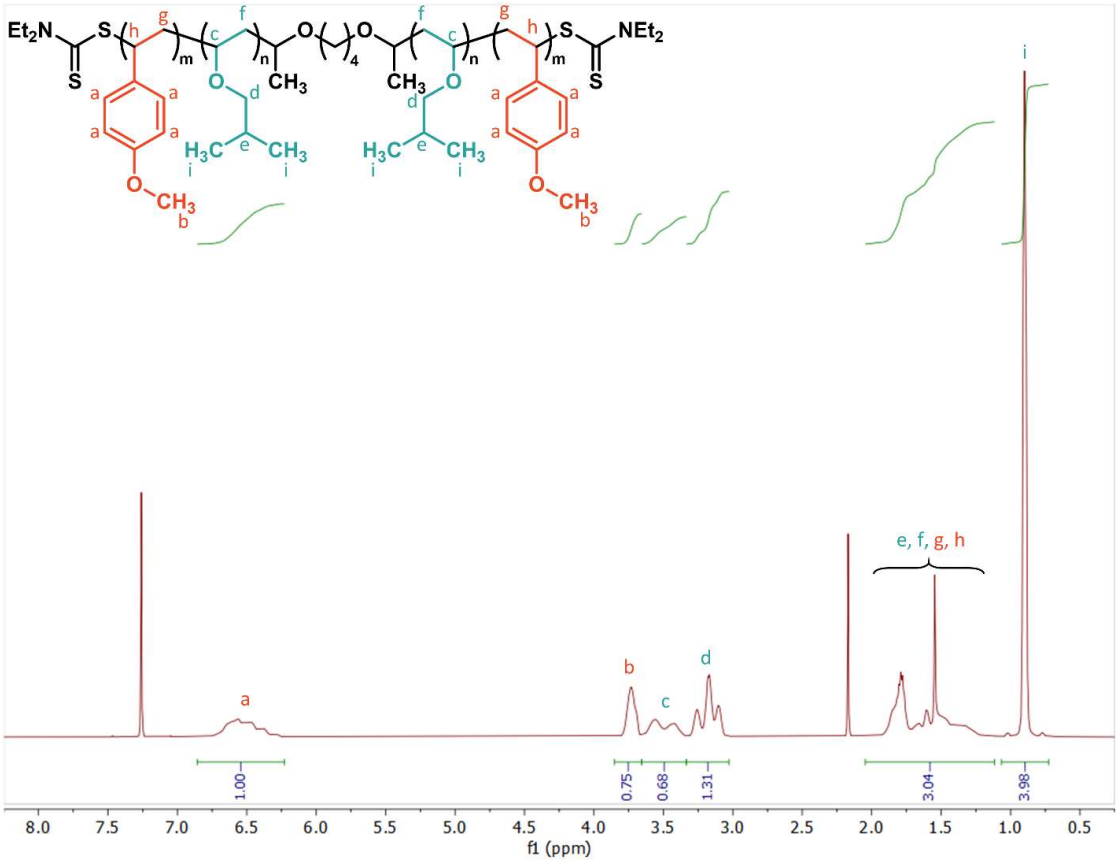

Figure 2.26: Quantitative ^{1}H NMR of PMOS-0.32 in $CDCl_3$

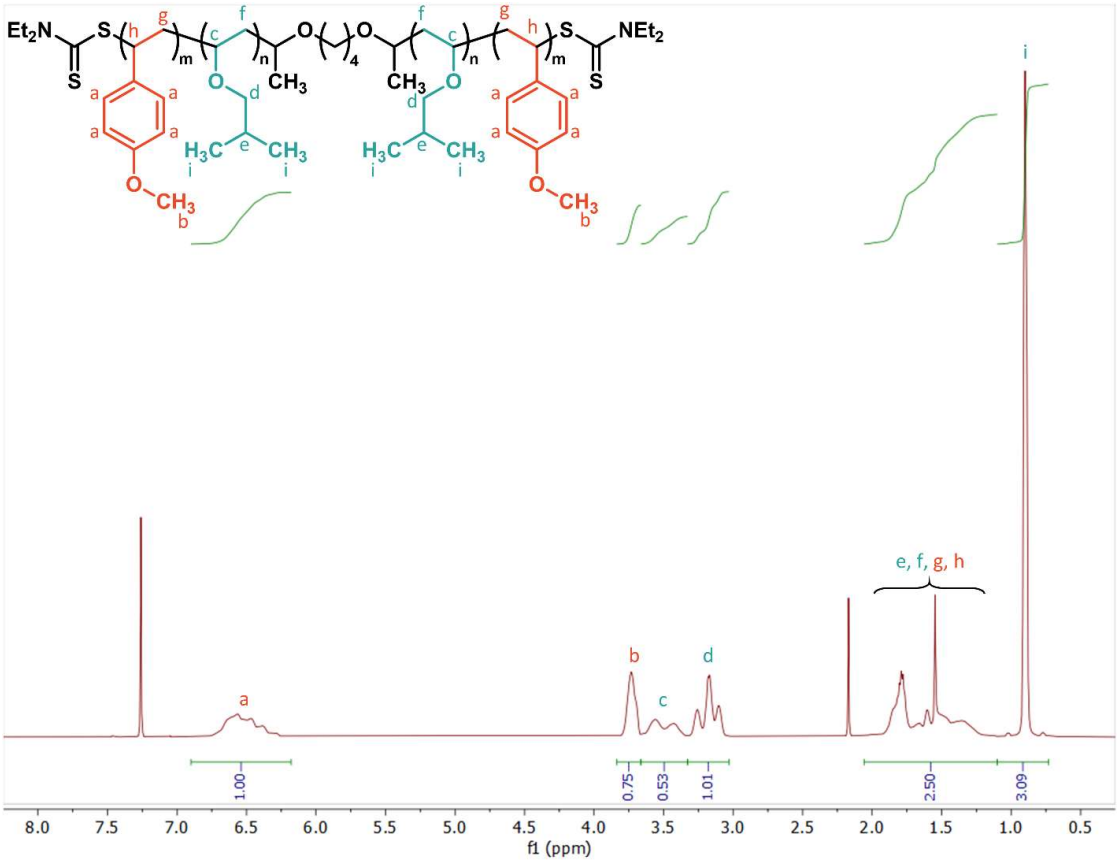

Figure 2.27: Quantitative ^{1}H NMR of PMOS-0.38 in $CDCl_3$

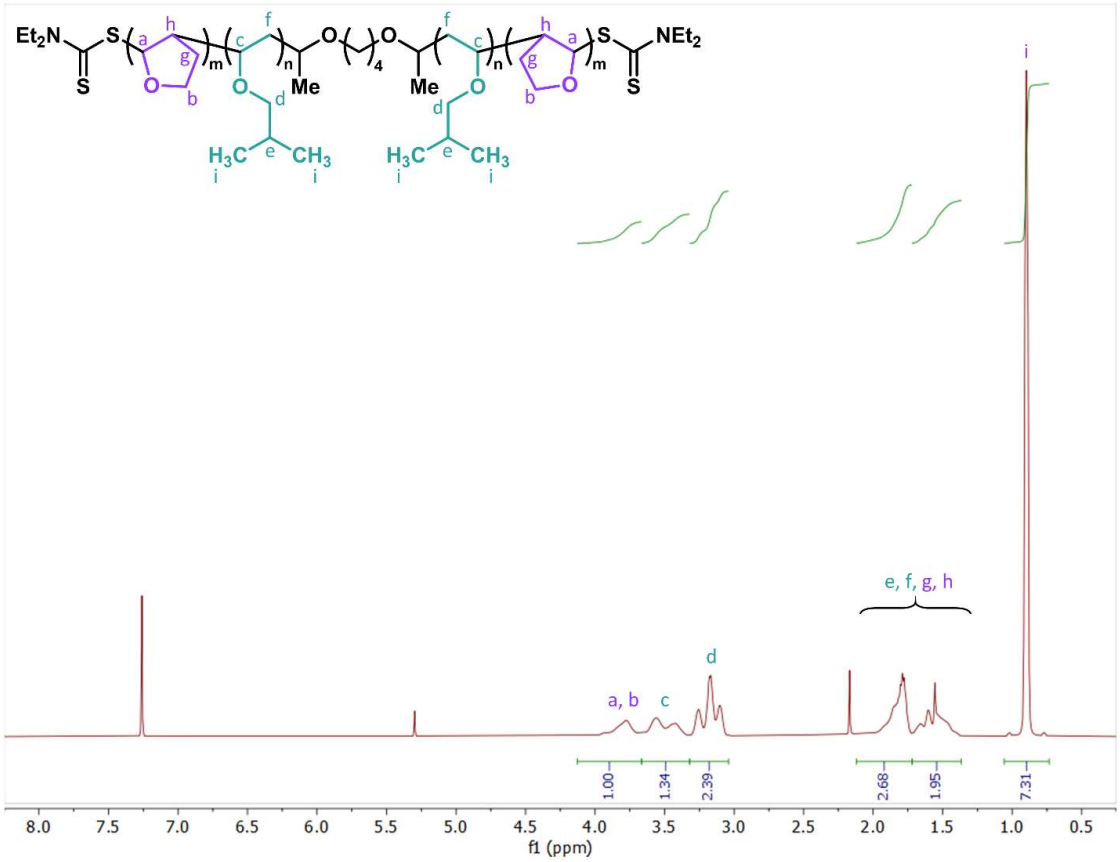

Figure 2.28: Quantitative ^{1}H NMR of PDHF-0.23 in $CDCl_3$

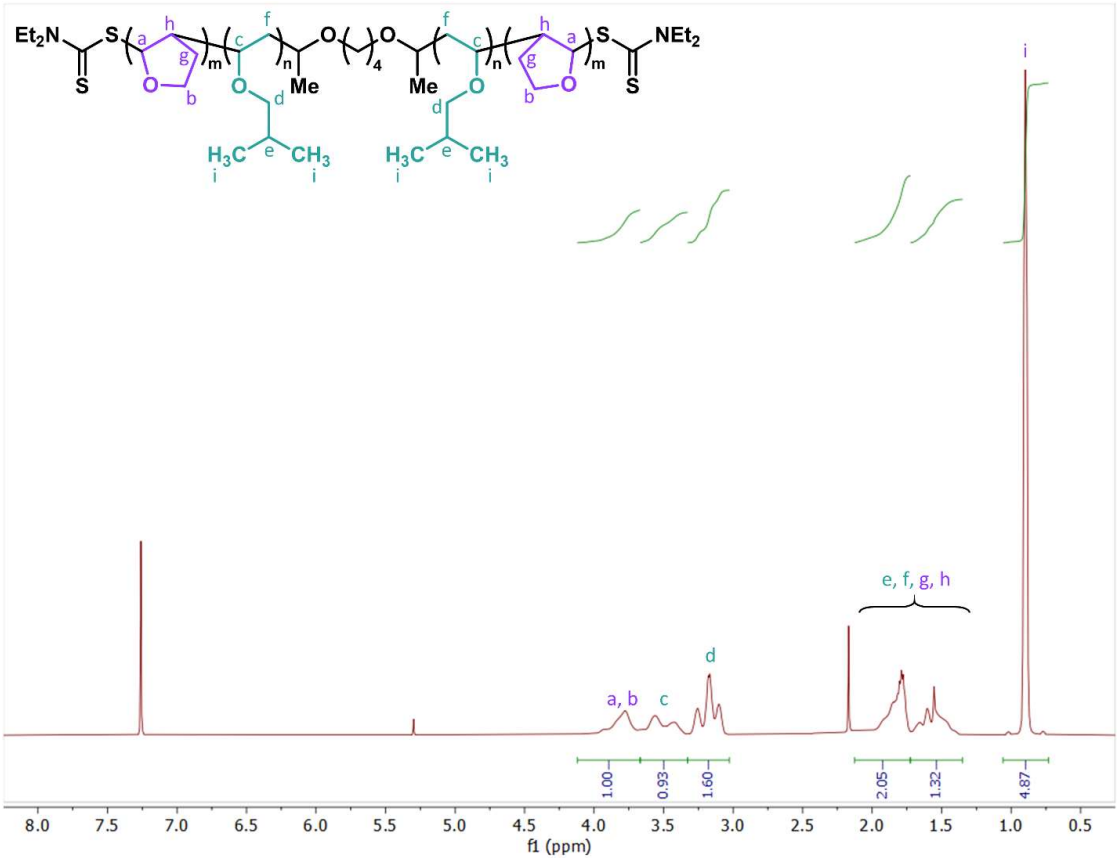

Figure 2.29: Quantitative ^{1}H NMR of PDHF-0.31 in $CDCl_3$

2.10 Green Metrics:

We evaluated the monomer and polymer syntheses disclosed herein using several widely accepted green metrics. Reported in Table S2 are the calculated isolated yields, atom economies (AEs) and process mass intensities (PMI). AE evaluates the percent molecular weight of the desired product compared to the molecular weight of all reactants.[5] For an account of all resources required in a process, the PMI is calculated as the mass of product divided by the mass of all reagents, solvents, and catalysts used in the reaction, workup, and purification.[6,7]

The synthesis of MOS has a high isolated yield (77%) over two steps on 25g scale. This reaction has a low AE due to the first step, decarboxylation of *p*-coumaric acid, resulting in mass loss from the original reactant. The methylation with methyl iodide is also inefficient due to the loss of iodide. The PMI is equally high for this process at 33 kg kg^{-1}. While this synthesis is not well-optimized in relation to green metrics, it does demonstrate the ability to source MOS, a common monomer in cationic RAFT polymerizations, from biomass.

The polymerizations of PMOS-PIBVE-PMOS and PDHF-PIBVE-PDHF are both ideal in AE, at 100%. This combined with high isolated yields (>70%), validates the efficiency of our cationic polymerization in producing ABA copolymers. While the PMI for each polymerization is high, this comes from the amount of methanol used to crash out the polymer for purification. However, the only byproducts left over are unreacted monomer, solvent, and ferrocene. The unreacted monomer and solvent can be removed under vacuum and, depending on the application of

the polymer, the removal of ferrocene (0.07 wt%) would not be required, reducing the PMI by over 200%.

Table 2.3: Atom Economy and Process Mass Intensity

Equation S6:

Product	Isolated Yield (%)	AE[a] (%)	PMI[b] (kg kg^{-1})	PMI without precipitation in MeOH (kg kg^{-1})
MOS	77	44	33	–
PMOS-PIBVE-PMOS	75	100	910	3.8
PDHF-PIBVE-PDHF	71	100	1146	4.3

[a] Defined as the percent molecular weight of the product compared to the molecular weight of all reactants.
[b] Defined as the mass of isolated product to mass of all materials used.

$$AE\ (\%) = \frac{molecular\ weight\ of\ product}{molecular\ weight\ of\ reactants} \times 100$$

Equation S7 was used to calculate the process mass index (PMI), which takes into account the mass of all reactants and solvents used in the reaction, work up, and purification.

Equation S7:

$$PMI = \frac{total\ mass\ of\ materials\ used\ in\ process\ (kg)}{mass\ of\ isolated\ product\ (kg)}$$

2.11 Peak Deconvolution of SEC Traces

In addition to the previously described method for estimating the molecular weight of these triblock copolymers, we also utilized peak deconvolution. Peak deconvolution is often performed to estimate molecular weights and mass fractions in multimodal polymer molecular weight distributions. To do so, we converted differential distributions to plots of mass fraction versus molecular weight. It is important to note that these molecular weights are calculated based

on polystyrene standards and are not absolute. Furthermore, without knowing the higher moments of the polymer molecular weight distributions, peak deconvolution does not afford highly accurate values. For these reasons, the data provided below is offered only as a comparison to the aforementioned method for calculating molecular weights. The Multipeak Fitting Package in Igor Pro 7 was utilized for peak deconvolution (Figure 2.30). PMOS triblock copolymers were assumed to have bimodal distributions whereas PDHF triblock copolymers were assumed to have trimodal distributions. All peaks were fit to a Gaussian function except for the highest molecular weight peaks in PDHF polymers (peak 3), which were fit to a Lorentzian function. From these peak fits were calculated M_n (equation S8) and the mass percent of each peak (equation S9). These values are displayed in Table 2.4.

Equation S8:

$$M_n = \frac{\sum M_i * N_i}{\sum N_i}$$

Equation S9:

$$mass\ \% = 100 \times \frac{\sum N_{i,peak\ 1}}{\sum (N_{i,peak\ 1} + N_{i,peak\ 2})}$$

Table 2.4: ABA copolymer composition calculated from peak fitting data.

Sample	Peak 1 M_n (kg/mol)	Peak 2 M_n (kg/mol)	Peak 3 M_n (kg/mol)	Mass % (Peak 1:Peak 2:Peak 3)
PMOS-0.21	11.6	82.0	–	16:84
PMOS-0.23	13.9	84.3	–	2:98
PMOS-0.32	18.4	85.9	–	16:84
PMOS-0.38	21.4	83.8	–	15:85
PDHF-0.23	11.5	80.3	167	1:67:32
PDHF-0.31	14.5	72.1	153	2:59:38

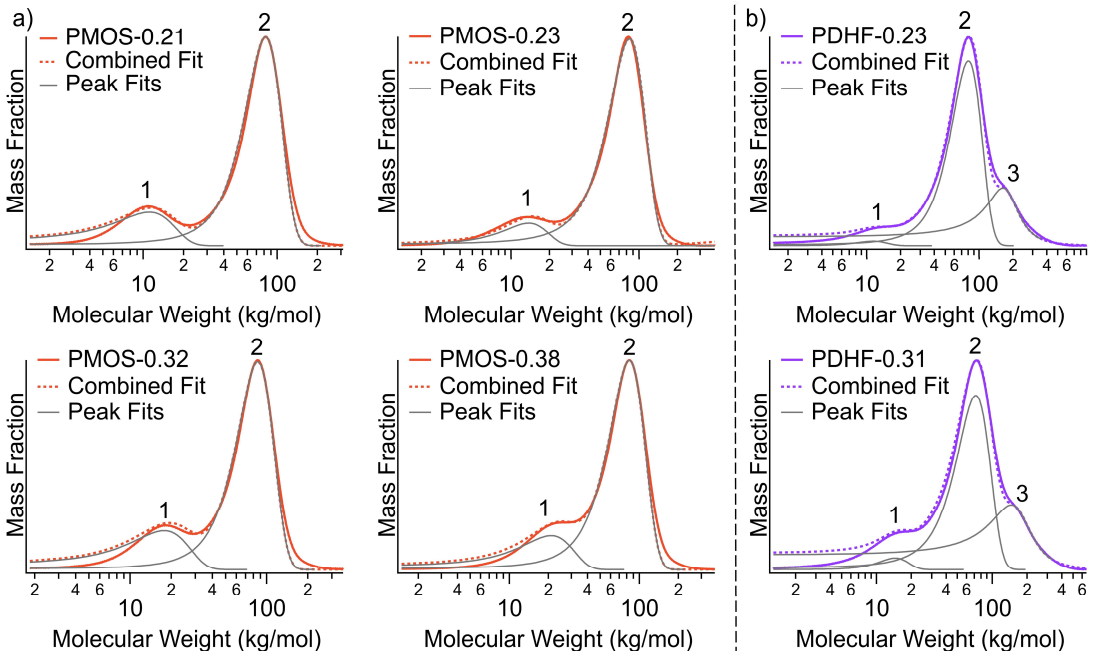

Figure 2.30: Peak deconvolution of a) PMOS-PIBVE-PMOS and b) PDHF-PIBVE-PDHF SEC traces calculated using the Multipeak Fitting Package in Igor Pro 7.

2.12 References

(1) Perkowski, A. J.; You, W.; Nicewicz, D. A. Visible Light Photoinitiated Metal-Free Living Cationic Polymerization of 4-Methoxystyrene. *J. Am. Chem. Soc.* **2015**, *137* (24), 7580–7583.

(2) Stoupin, S.; Ruff, J. P. C.; Krawczyk, T.; Finkelstein, K. D. X-Ray Reflectivity of Chemically Vapor-Deposited Diamond Single Crystals in the Laue Geometry. *Acta Crystallogr. Sect. A* **2018**, *74* (5), 567–577.

(3) Ilavsky, J. Nika: Software for Two-Dimensional Data Reduction. *J. Appl. Crystallogr.* **2012**, *45*, 324–328.

(4) Ilavsky, J.; Jemiana, P. R. Irena: Tool Suite for Modeling and Analysis of Small-Angle Scattering. *J. Appl. Crystallogr.* **2009**, *42*, 347—353.

(5) Tobiszewski, M.; Marć, M.; Gałuszka, A.; Namieśnik, J. Green Chemistry Metrics with Special Reference to Green Analytical Chemistry. *Molecules* **2015**, *20* (6), 10928–10946.

(6) Jimenez-Gonzalez, C.; Ponder, C. S.; Broxterman, Q. B.; Manley, J. B. Using the Right Green Yardstick: Why Process Mass Intensity Is Used in the Pharmaceutical Industry To Drive More Sustainable Processes. *Org. Process Res. Dev.* **2011**, *15* (4), 912–917.

(7) Jiménez-González, C.; Constable, D. J. C.; Ponder, C. S. Evaluating the "Greenness" of Chemical Processes and Products in the Pharmaceutical Industry—a Green Metrics Primer. *Chem. Soc. Rev.* **2012**, *41* (4), 1485–1498.

Chapter 3

Green Chain Transfer Agent for Cationic RAFT Polymerizations

3.1 Abstract

Cationic polymerization of vinyl ethers has gained prominence due to the the ability to produce robust, sustainable polymers. This has been enabled in part by the advent of cationic reversible addition-fragmentation chain-transfer (RAFT) polymerizations. However, the synthesis of chain transfer agents (CTAs) has hindered the success of this method, with many existing as viscous, coloured oils requiring complex syntheses and solvent-intense purification. Herein, we disclose a solid, colorless CTA produced through a green synthetic route in 83% yield on 50-gram scale. We demonstrate the utility of this CTA in chemical, electrochemical, photochemical, and acid-initiated methods to perform controlled cationic RAFT polymerization.

3.2 Results and Discussion

In 2009 Aoshima and Kanaoka reported on “a renaissance in living cationic polymerization”.[1] Since this point, controlled cationic polymerizations have continued to improve; the development of cationic reversible addition-fragmentation chain-transfer (RAFT) has led to new possibilities.[2,3] Previous methods for controlled cationic polymerizations relied on low temperatures, resulting in high energy costs when scaling up the reactions.[4,5] Cationic RAFT also offers greater control over the polymerization process through external stimuli

such as chemical, electrochemical, and photochemical.[6–9] This has enabled spatial and temporal control, leading to the production of well-defined block copolymers and thermosets with tunable properties.[10,11] However, some of the reagents and solvents used for cationic RAFT polymerizations are unsustainable and toxic, making adaptation to industry scale unlikely. Therefore, we envisage the adoption of facile reagents and non-toxic solvents would improve cationic RAFT's accessibility and industrial relevance.

To improve the accessibility and sustainability of cationic RAFT, we set out to develop a more facile and sustainable chain transfer agent (CTA). The synthesis and design of CTAs for radical RAFT is well understood, with several commercially available options.[12] There are also several radical CTAs that are solid, such as dithiobenzoates, allowing for purification by recrystallization rather than solvent-intense column chromatography. Another issue with many CTAs is their colour, which is generally present in the resulting polymers. To address these problems, we sought to develop a solid, colourless CTA with a facile synthesis.

We first set out to design and synthesize a solid, colorless CTA. Previous studies show dithiocarbamates and trithiocarbonates give the best control for cationic RAFT with low dispersity (*Đ*) and agreement with experimental molecular weight (M_n^{exp}) and predicted molecular weight (M_n^{theo}).[3,13] Based on our previous experiences generating dithiocarbamates and our work with 2,3-dihydrofuran (DHF) as a monomer, we envisioned a cyclic vinyl ether would increase the melting point of our product. Concurrently, changing the diethyl amine to cyclic

pyrrolidine should have the same effect without affecting the electronic properties of the dithiocabamate. Therefore, we predicted CTA-1 would provide a solid CTA, while retaining the ability to produce a controlled cationic RAFT polymerization. Serendipitously, we found an efficient, green synthesis of this dithiocabamate was recently reported by Halimehjani *et al.*[14] Indeed, we successfully employed this method in a 50 gram scale synthesis of CTA-1. The product was purified through recrystallization, and 41.4 grams of white, solid product was isolated (Figure 3.1a). Thus, we were eager to implement this CTA in our work and explore its utility in a variety of cationic RAFT polymerizations (Figure 3.1b).

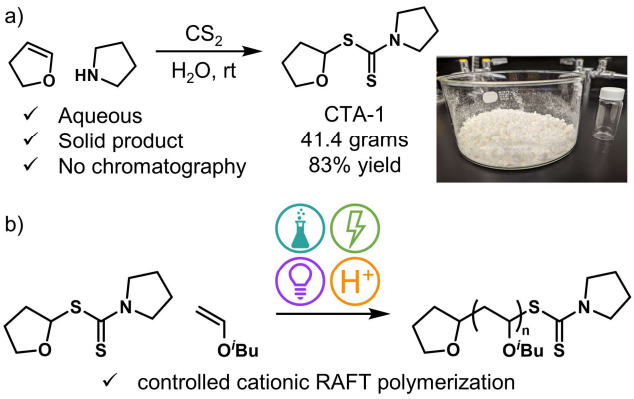

Figure 3.1: a) Solid, colorless CTA-1 generated with green, aqueous synthesis b) Cationic RAFT polymerizations of IBVE achieved through several methods, including external, temporal control.

To investigate the effectiveness of CTA-1 in cationic RAFT, we chose a test reaction using ferrocenium tetrafluoroborate ($FcBF_4$) as a chemical oxidant (Table 3.1). Initially, IBVE was added to a vial containing CTA-1 followed by a solution of $FcBF_4$ in dichloromethane (DCM). We observed good agreement between M_n^{theo}

and M_n^{exp} and narrow $Đ$ when targeting molecular weights from 10–30 kg/mol (Table 3.1, entries 1-3). We then expanded this to other vinyl ethers, including electron deficient 2-chloroethyl vinyl ether (Cl-EVE) (Table 3.1, entry 5), and the cyclic vinyl ether DHF (Table 3.1, entry 6). Notably, we could also polymerize the less active styrenic monomer, *p*-methoxystyrene (MOS) (Table 3.1, entry 7). These results demonstrate CTA-1 provides the same control over cationic RAFT polymerizations as previous CTAs when a chemical oxidant is used.

In addition, cationic RAFT polymerization methods reported previously were performed in toxic, unsustainable solvents, namely DCM. DCM is acutely toxic to humans and the environment, highly flammable, difficult to recover, and subject to costly waste disposal.[15–17] Some alternative solvents for cationic polymerizations such as toluene and tetrahydrofuran (THF) are not a major improvement in health and safety and present solubility issues for RAFT catalysts. In addition, THF is susceptible to ring opening under acidic conditions and for the same reason this also removes 2-methyl-THF as an option. However, based on reports of similar solubility properties and the lack of a heterocycle, we hypothesized cyclopentyl methyl ether (CPME) would be an effective green solvent for cationic RAFT polymerizations (Table 3.2).

Table 3.1: Cationic RAFT polymerization of vinyl ethers and p-methoxystyrene with CTA-1.

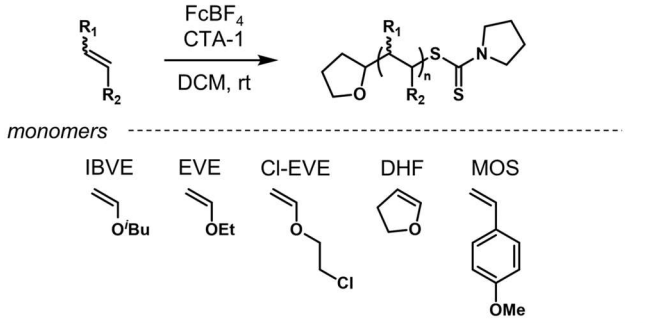

Entry	Monomer	[M]:[CTA-1]:[$FcBF_4$] [a]	M_n^{theo} (kg/mol) [b]	M_n^{exp} (kg/mol)	$Đ$
1	IBVE	100:1:0.01	10.0	10.3	1.11
2	IBVE	200:1:0.01	20.0	19.6	1.15
3	IBVE	300:1:0.01	30.0	29.0	1.21
4	EVE	100:1:0.01	9.7	9.4	1.14
5	Cl-EVE	100:1:0.03	10.0	9.1	1.08
6	MOS	100:1:0.04	9.5	9.2	1.19
7	DHF	100:1:0.01	10.0	11.4	1.23

[a] 0.02 mmol CTA-1, performed in nitrogen atmosphere. [b] M_n^{theo} calculated from NMR conversion. [c] M_n^{exp} and $Đ$ determined by light scattering. [d] M_n^{exp} and $Đ$ determined by GPC RI data.

We set out to explore the use of the green solvent CPME using IBVE and the $FcBF_4$ oxidant. Solubility of $FcBF_4$ was limited in CPME, so a stock solution of CTA-1 in CPME was added to a vial containing $FcBF_4$ followed by 100 equivalents of IBVE. The resulting polymer was 13.9 kg/mol with a narrow $Đ$ of 1.08 (Table 3.2, entry 1). Different M_ns were then targeted from 20–40 kg/mol by changing the equivalents of IBVE added (Table 3.2, entry 2-4). The ratio of [$FcBF_4$]:[IBVE] was maintained while [IBVE]:[CTA] was increased. Indeed, low $Đ$ and good agreement between M_n^{theo} and M_n^{exp} were observed, demonstrating a controlled polymerization in CPME solvent. Importantly, this eliminates the need for DCM in cationic RAFT polymerization, increasing the sustainability and accessibility of this method.

Table 3.2: Cationic RAFT polymerization of IBVE in cyclopentyl methyl ether.

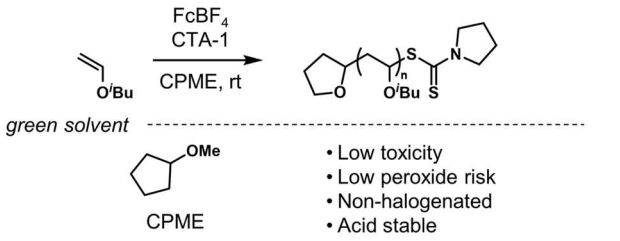

Entry	[M]:[CTA-1]:[$FcBF_4$]	Conversion (%)	M_n^{exp} (kg/mol)	M_n^{theo} (kg/mol)	$Đ$
1	100:1:0.02	99	10.0	13.9	1.07
2	200:1:0.04	99	20.0	25.6	1.08
3	300:1:0.06	99	30.0	35.1	1.13
4	400:1:0.08	99	40.0	45.4	1.12

[a] 0.02 mmol CTA-1, performed in nitrogen atmosphere. [b] M_n^{theo} calculated from NMR conversion. [c] M_n^{exp} and $Đ$ determined by light scattering.

Having achieved success with chemical oxidation, our next focus was to extend this study to other cationic RAFT techniques that have been developed in recent years (Figure 3.2). We began with electrochemistry, where Supej and coworkers demonstrated ferrocene (Fc) can be used as an electrochemical mediator.[18] In a divided cell, IBVE, Fc, CTA-1, Bu_4NClO_4, and DCM were added to the anode, while the cathode was loaded with Bu_4NClO_4 in DCM. 0.5 mA of anodic current was applied over 30 minutes and after 1 hour we obtained a 9.5 kg/mol polymer of narrow dispersity ($Đ$ = 1.09) (Figure 3.2b).

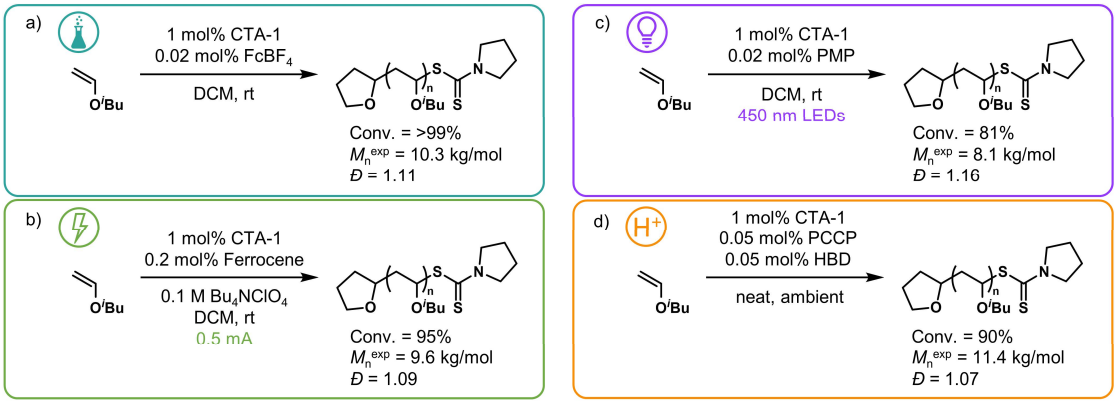

Figure 3.2: Controlled cationic RAFT polymerization initiated by a) chemical oxidant, b) electrochemistry, c) photochemistry, and d) bronsted acid.

Next, we investigated the use of CTA-1 in a photocontrolled RAFT polymerization. Our previous work demonstrated that dithiocabamate CTAs can be effectively oxidized by a photocatalyst to initiate cationic polymerization of vinyl ethers.[7,19] CTA-1 was added to a vial followed by IBVE and 2,4,6-tris(4-methoxyphenyl)pyrylium tetrafluoroborate (PMP) in DCM and the reaction was irradiated by 450 nm LEDs under air cooling. This produced an 8.14 kg/mol polymer with $Đ$ = 1.16 after 19.5 hours (Figure 3.2c). Monomer conversion was slower than previous results with S-1-isobutoxyethyl N,N-diethyl dithiocarbamate (CTA-2) and we observed a reduction in fluorescence of the photocatalyst (Figure 3.18). As a control, CTA-2 was produced using the green synthesis and performed as expected. ‡ We hypothesize that small quantities of leftover amine from the synthesis could be degrading the photocatalyst, so extra care must be taken during purification of the CTA.

Finally, we investigated polymerization using pentacarbomethoxycyclopentadiene (PCCP) as an acid initiator, with a hydrogen

bond donor catalyst, tris(3,5-bis(trifluoromethyl)phenyl) thiophosphotriamide (HBD). This system was developed by our group to achieve controlled cationic RAFT polymerizations under ambient conditions. IBVE was filtered through a plug of basic alumina before being added to a vial containing PCCP, HBD, and CTA-1. The reaction was stopped after 4.5 hours and produced a 11.4 kg/mol polymer with $Đ$ = 1.07 (Figure 3.2d). This technique highlights our ability to perform reactions without rigorous purification of monomer, under ambient conditions.

A major advancement afforded by cationic RAFT polymerizations is the external, temporal control over the reaction. Previous groups have demonstrated the ability to turn cationic RAFT polymerizations on and off through the application of an external stimuli, such as light[6,20,21] or electricity[8,9]. Having demonstrated that CTA-1 could perform a controlled polymerization through electrochemical oxidation of a Fc mediator, we envisaged reversing the current could enable temporal control. To test our hypothesis, we again added IBVE, Fc, CTA-1, Bu_4NClO_4, and DCM to the anode, and the cathode was loaded with Bu_4NClO_4 in DCM. 0.5 mA of anodic current (+) was then applied for 15 minutes to initiate polymerization (Figure 3.3). To turn off polymerization, a 0.5 mA cathodic current (−) was applied for 15 minutes. This first "on" period produced a 2.4 kg/mol polymer with $Đ$ = 1.08. After a 30 minute "off" period, no monomer conversion was observed, and the polymerization was reinitiated with a 15-minute, 0.5 mA anodic pulse. The polymerization proceeded for 30 minutes before a final 15-minute; 0.5 mA cathodic pulse was applied to stop the polymerization. The

resultant polymer was 3.9 kg/mol with a 1.17 dispersity. Another aliquot taken 30 minutes later confirmed the polymerization had stopped. This experiment successfully demonstrated CTA-1 can achieve temporal control through reversible termination of the polymerization.

Figure 3.3: Temporal control over monomer conversion achieved through anodic

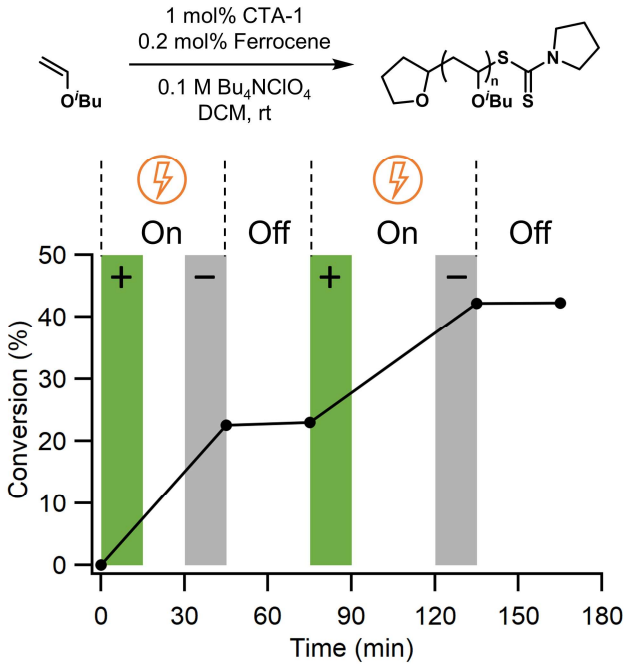

(+) and cathodic (−) 0.5 mA pulses.

3.3 Conclusions

We demonstrated a new solid CTA can perform as well as those used previously in a multitude of cationic RAFT polymerizations. CTA-1 can be synthesized on large scale, using an aqueous, room temperature synthesis that adheres to green chemistry principles. Additionally, CTA-1 is a white solid, enabling recrystallization for purification over solvent-intense column chromatography. CTA-1 was then utilized to controllably polymerize numerous

monomers using $FcBF_4$ as an initiator. This system was also performed in CPME, a green solvent alternative, eliminating the use of toxic solvents in cationic RAFT polymerizations. External initiation was achieved through photochemistry and electrochemistry, while a PCCP/HBD catalyst system enabled ambient reaction conditions. Finally, we demonstrated temporal control with electrochemical on/off pulses. This study showcases CTA-1 as a facile, green reagent, further expanding the accessibility of cationic RAFT polymerizations.

3.4 Conflicts of interest

There are no conflicts to declare.

3.5 Notes and references

‡ Ethyl acetate was used at the solvent, as we could not produce appreciable yield in deionized H_2O. This differs from the results reported by Halimehjani and coworkers.

(1) Aoshima, S.; Kanaoka, S. A Renaissance in Living Cationic Polymerization. *Chem. Rev.* **2009**, *109* (11), 5245–5287.

(2) Sugihara, S.; Okubo, S.; Maeda, Y. Metal-Free RAFT Cationic Polymerization of p-Methoxystyrene with HCl·Et2O Using a Xanthate-Type RAFT Cationogen. *Polym. Chem.* **2016**, *7* (44), 6854–6863.

(3) Uchiyama, M.; Satoh, K.; Kamigaito, M. Cationic RAFT Polymerization Using Ppm Concentrations of Organic Acid. *Angew. Chemie Int. Ed.* **2015**, *54* (6), 1924–1928.

(4) Yonezumi, M.; Kanaoka, S.; Aoshima, S. Living Cationic Polymerization of

Dihydrofuran and Its Derivatives. *J. Polym. Sci. Part A Polym. Chem.* **2008**, *46* (13), 4495–4504.

(5) Kanazawa, A.; Kanaoka, S.; Aoshima, S. A Stepping Stone to Stereospecific Living Cationic Polymerization: Cationic Polymerization of Vinyl Ethers Using Iron(II) Sulfate. *J. Polym. Sci. Part A Polym. Chem.* **2010**, *48* (16), 3702–3708.

(6) Peterson, B. M.; Kottisch, V.; Supej, M. J.; Fors, B. P. On Demand Switching of Polymerization Mechanism and Monomer Selectivity with Orthogonal Stimuli. *ACS Cent. Sci.* **2018**, *4* (9), 1228–1234.

(7) Kottisch, V.; Michaudel, Q.; Fors, B. P. Cationic Polymerization of Vinyl Ethers Controlled by Visible Light. *J. Am. Chem. Soc.* **2016**, *138* (48), 15535–15538.

(8) Peterson, B. M.; Lin, S.; Fors, B. P. Electrochemically Controlled Cationic Polymerization of Vinyl Ethers. *J. Am. Chem. Soc.* **2018**, *140* (6), 2076–2079.

(9) Supej, M. J.; Peterson, B. M.; Fors, B. P. Dual Stimuli Switching: Interconverting Cationic and Radical Polymerizations with Electricity and Light. *Chem* **2020**, *6* (7), 1794–1803.

(10) Spring, S. W.; Smith-Sweetser, R. O.; Rosenbloom, S. I.; Sifri, R. J.; Fors, B. P. Sustainable Thermoplastic Elastomers Produced via Cationic RAFT Polymerization. *Polym. Chem.* **2021**, *12*, 1097–1104.

(11) Ma, Y.; Kottisch, V.; McLoughlin, E. A.; Rouse, Z. W.; Supej, M. J.; Baker, S. P.; Fors, B. P. Photoswitching Cationic and Radical Polymerizations: Spatiotemporal Control of Thermoset Properties. *J. Am. Chem. Soc.* **2021**,

143 (50), 21200–21205.

(12) Perrier, S. 50th Anniversary Perspective: RAFT Polymerization—A User Guide. *Macromolecules* **2017**, *50* (19), 7433–7447.

(13) Michaudel, Q.; Chauviré, T.; Kottisch, V.; Supej, M. J.; Stawiasz, K. J.; Shen, L.; Zipfel, W. R.; Abruña, H. D.; Freed, J. H.; Fors, B. P. Mechanistic Insight into the Photocontrolled Cationic Polymerization of Vinyl Ethers. *J. Am. Chem. Soc.* **2017**, *139* (43), 15530–15538.

(14) Halimehjani, A. Z.; Marjani, K.; Ashouri, A. Synthesis of Dithiocarbamate by Markovnikov Addition Reaction in Aqueous Medium. *Green Chem.* **2010**, *12* (7), 1306–1310.

(15) Taygerly, J. P.; Miller, L. M.; Yee, A.; Peterson, E. A. A Convenient Guide to Help Select Replacement Solvents for Dichloromethane in Chromatography. *Green Chem.* **2012**, *14* (11), 3020–3025.

(16) Henderson, R. K.; Jiménez-González, C.; Constable, D. J. C.; Alston, S. R.; Inglis, G. G. A.; Fisher, G.; Sherwood, J.; Binks, S. P.; Curzons, A. D. Expanding GSK's Solvent Selection Guide – Embedding Sustainability into Solvent Selection Starting at Medicinal Chemistry. *Green Chem.* **2011**, *13* (4), 854–862.

(17) Alfonsi, K.; Colberg, J.; Dunn, P. J.; Fevig, T.; Jennings, S.; Johnson, T. A.; Kleine, H. P.; Knight, C.; Nagy, M. A.; Perry, D. A.; et al. Green Chemistry Tools to Influence a Medicinal Chemistry and Research Chemistry Based Organisation. *Green Chem.* **2008**, *10* (1), 31–36.

(18) Supej, M. J.; Peterson, B. M.; Fors, B. P. Dual Stimuli Switching: Interconverting Cationic and Radical Polymerizations with Electricity and Light. *Chem* **2020**, *6* (7), 1794–1803.

(19) Kottisch, V.; Supej, M. J.; Fors, B. P. Enhancing Temporal Control and Enabling Chain-End Modification in Photoregulated Cationic Polymerizations by Using Iridium-Based Catalysts. *Angew. Chemie Int. Ed.* **2018**, *57* (27), 8260–8264.

(20) Kottisch, V.; Michaudel, Q.; Fors, B. P. Photocontrolled Interconversion of Cationic and Radical Polymerizations. *J. Am. Chem. Soc.* **2017**, *139* (31), 10665–10668.

(21) Kottisch, V.; O'Leary, J.; Michaudel, Q.; Stache, E. E.; Lambert, T. H.; Fors, B. P. Controlled Cationic Polymerization: Single-Component Initiation under Ambient Conditions. *J. Am. Chem. Soc.* **2019**, *141* (27), 10605–10609.

3.6 Experimental Section

3.6.1 Materials

For chain transfer agent synthesis, isobutyl vinyl ether (IBVE) (99%, TCI), 2,3-dihydrofuran (DHF) (99%, TCI), pyrrolidine (99%, Alfa Aesar) and diethylamine (99%, Alfa Aesar) were filtered through a plug of basic alumina prior to use. Carbon disulfide (CS_2) (99%, Fisher) was used as received. For most polymerization procedures, isobutyl vinyl ether (IBVE) (99%, TCI), 2,3-dihydrofuran (DHF) (99%, TCI), ethyl vinyl ether (EVE) (99%, TCI), *p*-methoxystyrene (MOS) (99%, Sigma Aldrich), 2-chloroethyl vinyl ether (Cl-EVE) (99%, Sigma Aldrich), and cyclopentyl methyl ether (CPME) (99%, TCI) were dried over calcium hydride (CaH_2) (ACROS organics, 93% extra pure, 0–2 mm grain size) for 12 hours, distilled under vacuum, and degassed by three freeze-pump-thaw cycles. For reactions set up under ambient conditions, IBVE was filtered through a plug of activated basic alumina to remove inhibitors prior to use. Sodium N,N-diethylcarbamate trihydrate (NaDTC) (98%, Alfa Aesar) was azeotropically dried with benzene. Ferrocene (FC) (98%, TCI), sodium sulfate (Na_2SO_4, anhydrous, Fisher), and alumina (activated, basic, Brockmann Grade I, 58 Ångstroms, Alfa Aesar) were used as received. Tetrabutylammonium perchlorate (Bu_4NClO_4) (98%, TCI) was purified by recrystallization from ethyl acetate three times, and dried in vacuo. Dichloromethane (DCM) and acetonitrile (MeCN) were purchased from J.T. Baker and was purified by purging with argon for 1 hour, followed by passing through two packed columns of neutral alumina under argon pressure.

Benzene (C6H6), hexanes, ethyl acetate (EtOAc), methanol (MeOH), and triethylamine (NEt_3) were purchased from Fischer Scientific and used as received. Alumina (1.0, 0.3, 0.05 µm pore size) was purchased from Extec. Reticulated vitreous carbon was purchased from ERG Aerospace. 2,4,6-tri-(p-methoxyphenyl)pyrylium tetrafluoroborate (PMP), Pentacarbomethoxycyclopentadiene (PCCP), hydrogen bond donor (HBD) tris(3,5-tris(trifluoromethyl)phenyl)thiophosphotriamide were synthesized according to literature procedures.[1–3]

3.6.2 General Electrochemical Cell and Electrode Setup

Preparation of Electrochemical Cell and Caps

Two-chambered electrochemical cells, separated by a fine frit and joined by a narrow passage above the volume of the reaction contents, were used for all electrochemical experiments. Ground glass joints (14/20) sealed with septa were used for addition of liquid reagents and held the electrodes.

Preparation of Reticulated Vitreous Carbon (RVC) Electrodes

The RVC electrodes were constructed by driving a 2 mm pencil lead through a 50 mm x 50 mm x 100 mm section of RVC. For use in the electrochemical cell, the other end of the pencil lead was inserted into the septa sealing the electrochemical cells. The pencil lead was cut to the desired length with a razor blade to maximize electrode surface area in contact with the reaction while allowing for space for magnetic stirring.

3.6.3 General Measurements

All polymer samples were analyzed using a Tosoh EcoSec HLC 8320 GPC system with two SuperHM-M columns in series at a flow rate of 0.350 mL/min. THF was used as the eluent and number-average molecular weights (M_n), weight-average molecular weights (M_w), and dispersities ($Đ$) for PIBVE and PDHF were determined by light scattering using a Wyatt miniDawn Treos multi-angle light scattering detector and a calculated dn/dc assuming 100% mass recovery. The reported M_ns for pEVE, pCl-EVE, and pMOS were calculated from refractive index chromatograms against TSKgel polystyrene standards. Nuclear magnetic resonance (NMR) spectra were recorded on a Varian 400 MHz, a Varian 600 MHz, or a Bruker 500 MHz instrument.

3.6.4 50-gram Scale Synthesis of tetrahydrofuran-2-yl pyrrolidine-1-carbodithioate (CTA-1)

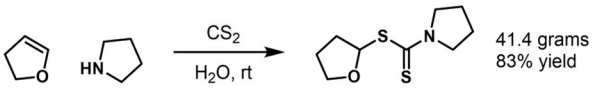

This synthesis was adapted from a previous literature procedure.[4] 150 mL of distilled H_2O was added to a 500 mL round bottom flask equipped with a large stir bar, an addition funnel, and septum. To this, pyrrolidine (18.9 mL, 0.23 mol, 1 equiv.) was added slowly under vigorous stirring. CS_2 (16.0 mL, 0.27 mol, 1.15 equiv.) was then added dropwise *via* the addition funnel. DHF (20.0 mL, 0.27 mol, 1.15 equiv.) was then added dropwise *via* addition funnel. The reaction was stirred vigorously overnight (19 hours). The organic and aqueous layers were separated in an addition funnel and the organic layer quickly solidified. This solid was then

dried under vacuum to remove starting material, yielding a crude mass of 43.3 grams, 87% yield. The crude product was then recrystallized in hexanes and ethyl acetate. It was noted previously that heating during recrystallization led to the formation of a yellow degradation product, so heat was not used when dissolving the product. The dissolved product was placed in a −30 °C freezer for 24 hours to facilitate crystal growth. The white crystals were then filtered and washed with cold hexanes. The product was then dried under vacuum to yield 41.4 grams of product, 83% isolated yield. The spectroscopic data for this compound were identical to those reported in the literature.[4] ^{1}H NMR (500 MHz, $CDCl_3$) δ 6.43 (dd, *J* = 7.2, 3.9 Hz, 1H), 4.03 – 3.86 (m, 4H), 3.72 – 3.63 (m, 1H), 3.61 – 3.52 (m, 1H), 2.47 (ddt, *J* = 13.9, 8.7, 7.1 Hz, 1H), 2.21 (dddd, *J* = 13.7, 7.9, 6.1, 3.9 Hz, 1H), 2.10 – 1.90 (m, 6H). ^{13}C NMR (126 MHz, $CDCl_3$) δ 191.32, 89.90, 77.29, 77.04, 76.78, 68.55, 54.41, 50.87, 32.11, 26.01, 24.95, 24.26.

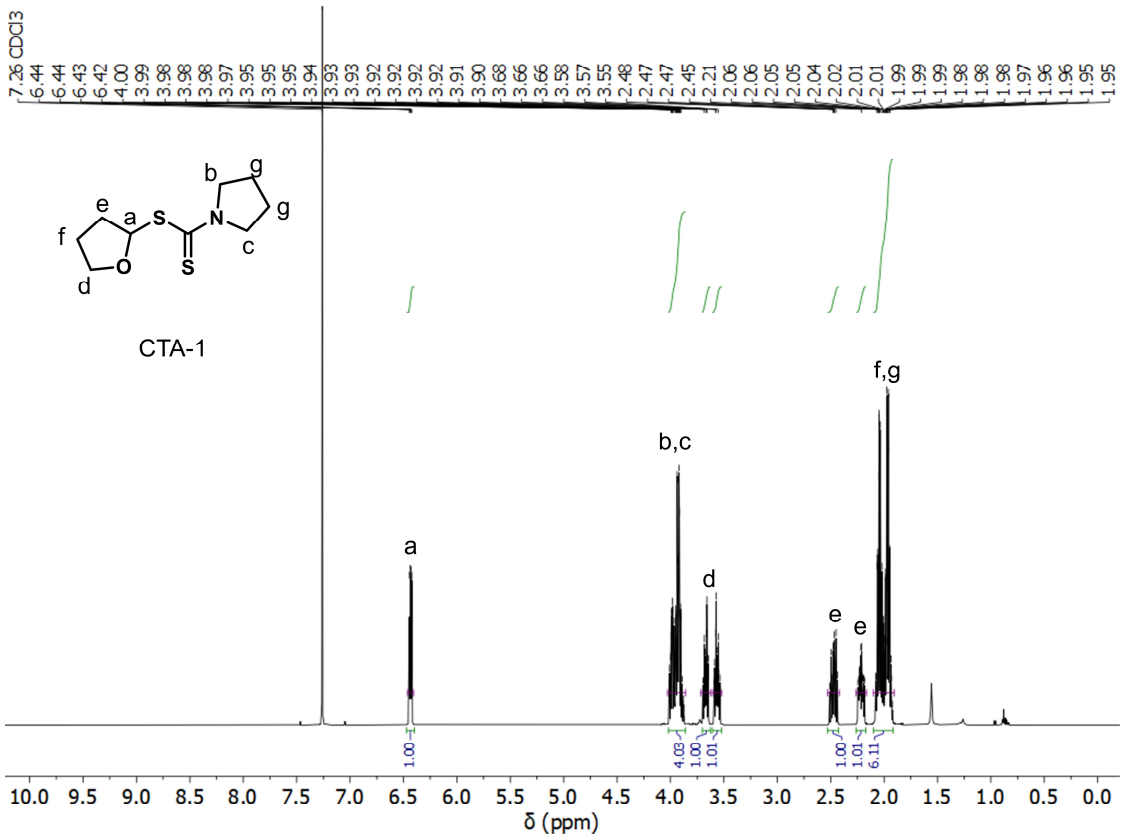

Figure 3.4: ^{1}H NMR of CTA-1 in $CDCl_3$.

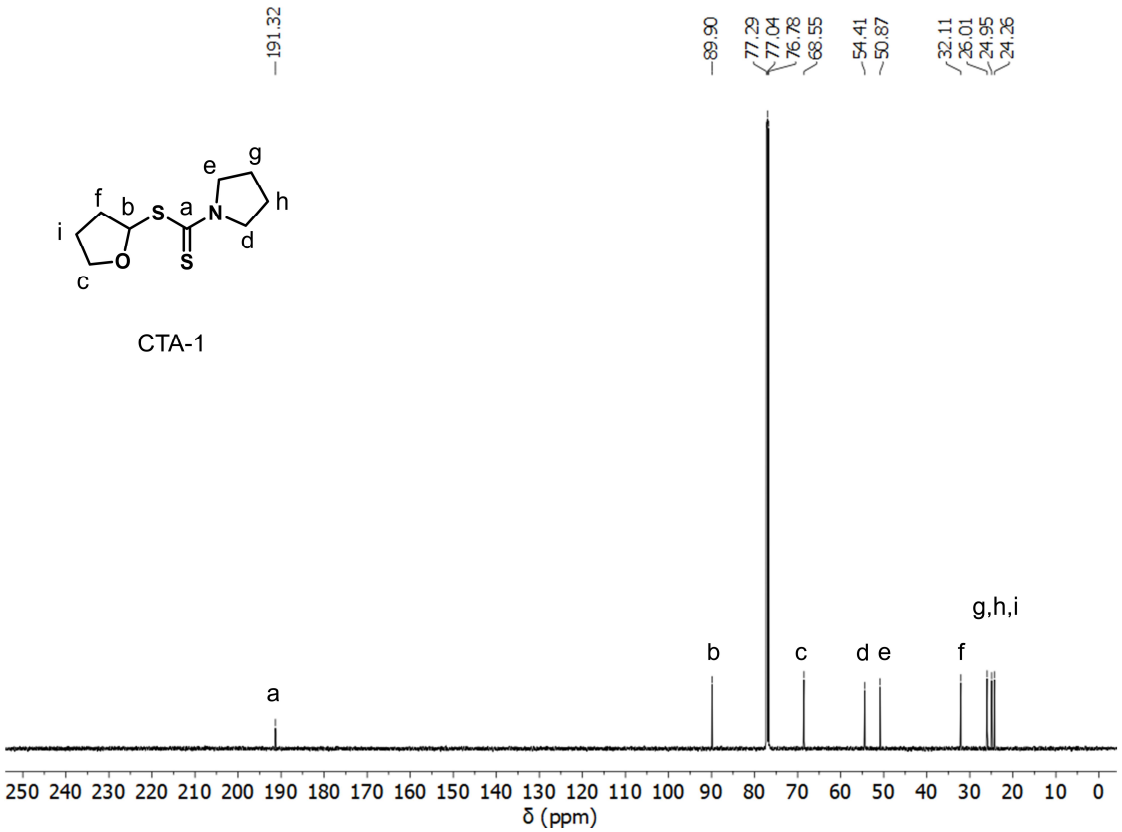

CTA-1

Figure 3.5: ^{13}C NMR of CTA-1 in $CDCl_3$.

3.6.5 Synthesis of S-1-isobutoxyethyl N,N-diethyl dithiocarbamate (CTA-2)

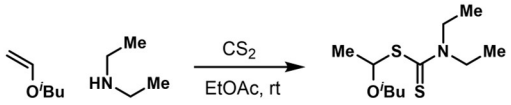

This synthesis was adapted from a previous literature procedure.[4] 10 mL ethyl acetate was added to a 20 x 125 mm threaded reaction tube equipped with a stir bar and sealed with a cap and Teflon septum. To this, pyrrolidine (0.52 mL, 5 mmol, 1 equiv.), CS_2 (0.36 mL, 6 mmol, 1.2 equiv.), and IBVE (0.78 mL, 6 mmol, 1.2 equiv.) were added, respectively. The reaction was then stirred vigorously overnight (24 hours). The reaction was extracted 3x with ~3 mL ethyl acetate. The combined organic layers were then washed with brine and dried over sodium sulfate before being filtered and concentrated *via* rotary evaporation. The crude

product was a yellow viscus oil. The product was purified by column chromatography using 10% ethyl acetate in hexanes. 405 mg (32% yield) of the pale-yellow product was isolated. The spectroscopic data for this compound were identical to those reported in the literature.[5] ^{1}H NMR (500 MHz, $CDCl_3$) δ 5.88 (q, *J* = 6.3 Hz, 1H), 4.09 – 3.94 (m, 2H), 3.82 – 3.68 (m, 2H), 3.46 (dd, *J* = 9.4, 6.9 Hz, 1H), 3.34 (dd, *J* = 9.4, 6.4 Hz, 1H), 1.92 – 1.80 (m, *J* = 6.7 Hz, 1H), 1.72 (d, *J* = 6.3 Hz, 3H), 1.27 (dt, *J* = 9.6, 7.0 Hz, 6H), 0.89 (d, *J* = 6.7 Hz, 6H).

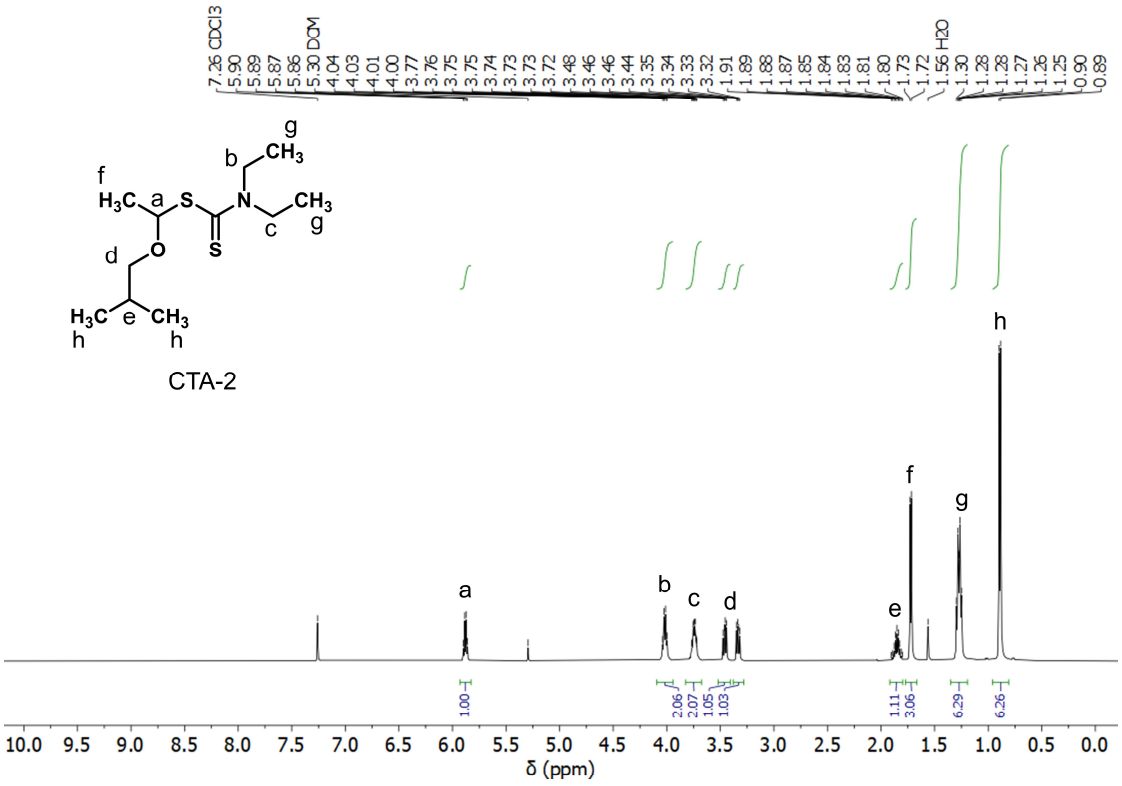

Figure 3.6: ^{1}H NMR of CTA-2 in $CDCl_3$.

3.7 Polymerization Procedures

3.7.1 Polymerization of IBVE with CTA-1 and $FcBF_4$ in DCM

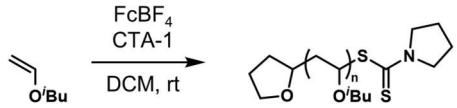

In a nitrogen glovebox, a dram vial equipped with a magnetic stir bar was charged with CTA-1 (0.02 mL, 0.5 M, 0.01 mmol, 1 equiv.) in DCM. IBVE (0.13 to 0.39 mL, 1 to 3 mmol, 100 to 300 equiv.) was then added, followed by 0.10 mL of 1 mg/mL $FcBF_4$ solution in DCM (0.2 µmol, 0.01 mol% to IBVE). The reaction was sealed with a Teflon-lined cap, then removed from the glove box and stirred for 4-18 hours. The reaction was terminated by the addition of 20 µL of 1 mg/mL NaDTC in 1:1 DCM:MeCN. 89 µL (1 mmol) of benzene was added as an internal standard. Aliquots were taken for ^{1}H NMR and GPC.

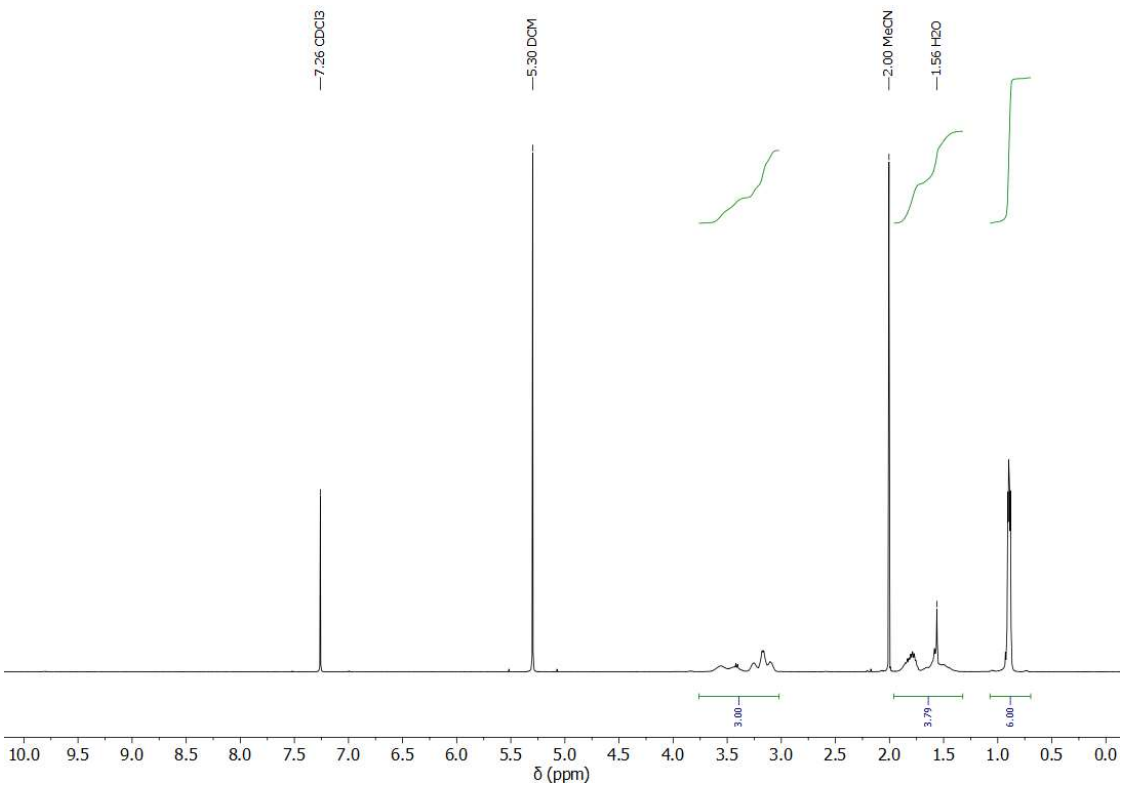

Figure 3.7: ^{1}H NMR of PIBVE in $CDCl_3$

3.7.2 Polymerization of EVE with CTA-1 and $FcBF_4$ in DCM

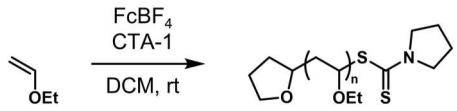

In a nitrogen glovebox, a dram vial equipped with a magnetic stir bar was charged with CTA-1 (0.03 mL, 0.5 M, 0.015 mmol, 1 equiv.) in DCM. EVE (0.19 mL, 2 mmol, 133 equiv.) was then added, followed by 0.05 mL $FcBF_4$ solution in DCM (0.2 µmol, 0.01 mol% to EVE). The reaction was sealed with a Teflon-lined cap, then removed from the glove box and stirred for 3.5 hours. The reaction was terminated by the addition of 20 µL of 1 mg/mL NaDTC in 1:1 DCM:MeCN. 89 µL (1 mmol) of benzene was added as an internal standard. Aliquots were taken for ^{1}H NMR and GPC.

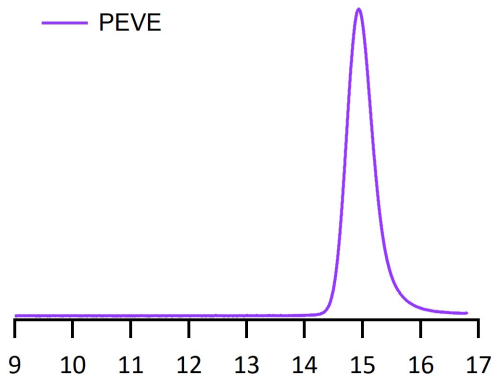

Figure 3.8: GPC trace of PEVE from Table 1, entry 4.

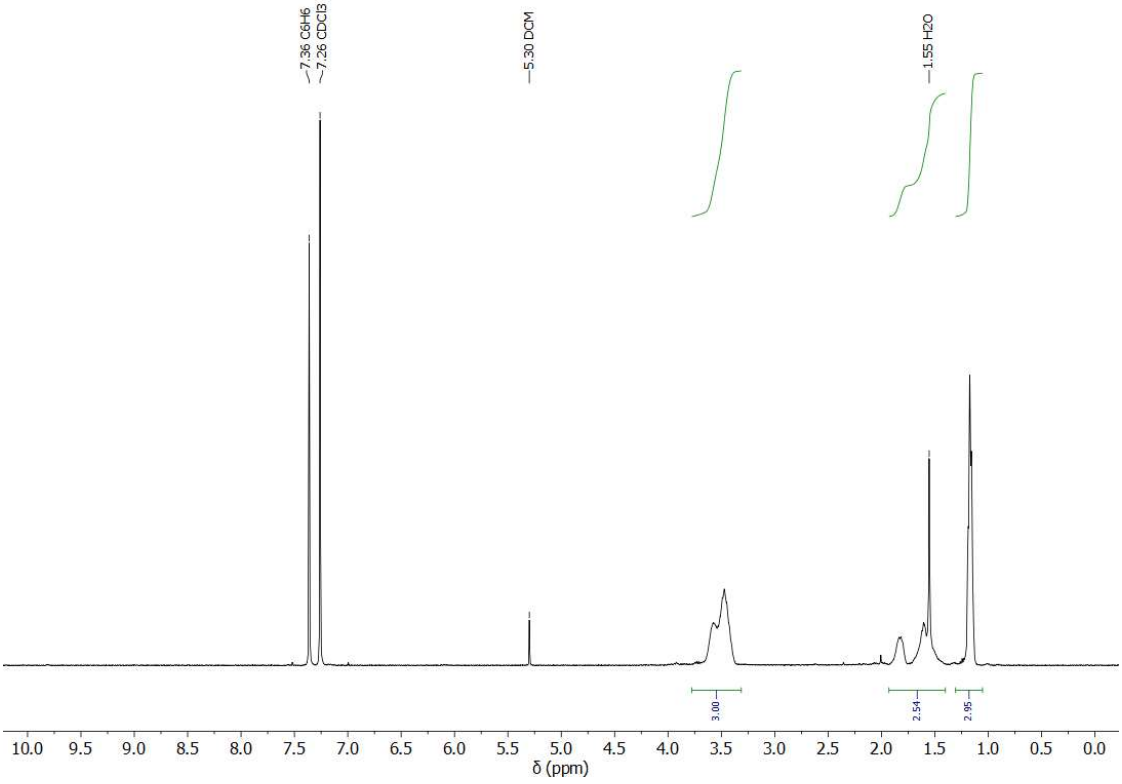

Figure 3.9: ^{1}H NMR of PEVE in $CDCl_3$

3.7.3 Polymerization of Cl-EVE with CTA-1 and $FcBF_4$ in DCM

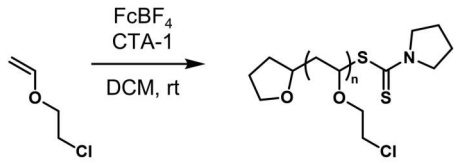

In a nitrogen glovebox, a dram vial equipped with a magnetic stir bar was charged with CTA-1 (0.04 mL, 0.5 M, 0.02 mmol, 1 equiv.) in DCM. Cl-EVE (0.20 mL, 2 mmol, 94 equiv.) was then added, followed by 0.15 mL $FcBF_4$ solution in DCM (0.5 µmol, 0.03 mol% to Cl-EVE). The reaction was sealed with a Teflon-lined cap, then removed from the glove box and stirred for 18 hours. The reaction was terminated by the addition of 20 µL of 1 mg/mL NaDTC in 1:1 DCM:MeCN. 89 µL (1 mmol) of benzene was added as an internal standard. Aliquots were taken for ^{1}H NMR and GPC.

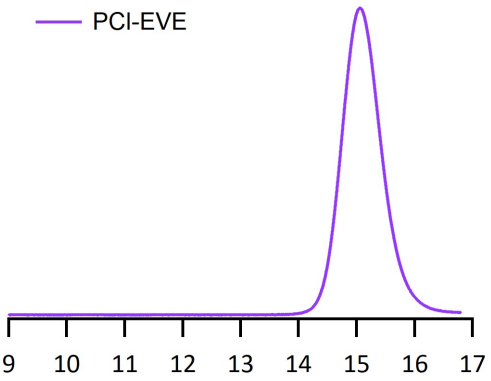

Figure 3.10: GPC trace of PCl-EVE from Table 1, entry 5.

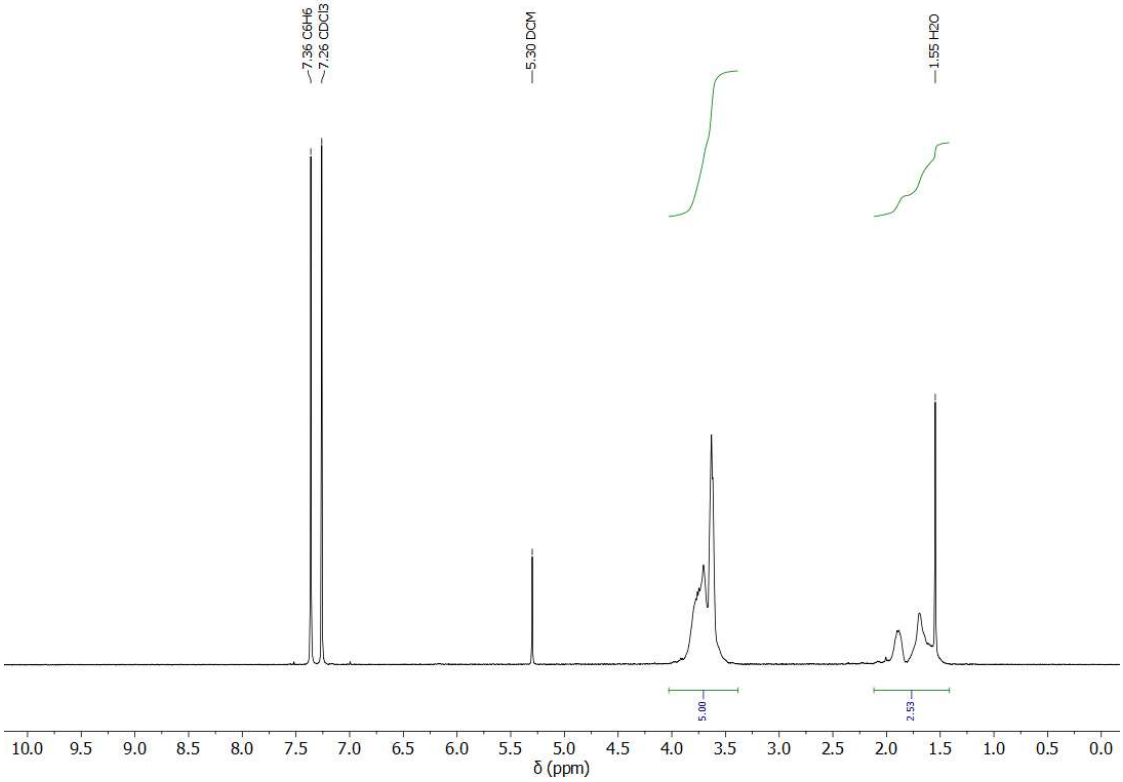

Figure 3.11: ^{1}H NMR of PCl-EVE in $CDCl_3$

3.7.4 Polymerization of MOS with CTA-1 and $FcBF_4$ in DCM

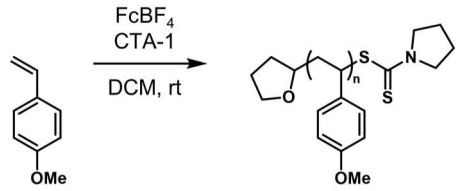

In a nitrogen glovebox, a dram vial equipped with a magnetic stir bar was charged with CTA-1 (0.04 mL, 0.5 M, 0.02 mmol, 1 equiv.) in DCM. MOS (0.20 mL, 1.5 mmol, 75 equiv.) was then added, followed by 0.20 mL $FcBF_4$ solution in DCM (0.7 µmol, 0.05 mol% to MOS). The reaction was sealed with a Teflon-lined cap, then removed from the glove box and stirred for 24 hours. The reaction was terminated by the addition of 20 µL of 1 mg/mL NaDTC in 1:1 DCM:MeCN. 89 µL (1 mmol) of benzene was added as an internal standard. Aliquots were taken for ^{1}H NMR and GPC.

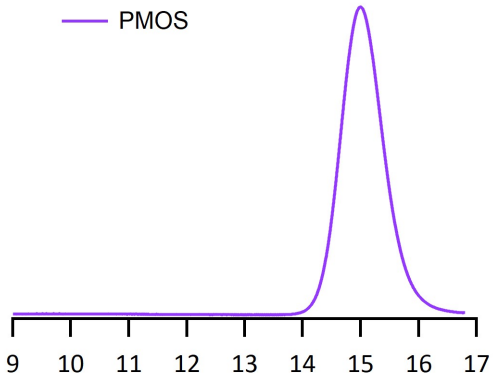

Figure 3.12: GPC trace of PMOS from Table 1, entry 6.

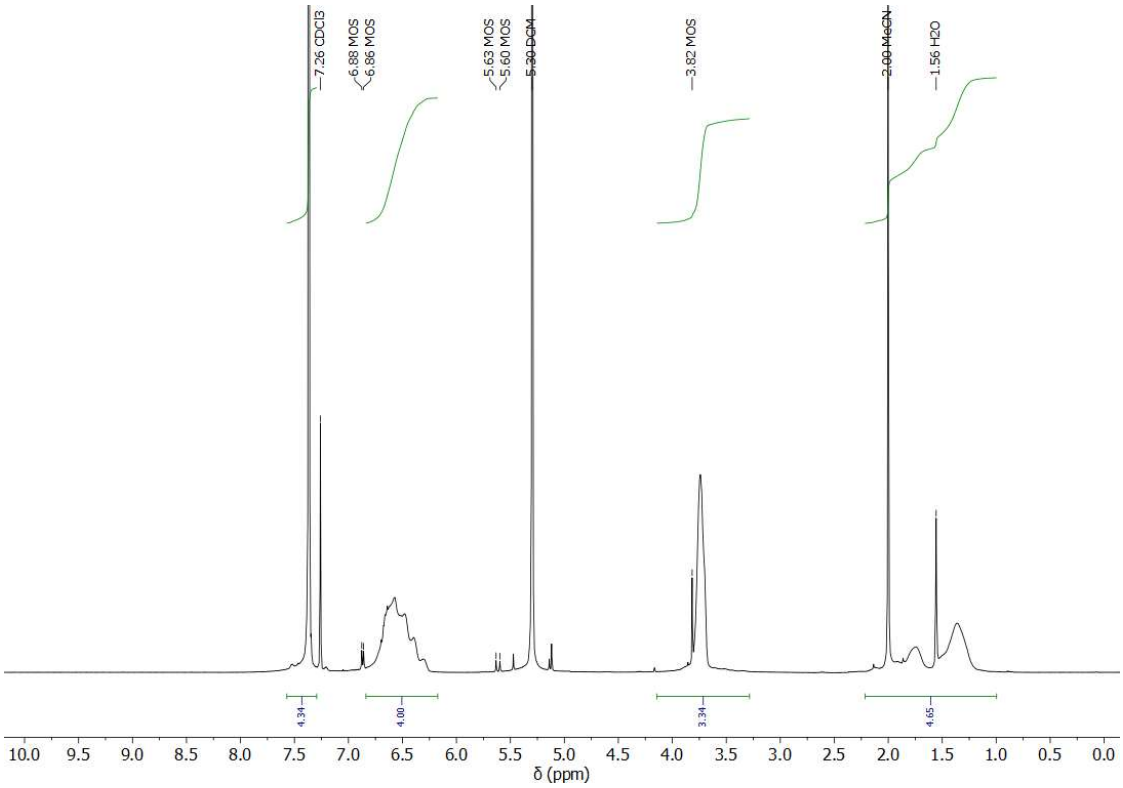

Figure 3.13: ^{1}H NMR of PMOS in $CDCl_3$

3.7.5 Polymerization of DHF with CTA-1 and $FcBF_4$ in DCM

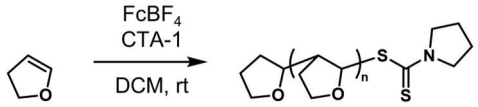

In a nitrogen glovebox, a dram vial equipped with a magnetic stir bar was charged with CTA-1 (0.06 mL, 0.5 M, 0.028 mmol, 1 equiv.) in DCM. DHF (0.32 mL, 4.3 mmol, 143 equiv.) was then added, followed by 0.08 mL $FcBF_4$ solution in DCM (0.3 µmol, 0.01 mol% to DHF) and an additional 0.18 mL DCM. The reaction was sealed with a Teflon-lined cap, then removed from the glove box and stirred for 20 minutes. The reaction was terminated by the addition of 20 µL of 1 mg/mL NaDTC in 1:1 DCM:MeCN. 89 µL (1 mmol) of benzene was added as an internal standard. Aliquots were taken for ^{1}H NMR and GPC.

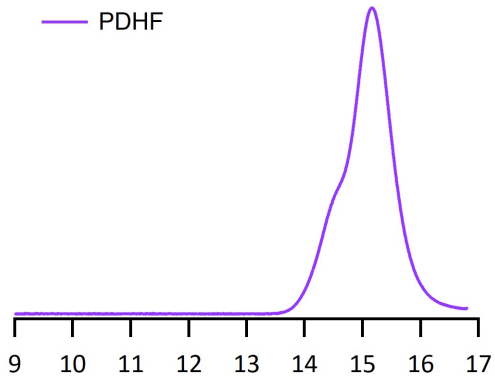

Figure 3.14: GPC trace of PDHF from Table 1, entry 7.

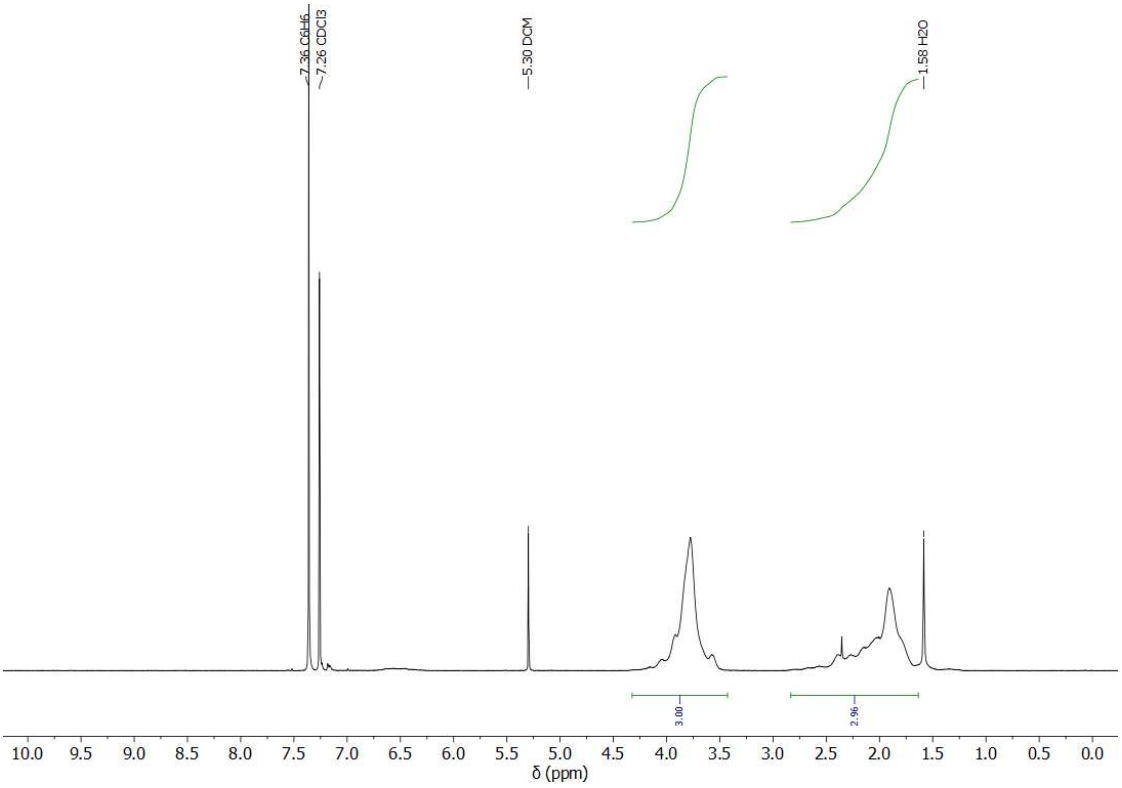

Figure 3.15: ^{1}H NMR of PMOS in $CDCl_3$

3.7.6 Polymerization of IBVE with CTA-1 and $FcBF_4$ in CPME

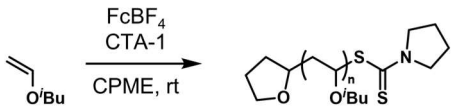

In a nitrogen glovebox, a dram vial equipped with a magnetic stir bar was charged with CTA-1 (0.02 mL to 0.04 mL, 0.5 M, 0.01 to 0.02 mmol, 1 equiv.) in CPME. IBVE (0.13 to 0.52 mL, 1 to 4 mmol, 100 to 400 equiv.) was then added, followed by $FcBF_4$ (0.1 mg to 0.2 mg, 0.4 to 0.8 µmol, 0.02 mol% to IBVE) and 0.10 to 0.22 mL. The reaction was sealed with a Teflon-lined cap, then removed from the glove box and stirred for 18 hours. The reaction was terminated by the addition of 20 µL of 1 mg/mL NaDTC in 1:1 DCM:MeCN. 89 µL (1 mmol) of benzene was added as an internal standard. Aliquots were taken for ^1H NMR and GPC.

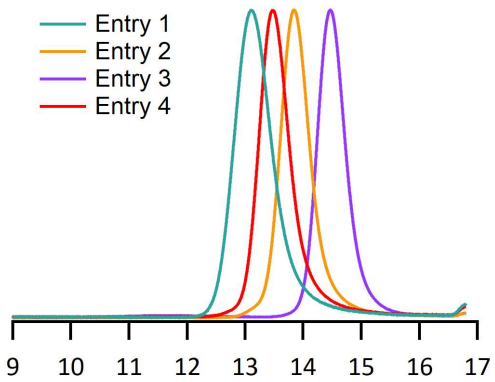

Figure 3.16: GPC traces of PIBVE from Table 2.

3.7.7 Procedure for Ferrocene-Mediated Electrochemically Controlled Cationic Polymerization of IBVE

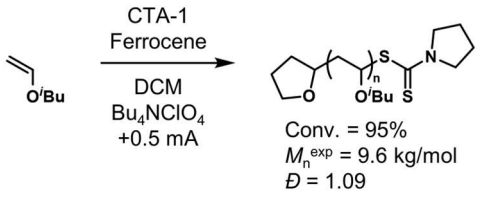

To an oven dried electrochemical cell, a magnetic stir bar was added to both the working and counter compartment. The cell was equipped with a reticulated vitreous carbon (RVC) anode and RVC cathode and then sealed with the rubber septa. The electrochemical cell was then evacuated and backfilled with positive pressure of nitrogen. Once the electrochemical cell had cooled to room temperature, ferrocene (6.0 mg, 0.032 mmol, 0.2 mol% relative to IBVE) and CTA-1 (35.0 mg, 0.16 mmol, 1 equiv.) were added to the working compartment and Bu_4NClO_4 (171 mg, 0.60 mmol) was added to both the working and counter compartments. The cell was then evacuated and backfilled with positive pressure of nitrogen three times. Then the working compartment was charged with IBVE (2.1 mL, 16 mmol, 100 equiv.) and DCM to bring the total volume to 5.0 mL. The counter compartment was charged with 5.0 mL of DCM. The leads of the DC power supply were connected to the electrodes. Stirring began and an anodic current (0.5 mA) was applied for 30 min, and the reaction was left to stir for 1 h. Aliquots taken by syringe under a blanket of N_2 and were then analyzed by NMR and GPC.

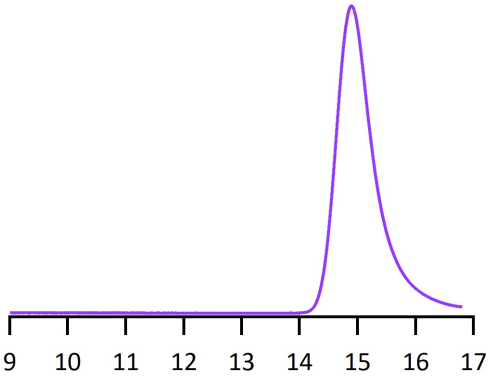

Figure 3.17: GPC trace of PIBVE produced electrochemically.

3.7.8 Procedure for Photocontrolled Cationic Polymerization of IBVE

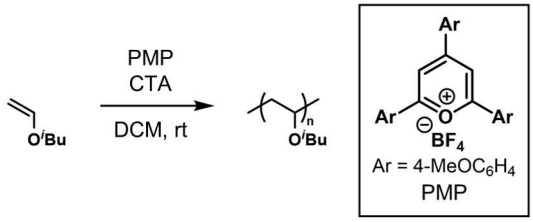

In a nitrogen glovebox, a dram vial equipped with a magnetic stir bar was charged with CTA-1 or CTA-2 (0.04 mL, 0.5 M, 0.02 mmol, 1 equiv.) in DCM. IBVE (0.26 mL, 2 mmol, 100 equiv.) was then added, followed by PMP (0.20 mL, 1mg/mL, 0.2 µmol, 0.01 mol% to IBVE). The reaction was sealed with a Teflon-lined cap, then removed from the glove box and stirred for 4-18 hours. The reaction was terminated by the addition of 20 µL of 1 mg/mL NaDTC in 1:1 DCM:MeCN. 89 µL (1 mmol) of benzene was added as an internal standard. Aliquots were taken for ^{1}H NMR and GPC. The polymerization performed with CTA-1 reached 81% conversion and produced an 8.1 kg/mol polymer with $Đ$ = 1.16. The polymerization performed with CTA-2 reached 99% conversion and produced a 10.5 kg/mol polymer with $Đ$ = 1.07.

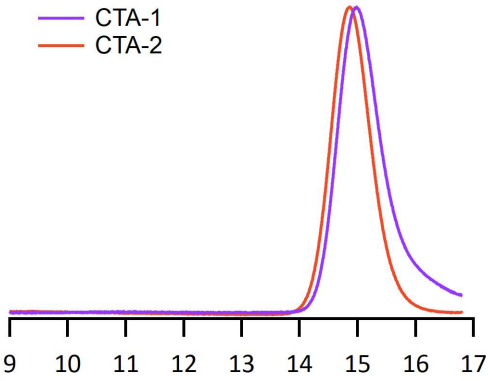

Figure 3.18: GPC traces of PIBVE produced by photochemistry.

3.7.9 Procedure for Ambient Cationic Polymerization

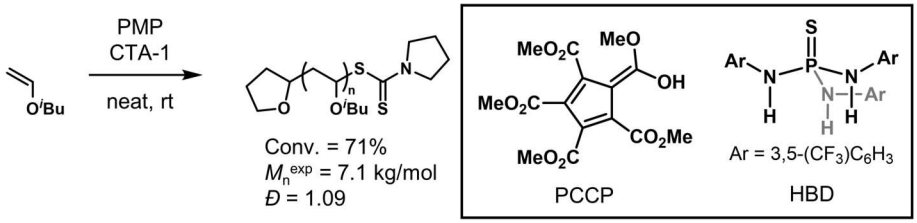

A dram vial equipped with a magnetic stir bar was charged with CTA-1 (12 mg, 0.056 mmol, 1 equiv.), PCCP (1.0 mg, 2.8 µmol, 0.05 equiv.), and HBD (2.0 mg, 2.8 µmol, 0.05 equiv.). IBVE (0.73 mL, 5.6 mmol, 100 equiv.) was then added. The reaction was sealed with a Teflon-lined cap and stirred for 4.5 hours. The reaction was terminated by the addition of 20 µL of 1 mg/mL NaDTC in 1:1 DCM:MeCN. 89 µL (1 mmol) of benzene was added as an internal standard. Aliquots were taken for ^{1}H NMR and GPC.

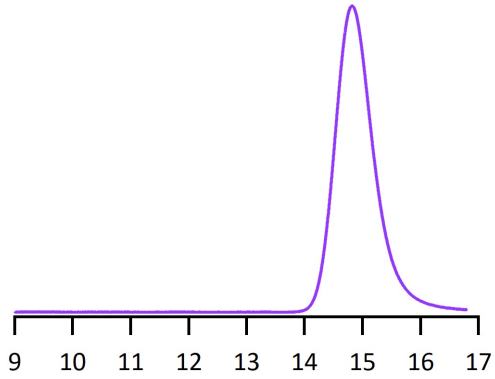

Figure 3.19: GPC trace of PIBVE produced under ambient conditions.

3.7.10 Procedure for Temporally Controlled Electrochemical Cationic Polymerization of IBVE

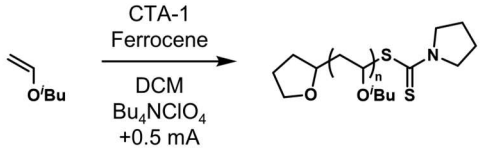

To an oven dried electrochemical cell, a magnetic stir bar was added to both the working and counter compartment. The cell was equipped with a reticulated vitreous carbon (RVC) anode and RVC cathode and then sealed with the rubber septa. The electrochemical cell was then evacuated and backfilled with positive pressure of nitrogen. Once the electrochemical cell had cooled to room temperature, ferrocene (4.7 mg, 0.025 mmol, 0.2 mol% relative to IBVE) and CTA-1 (28 mg, 0.13 mmol, 1 equiv.) were added to the working compartment and Bu_4NClO_4 (137 mg, 0.40 mmol) was added to both the working and counter compartments. The cell was then evacuated and backfilled with positive pressure of nitrogen three times. Then the working compartment was charged with IBVE (1.7 mL, 13 mmol, 100 equiv.) and DCM to bring the total volume to 4.0 mL. The

counter compartment was charged with 4.0 mL of DCM. The leads of the DC power supply were connected to the electrodes. Stirring began and 0.5 mA of anodic current (+) was then applied for 15 minutes to initiate polymerization. The reaction was allowed to continue for 15 minutes. To turn off polymerization, a 0.5 mA cathodic current (−) was applied for 15 minutes. After a 30 minute "off" period, no monomer conversion was observed, and the polymerization was reinitiated with a 15-minute, 0.5 mA anodic pulse. The polymerization proceeded for 30 minutes before a final 15-minute; 0.5 mA cathodic pulse was applied to stop the polymerization. Another aliquot taken 30 minutes later confirmed the polymerization had stopped. Aliquots taken by syringe under a blanket of N2 and were then analyzed by NMR and GPC.

Table 3.3: Temporally Controlled Electrochemical Polymerization of IBVE

Aliquot	Time (min)	Conv. (%)	M_n^{theo} (kg/mol)	M_n^{exp} (kg/mol)	$Đ$
1	45	23	2.3	2.4	1.08
2	75	23	2.3	2.4	1.17
3	135	42	4.2	3.9	1.17
4	165	42	4.2	3.9	1.22

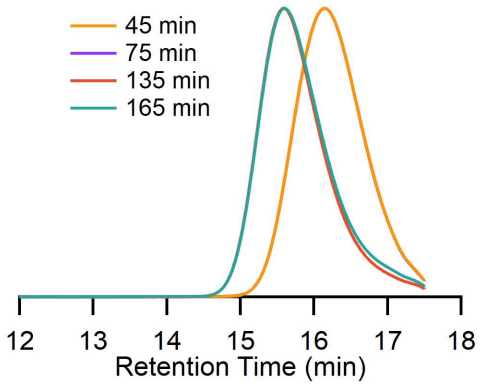

Figure 3.20: GPC traces from the temporally controlled electrochemical polymerization of IBVE

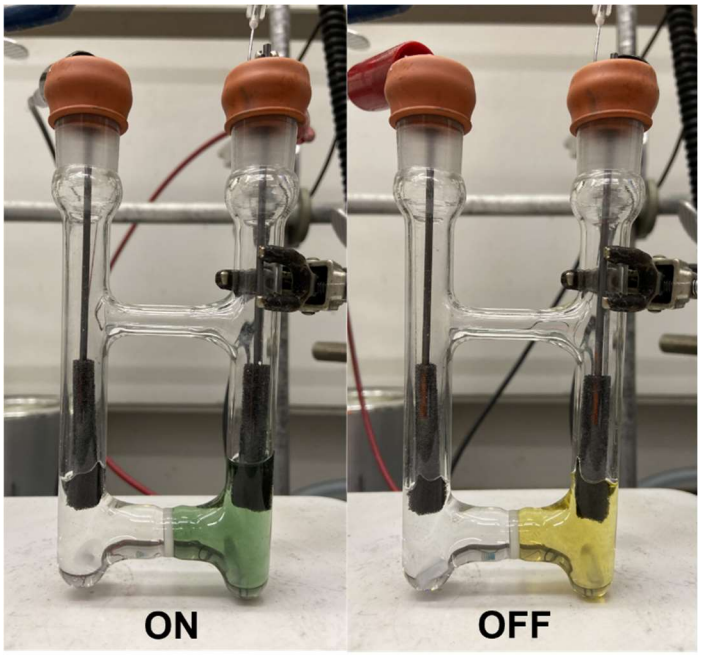

Figure 3.21: Images of electrochemical polymerization setup during “on” and “off” pulses

3.8 Cyclic Voltammetry of Chain Transfer Agents

Cyclic voltammetry experiments were performed using a Bio-Logic SP-50 Potentiostat at ambient temperature under an ambient atmosphere. A typical electrochemical cell consisted of a three-electrode setup using a glassy carbon working electrode, a platinum wire counter electrode,and a Ag/AgCl reference electrode. All electrochemical experiments in DCM were performed with 0.1 M tetrabutylammonium perchlorate (Bu_4NClO_4) as supporting electrolyte. The glassy carbon working electrode was polished between each scan. All potentials recorded in DCM are referenced to Ag/Ag^+ redox couple (0.0V).

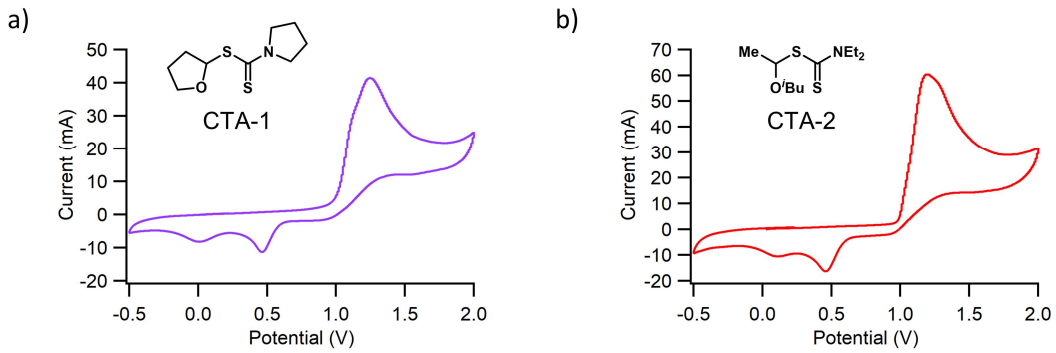

Figure 3.22: Cyclic voltammograms of CTA-1 (a) and CTA-2 (b)

Table 3.4: Oxidation and reduction peaks from cyclic voltammograms of CTAs

CTA	Oxidation (V)	Reduction 1 (V)	Reduction 2(V)
CTA-1	1.24	0.46	0.0
CTA-2	1.20	0.45	-0.1

References

(1) Martiny, M.; Steckhan, E.; Esch, T. Cycloaddition Reactions Initiated by Photochemically Excited Pyrylium Salts. *Chem. Ber.* **1993**, *126* (7), 1671–1682.

(2) Kottisch, V.; O'Leary, J.; Michaudel, Q.; Stache, E. E.; Lambert, T. H.; Fors, B. P. Controlled Cationic Polymerization: Single-Component Initiation under Ambient Conditions. *J. Am. Chem. Soc.* **2019**, *141* (27), 10605–10609.

(3) Kottisch, V.; Jermaks, J.; Mak, J.-Y.; Woltornist, R. A.; Lambert, T. H.; Fors, B. P. Hydrogen Bond Donor Catalyzed Cationic Polymerization of Vinyl Ethers. *Angew. Chemie Int. Ed.* **2021**, *60* (9), 4535–4539.

(4) Halimehjani, A. Z.; Marjani, K.; Ashouri, A. Synthesis of Dithiocarbamate by Markovnikov Addition Reaction in Aqueous Medium. *Green Chem.* **2010**, *12* (7), 1306–1310.

(5) Kottisch, V.; Michaudel, Q.; Fors, B. P. Cationic Polymerization of Vinyl Ethers Controlled by Visible Light. *J. Am. Chem. Soc.* **2016**, *138* (48), 15535–15538.

Chapter 4

Poly(2,3-dihydrofuran): A strong, biorenewable, and degradable thermoplastic synthesized via room temperature cationic polymerization

4.1 Abstract

The development of economically viable biorenewable plastics is often hindered by the production and availability of chemical feedstocks as well as the efficiency of monomer synthesis. There exists the additional challenge of creating strong and tough materials from these sustainable sources. Herein, we demonstrate the utility of 2,3-dihydrofuran (DHF), a monomer synthesized in one step from 1,4-butanediol, a bioalcohol already produced on plant scale. In a single-component, metal-free, and ambient temperature cationic polymerization, we produced poly(2,3-dihydrofuran) (PDHF) with molecular weights of up to 256 kg/mol. We further characterized material properties, establishing high molecular weight PDHF as a strong thermoplastic with high tensile strength and toughness (70 and 14 MPa, respectively) comparable to commercial polycarbonate (63 and 22 MPa, respectively). PDHF films were evaluated, revealing high optical clarity and good barrier properties to oxygen, carbon dioxide, and water, making the material amenable for food packaging applications. Finally, we developed a facile method for the accelerated oxidative degradation of PDHF into oligomers, suggesting potential for further development of end-of-life solutions.

4.2 Introduction

The annual production of plastics exceeded 381 million metric tons in 2015.[1] With ninety percent of polymers produced from petroleum feedstocks, plastics are projected to account for 20% of annual petroleum consumption by 2050 without intervention. To reduce the carbon footprint and oil consumption of the plastics industry, there is a concerted effort to generate sustainable materials from biomass. In a recent review, Hillmyer and coworkers summarized three grand challenges of sustainable polymers: "The polymers of tomorrow should be derived from sustainable resources, should be highly effective in their intended use, and should offer sustainable solutions after use."[2] We envision that poly(2,3-dihydrofuran) (PDHF) is an excellent candidate to meet these aims, given that it can be sourced from a bioalcohol, provides a strong and tough thermoplastic, and can be degraded back to small molecules for potential biodegradation or chemical recycling (Figure 4.1). However, efficient polymerization of PDHF to high molecular weight has proven difficult, and no comprehensive study of its material properties has been reported.

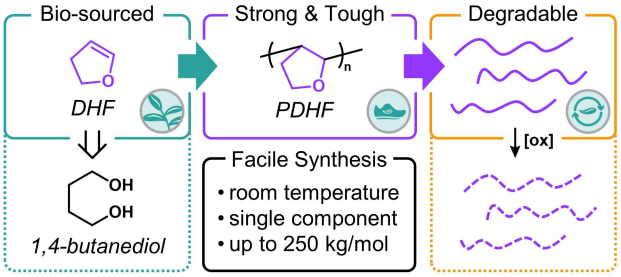

Figure 4.1: Poly(2,3-dihydrofuran) as a strong, tough, and degradable thermoplastic sourced sustainably from a bioalcohol

Bioalcohols represent a largely untapped resource in the production of biorenewable plastics. Several alcohols are already produced on plant scale from biomass for use as transportation fuel. In 2019 the United States produced 15.7 billion gallons of bio-ethanol and 1 million gallons of bio-isobutanol, and recently, Novamont and Genomatica built the first plant dedicated to production of 1,4-butanediol from biomass.[3,4] In recognizing the facile methods available to transform biorenewable alcohols into vinyl ether monomers, we were inspired by the one-step cyclization of 1,4-butanediol to generate 2,3-dihydrofuran (DHF) developed by Leite and coworkers.[5,6] Based on our previous work in which we incorporated this monomer as the glassy block of sustainable thermoplastic elastomers, we hypothesized that achieving high molecular weight (M_n) PDHF would produce a strong and tough thermoplastic.[7]

DHF has captured the interest of polymer chemists since the 1950s.[8] This cyclic vinyl ether results in a polymer with a restricted backbone, leading to a material with a high glass transition temperature (T_g) of ~135 °C. Higashimura and coworkers published the first controlled polymerization of DHF using iodine as an initiator at −40 °C.[9] Sanda and Matsumoto implemented a Lewis acid initiator to obtain a controlled polymerization at −78 °C and characterized the relationship between PDHF diastereoselectivity and T_g.[10,11] More recently, Aoshima and coworkers published a base-stabilized method that resulted in a controlled polymerization at 0 °C.[12] Tangentially, Xia and coworkers showed that ring opening metathesis polymerization (ROMP) of DHF produced a rubbery poly(enol ether)

that could be depolymerized back to monomer or acid-degraded to small molecules.[13] Overall, this extensive interest in DHF is underlined by the various patents issued for the synthesis and application of PDHF as a degradable fiber and thermoplastic.[14–28] Despite these many advances, all methods require low temperatures and low monomer concentrations, resulting in substantial energy and solvent costs at plant scale. In addition to these drawbacks, only low molecular weight (M_n) PDHF has been produced, leaving the material properties of high M_n PDHF unknown. Thus, the development of an energy- and solvent-efficient controlled polymerization for high M_n PDHF remains a challenge.

Previous Lewis acid methods for controlled cationic polymerizations required low temperatures, likely to reduce reactivity and counteract exothermal heat generation and chain transfer.[9,12] We recently demonstrated pentakis-(methoxycarbonyl)cyclopentadiene (PCCP) could initiate controlled polymerization of vinyl ethers under ambient conditions.[29] PCCP is a readily available, highly acidic reagent which provides a unique reactivity profile due to its extended carbanionic π-system. We hypothesized the strong coordination of the cyclopentadienyl anion to the propagating oxocarbenium chain end directed monomer addition and prevented termination from adventitious nucleophiles while tempering the reactivity of the chain end, allowing for room temperature polymerization. We posited that this new method could allow us to synthesize and characterize the properties of high M_n PDHF for the first time.

Herein, we disclose the metal-free, room temperature synthesis of high molecular weight PDHF. Our polymerization method utilizes PCCP to target molecular weights from 20 to 250 kg/mol. Tensile characterization of PDHF demonstrated high ultimate tensile strength of up to 70 MPa, and high molecular weight samples achieved high toughness of up to 14 MPa. In addition, we produced optically transparent films with low gas and water permeability. As an end-of-life solution, we developed a facile degradation of PDHF under oxidizing conditions. This comprehensive study of PDHF provides a green method for the production of a strong and tough high T_g thermoplastic from a readily available bioalcohol feedstock and provides an end-of-life strategy for this material.

4.3 Results and Discussion

4.3.1 Room-temperature, Single-component Polymerization of Poly(2,3-dihydrofuran)

Our initial studies focused on the polymerization of DHF using PCCP as the initiator (Figure 4.2). Mixing PCCP and DHF in a 1:290 ratio in DCM resulted in 99% conversion of the monomer after 2 h at room temperature to yield a 24.2 kg/mol polymer with a narrow dispersity (*Đ*) of 1.23 (Table 4.1, entry 1). Critically, the experimental (24 kg/mol) and theoretical (20.0 kg/mol) molar masses were in good agreement, suggesting that each PCCP led to a polymer chain and providing evidence that significant chain transfer was not occurring. By varying the ratio of the monomer to initiator we successfully targeted a wide range of molar masses up to 256 kg/mol (Table 4.1, entries 1-6)—these high molar mass samples are an

order of magnitude larger than what has been obtained by previous methods and, importantly, are still polymerized at room temperature. We found when targeting molecular weights above 100 kg/mol, the distributions did broaden slightly (Figure 4.3); however, good agreement between theoretical and experimental M_ns were still maintained.† Notably, this method was also amenable to large scale polymerizations and we were able to successfully produce a 250 kg/mol PDHF on a 14 g scale with an isolated yield of 95% (Table 4.1, entry 6).

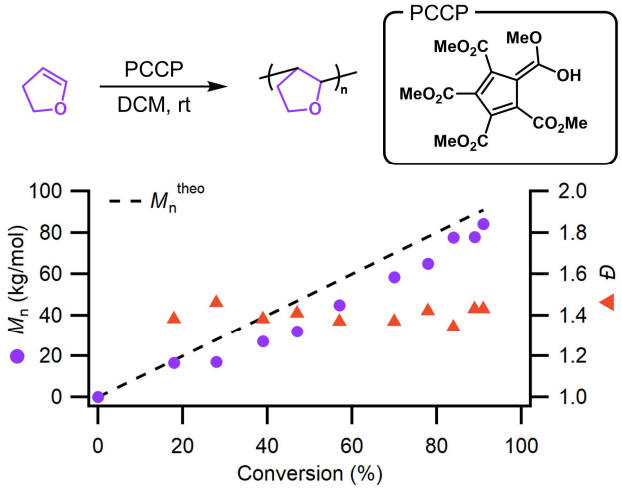

Figure 4.2: M_n of PDHF increases linearly with conversion.

Table 4.1: Controlled polymerization of PDHF to high M_n using PCCP initiator.

Entry	[PCCP]:[DHF]:[HBD]	Solvent [e]	Time (h)	Conversion [f]	M_n^{theo} (kg/mol)	M_n^{exp} (kg/mol) [g]	$Đ$
1[a]	1:290:0	DCM	2	99%	20.0	24.2	1.23
2[a]	1:572:0	DCM	4	94%	37.6	37.9	1.27
3[a]	1:1420:0	DCM	17.5	99%	100	99.0	1.50
4[b]	1:2140:0	DCM	19.5	94%	142	140	1.51
5[b]	1:3570:0	DCM	26	99%	250	237	1.49
6[c]	1:3530:0	DCM	22	99%	248	256	1.62
7[d]	1:3570:0	CPME	168	39%	97.5	82.3	2.16
8[d]	1:3570:1	CPME	77	91%	229	214	1.42
9[d]	1:1427:1	CPME	23	96%	96.0	89.2	1.61
10[d]	1:713:1	CPME	3	85%	42.5	40.5	1.31

[a]40 mmol DHF [b]60 mmol DHF [c]200 mmol DHF [d]30 mmol DHF [e][DHF] = 6.7M [f]Conversion calculated from 1H NMR. [g]M_n and $Đ$ determined by light scattering.

Our initial results suggested that the polymerization of DHF was proceeding

through a chain-growth process with living characteristics. To further support this suggestion, we monitored a polymerization by NMR and gel permeation chromatography (Figure 4.2). As expected, we saw linear growth in the molar mass of the polymer relative to conversion (Figure 4.3).

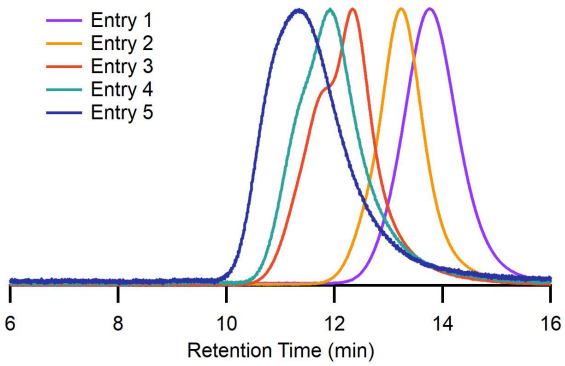

Figure 4.3: GPC traces of polymers listed in Table 1, Entry 1-5.

We next sought to improve the sustainability of our method by employing a green solvent in place of halogenated DCM. We have observed the solubility of PDHF in tetrahydrofuran (THF), but this is not an effective solvent for cationic polymerizations because it degrades by ring-opening under acidic conditions. In addition, THF readily forms peroxides adding risk to large scale reactions. Cyclopentyl methyl ether (CPME) has recently captured attention in process chemistry as an alternative to THF and other ether solvents (Figure 4.4).[30,31] Watanabe and coworkers reported CPME does not readily form peroxides like other ethers and exhibits low toxicity.[32] In addition, its high boiling point and low energy of vaporization are favorable for solvent recovery. Because CPME has similar solubility properties to THF and is stable to acidic conditions, we hypothesized CPME would be an effective substitute for DCM.

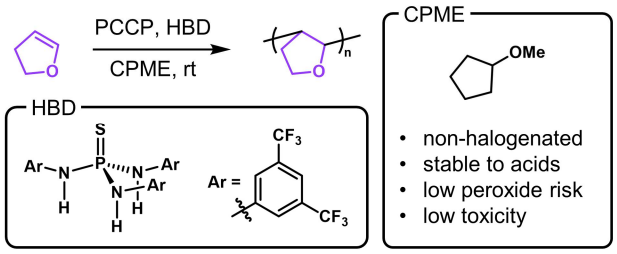

Figure 4.4: Hydrogen bond donor (HBD) enables polymerization of DHF in the green solvent cyclopentyl methyl ether (CPME).

We first attempted a polymerization targeting 250 kg/mol with our standard conditions in CPME. This reaction reached only 39% conversion after 168 h, yielding an 82 kg/mol polymer with a broad dispersity of 2.16 (Table 4.1, entry 7). We attributed the slow rate of polymerization to the lower polarity of the solvent leading to a stronger interaction between the PCCP anion and polymer chain end. To overcome this limitation, we took inspiration from our recent report that demonstrated the addition of a hydrogen bond doner catalyst, tris(3,5-bis(trifluoromethyl)phenyl)thiophosphotriamide (HBD), increases the reaction rate of PCCP-promoted reactions and reduces chain transfer (Figure 4.4). Addition of an equivalent of HBD relative to PCCP led to 91% conversion after 77 h and yielded a 214 kg/mol PDHF sample with a narrow dispersity ($Đ$ = 1.42) and good agreement between experimental and theoretical molar masses (Table 4.1, entry 8). We then extended this strategy to target various molar masses while maintaining excellent control over the polymerization (Table 4.1, entries 9 and 10). We propose that the HBD effectively weakens the association of the PCCP anion with the oxocarbenium ion chain end to enable the use of the less polar CPME solvent as a green alternative to DCM.

4.3.2 Tensile Properties

We hypothesized that PDHF had not seen widespread use because the low molar mass polymers that had previously been made led to brittle materials. We posited that by accessing higher molar mass samples of PDHF we could increase the toughness and thus gain access to a material with highly desirable properties. Using the polymers synthesized with our new method (*vida supra*), we tested the tensile properties of PDHF samples with M_ns ranging from 53 – 198 kg/mol (Table 4.2). Dogbone tensile bars were subjected to uniaxial tensile stress at a rate of 2 mm min^{-1}. All the PDHF samples demonstrated high ultimate tensile strength (UTS), ranging from 65 to 70 MPa. Significantly, we found that high molecular weight samples exhibited a definitive yield event, or neck, and subsequent cold-drawing phase (Figure 4.5, *photo inset*). This drawing behavior dramatically increased strain-at-break up to 52% (PDHF-198), which improved the toughness to a maximum of 14 MPa. Interestingly, strain hardening was not observed, and the polymer failed before full propagation of the neck through the entire gauge length. This behavior is indicative of unstable crazing leading to premature failure during the cold-drawing.[33–35] We hypothesize that the addition of plasticizing agents could stabilize this cold-drawing behavior and further improve both strain-at-break and toughness.

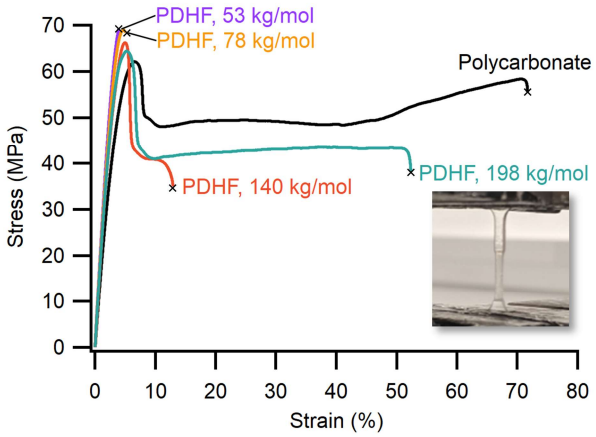

Figure 4.5: Stress-strain curves for PDHF samples compared to PC at a strain rate of 2 mm min^{-1} to failure, indicated by x.

Encouraged by the tensile properties displayed by PDHF-198, we compared it to a benchmark commercial polymer known for strength and toughness. Hence, a 45 kg/mol poly(bisphenol A carbonate) (PC-45) sample was prepared and tested under the same conditions (Table 4.2, Figure 5). Notably, the yield strength of PDHF-198 was comparable to PC-45 (65 vs. 63 MPa, respectively). The strain-at-break for PC-45 exceeded that of PDHF-198 and the PC-45 sample underwent strain hardening, resulting in an overall tougher thermoplastic (22 vs. 14 MPa, respectively). The high strength and toughness of unformulated PDHF as compared to PC-45, showcases its promise as a renewable engineering plastic.

Table 4.2: Tensile properties of PDHF at different M_n compared with PC.

Polymer-M_n	M_n [b] (kg/mol)	$Đ$ [a]	Ultimate Tensile Strength (MPa) [c]	Strain at Break (%)	Toughness (MPa)
PDHF-53	53.4	1.45	69 ± 2	4.0 ± 0.2	1.6 ± 0.1
PDHF-78	78.0	1.50	70 ± 1	5.3 ± 0.2	2.5 ± 0.2
PDHF-140	140	1.51	65.9 ± 0.6	16 ± 2	6.1 ± 0.8
PDHF-198	198	1.47	65 ± 1	33 ± 14	14 ± 6
PC-45[a]	45	N/A	62.8 ± 0.8	45 ± 19	22 ± 10

[a] Poly(bisphenol A carbonate) sample obtained from Millipore-Sigma. [b] Mn and $Đ$ determined from light scattering.
[c] Reported tensile data is the average of at least 3 samples.

4.3.3 Thermal Properties and Rheology

PDHF is unique as a poly(vinyl ether) due to the retained cyclic backbone structure giving the polymer a high glass transition temperature. We measured a T_g of 135 °C for PDHF, matching previous reports.[7,10] PDHF also has exceptional thermal stability, with a 5% mass loss temperature of 364 °C. These thermal properties demonstrate a large processing window for PDHF, where heat molding and polymer melt processing can take place. Sanda and coworkers reported the influence of reaction temperature on the distereoselectivity and consequently the T_g of PDHF.[10] Lower reaction temperatures favored the kinetic *cis*-isomer with a higher T_g while higher temperatures favored the thermodynamic *trans*-isomer with a lower T_g. Sanda's reported uncontrolled room temperature polymerization led to a low T_g of ~112 °C for the of 68% *trans*-PDHF. In contrast, our controlled room temperature polymerization generated 65% *trans*-PDHF with a high T_g of 131 °C for the same M_n (~30 kg/mol). We attribute this to the better control achieved in our polymerization and we believe the relationship between distereoselectivity and T_g is more nuanced than previously reported. Consequently, our controlled polymerization provides access to high T_g PDHF at room temperature.

To evaluate the melt stability of PDHF, we subjected a batch of polymer to different processing conditions and evaluated the complex viscosity (η*) in parallel plate rheology. It was previously reported that PDHF is sensitive to thermo-oxidative degradation.[11] We hypothesized the addition of a commercial phenolic inhibitor (Irganox® 1010) would stabilize the polymer at elevated

temperatures. PDHF samples from the same batch were prepared without inhibitor and with 0.07 wt% inhibitor. Constant 0.1% oscillatory strain was applied at a frequency of 0.1 rad s^{-1} for 20 minutes at 180 °C (Figure 4.6). Uninhibited PDHF showed a greater increase in η* over 20 minutes when compared to the inhibited PDHF. In addition, uninhibited samples would often turn yellow during heat molding, while inhibited samples remained clear. This provided discernible evidence that the inhibitor increased the thermal stability of PDHF.

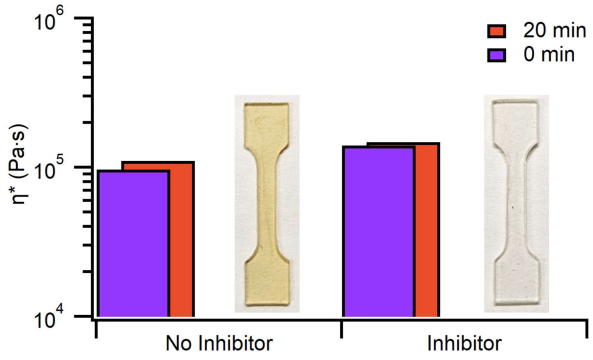

Figure 4.6: Melt stability of PDHF evaluated through complex viscosity (η*) monitored at 180 °C with 0.1% oscillatory strain applied at a frequency of 0.1 rad s^{-1} for 20 min.

Another key parameter that influences polymer properties is the entanglement molecular weight (M_e). Using time-temperature superposition to generate a master curve, the M_e was calculated to be ~3 kg/mol using the equation given by Ferry (Figure 4.23, Equation 1).[36,37] In reference to other polymers, this is quite low; for example, the value for polystyrene is estimated to be 18 kg/mol.[37] Generally, a low M_e is associated with a strong thermoplastic, such as observed with PC (M_e = 2.5 kg/mol).[38] Consequently, we believe PDHF derives its strength from being well

entangled, where $M_n >> M_e$. In addition, because PDHF is amorphous with a high T_g, it should maintain melt strength making it amenable to extrusion and other polymer processing techniques where high melt viscosity at low frequencies is desirable.

The influence of M_n on melt properties was then examined with frequency sweeps performed at 170 °C from 0.1 to 100 rad s^{-1}. Storage (G') and loss (G") moduli showed a clear crossover frequency that shifted to lower frequencies with increased M_n (Figure 4.24). The crossover between G' and G" indicates the frequency at which the polymer transitions from fluid-like to solid-like, giving insight into the sheer rates needed for melt-processing.[39] The plot of η* at 180 °C shows an increase in η* with respect to increasing M_n at low frequency (<0.1 rad s^{-1}), indicative of the increased zero-shear viscosity (Figure 4.7). Above 100 rad s^{-1} the η* for all samples converge as a result of shear thinning.[40] The onset of shear thinning indicates the shear rate at which viscosity diminishes with increased frequency, an important consideration in many polymer processing techniques, allowing PDHF of varying molecular weight to be processed with similar η* above 10 rad/sec .[40] Finally, the range of complex viscosities observed suggests that PDHF could be well suited for hot-melt extrusion processing, as the optimal viscosity range has been cited as 1000–10000 Pa·s.[41]

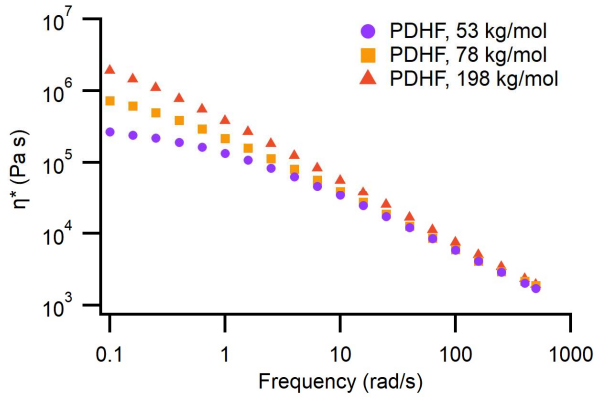

Figure 4.7: Frequency sweeps of PDHF-53, PDHF-84, and PDHF-198 showing the effect of M_n on complex viscosity (η*).

4.3.4 Film Barrier Properties

To study how PDHF may perform as a barrier material for food packaging applications, we produced free standing films for analysis. These films were solvent cast then pressed at 170 °C to ensure the polymer was thermally relaxed. This produced uniform films ~38 µm thick with >89% transmittance across visible wavelengths (380-700 nm) (Figure 4.8a). For gas permeation measurements, PDHF films were tested by introducing an upstream pressure (1-17 atm) of single gas penetrants (O_2 or CO_2) and measuring downstream pressure.[42–44] Water vapor transmission rate (WVTR) was tested using previously described methods, in accordance with ASTM-E96.[45–47] The values recorded for PDHF were compared to data from a recent publication on sustainable packaging materials (Figure 4.8).[48] O_2 permeability (PO_2) for PDHF at was lower than LDPE, but higher than PLLA and PET. CO_2 permeability (PCO_2) for PDHF was again lower than LDPE, and comparable to PLLA, but not as low as PET. Measured values for PDHF WVTR were

low, at 2.7 g mm m^{-2} day^{-1}. This is comparable to PET, (1.49 g mm m^{-2} day^{-1}) and a significant improvement over PLLA (5.7 g mm m^{-2} day^{-1}). The lower WVTR and resistance to hydrolysis gives PDHF clear advantages over PLLA for water-exposed applications. PDHF combines moderate gas and water permeability with robust material properties to produce a biorenewable polymer that could be attractive for food packaging applications.

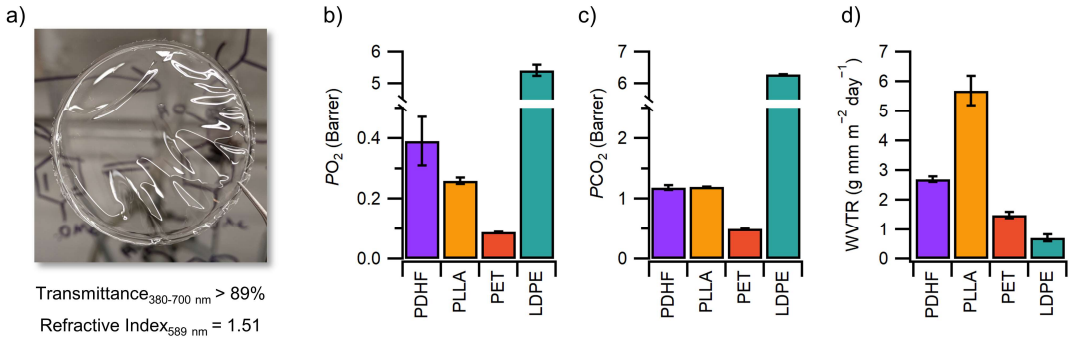

Figure 4.8: PDHF films demonstrate desirable optical properties (a) and moderate permeability for O_2 (b), CO_2 (c), and water vapor (d).

4.3.5 Accelerated Oxidative Degradation of PDHF

In the development phase of any new plastic, it is imperative to examine the end-of-life solutions available for recycling and/or degradation. Being a stable thermoplastic, PDHF can be mechanically recycled. However, we also wanted to investigate the chemical degradation of this material. Early work by Sanda and Matsumoto demonstrated the slow degradation of PDHF in the presence of air and proposed an oxidative chain scission mechanism.[11] They reported a reduction in M_n from 85 to 4.5 kg/mol occurred after an uninhibited, high surface area sample was exposed to air for 130 days at room temperature. Motivated by this work, we sought to develop a method by which we could chemically

accelerate PDHF degradation to oligomeric and small molecule fragments, which may hold potential for more favorable biodegradation or for waste valorization through chemical upcycling.

It is well known that the combination of hydrogen peroxide (H_2O_2) and a ferrous salt (Fe(II)), "Fenton's reagent," results in the formation of a strongly oxidizing hydroxyl radical species.[49] Due to the relative abundance and low cost of H_2O_2 and Fe(II), we sought to use a Fenton's reagent oxidation to demonstrate a facile, accelerated chemical degradation of PDHF. PDHF was first dissolved in DCM before adding H_2O_2/H_2O (30 wt %) and Fe(II) in the form of $(NH_4)_2Fe(SO_4)_2 \bullet 6H_2O$. The biphasic reaction mixture was then monitored by GPC, revealing a reduction in M_n from 50 kg/mol to ~1 kg/mol over 48 h (Figure 4.9). The plot of M_n^{-1} versus time exhibited a linear relationship, suggesting a chain scission mechanism (). When PDHF was stirred in only water and DCM, no reduction in M_n was observed, and when PDHF was stirred in H_2O_2, H_2O, and DCM but no Fe(II), the M_n only decreased to 42.7 kg/mol after 48 hours. These results demonstrate Fenton's reagent as an effective method for the rapid, facile degradation of PDHF.

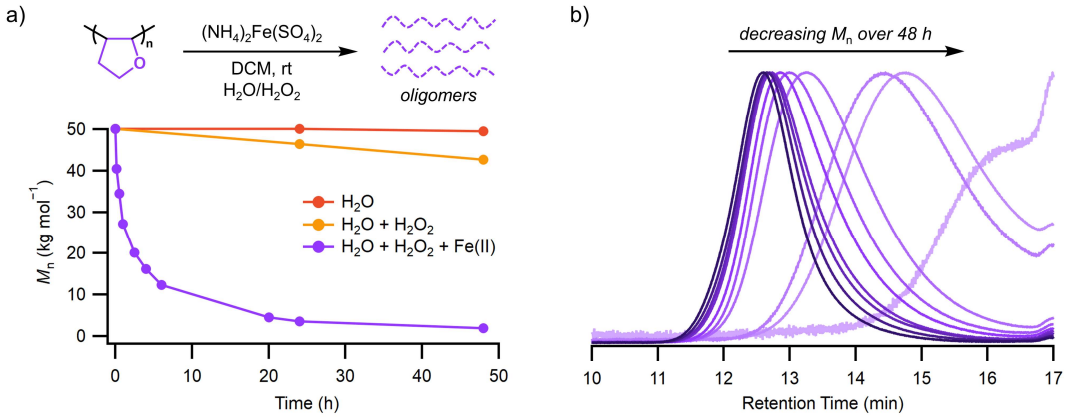

Figure 4.9: Facile oxidative degradation of PDHF using Fenton's reagent ($Fe(II)/H_2O_2$). PDHF was reduced to oligomers within 24 hours by GPC (a), far outperforming controls (b).

^1H NMR, ^{13}C NMR, and FT-IR spectra of the degradation products provided initial insight into the mechanism. By ^1H NMR (Figure 4.32), we observed signals consistent with a carboxylic acid (10.70 ppm), aldehyde (9.11 ppm), as well as an acetal (5.43 ppm), and in the ^{13}C NMR spectrum (Figure 4.33), a peak consistent with that of a lactone (162.07 ppm) was visible. These assignments were supported by FT-IR spectra (Figure 4.34), in which new absorptions for C=O stretching were observed at 1730 and 1770 cm^{-1} in addition to a broad absorption ranging from 3050 to 3500 cm^{-1} corresponding to O-H stretching. These observations align with those made previously for PDHF degradation, and we expect that our accelerated oxidation proceeds through a similar mechanism.[11] This degradation study sets the groundwork for the development of a method to chemically recycle PDHF.

4.4 Conclusions

PDHF represents a unique opportunity to source a strong and degradable thermoplastic from a commercial bioalcohol. We demonstrated that PCCP is an effective organic acid initiator for cationic polymerization of DHF at room temperature to achieve high M_n PDHF (256 kg/mol) at 14 g scale. The addition of HBD enabled polymerization in an industrially relevant green solvent, CPME. Tensile properties revealed that high M_n PDHF is a strong (≤ 70 MPa) and tough (≤ 14 MPa) thermoplastic, comparable to PC. Film barrier properties showed promising results for food packaging, with low permeability to O_2 (0.42 barrer), CO_2 (1.2 barrer), and water vapor (2.7 g mm m^{-2} day^{-1}). Finally, we demonstrated an accelerated chemical degradation of PDHF under oxidizing conditions. This comprehensive evaluation of PDHF lays a roadmap for developing this next-generation sustainable thermoplastic, where we have provided an efficient bioalcohol source, robust material properties, and facile degradability.

4.5 Acknowledgments

This material is based upon work supported by the National Science Foundation Graduate Research Fellowship Program under Grant No. DGE-1650441. Any opinions, findings, and conclusions or recommendations expressed in this material are those of the author(s) and do not necessarily reflect the views of the National Science Foundation. This work was supported by the National Science Foundation Center for Sustainable Polymers at the University of Minnesota, a Center for Chemical Innovation (CHE-1901635). This work made use

of the Cornell Center for Materials Research Shared Facilities that are supported through the NSF MRSEC program (DMR- 1120296). This work made use of the NMR Facility at Cornell University that is supported, in part, by the NSF under the award number CHE-1531632. We would like to thank Meredith Silberstein and her group for generous use of their tensile tester.

4.6 References

† We discuss a possible chain-transfer and chain-coupling mechanism in the Supporting Information.

† We discuss a possible chain-transfer and chain-coupling mechanism in the Supporting Information.

(1) Ellen MacArthur Foundation. The New Plastics Economy: Rethinking the Future of Plastics and Catalysing Action; 2017.

(2) Haque, F. M.; Ishibashi, J. S. A. A.; Lidston, C. A. L. L.; Shao, H.; Bates, F. S.; Chang, A. B.; Coates, G. W.; Cramer, C. J.; Dauenhauer, P. J.; Dichtel, W. R.; et al. Defining the Macromolecules of Tomorrow through Synergistic Sustainable Polymer Research. Chem. Rev. **2022**, 122 (6), 6322–6373.

(3) Bomgardner, M. M. Novamont Opens Bio-BDO Plant. C&EN **2016**, 94 (40).

(4) U.S. Fuel Ethanol Plant Production Capacity; 2020.

(5) Ludmila, L.; Stonkus, V.; Edolfa, K.; Ilieva, L.; Plyasova, L.; Zaikovskii, V. Copper-Promoted Cobalt Catalysts for 2,3-Dihydrofuran Synthesis. Appl. Catal. A Gen. **2006**, 311, 86–93.

(6) Matake, R.; Adachi, Y.; Matsubara, H. Synthesis of Vinyl Ethers of Alcohols Using Calcium Carbide under Superbasic Catalytic Conditions (KOH/DMSO). Green Chem. **2016**, 18 (9), 2614–2618.

(7) Spring, S. W.; Smith-Sweetser, R. O.; Rosenbloom, S. I.; Sifri, R. J.; Fors, B. P. Sustainable Thermoplastic Elastomers Produced via Cationic RAFT Polymerization. Polym. Chem. **2021**, 12, 1097–1104.

(8) Barr, D. A.; Rose, J. B. Cationic Polymerisation of 2: 3-Dihydrofurans. J. Chem. Soc. **1954**, 3766–3769.

(9) Ogawa, Y.; Sawamoto, M.; Higashimura, T. Living Cationic Polymerization of Cyclic Unsaturated Ethers. Polym. J. **1984**, 16 (5), 415.

(10) Sanda, F.; Matsumoto, M. Cationic Polymerization of 2,3-Dihydrofuran. Study on the Relationship between Glass Transition Temperature and Tacticity of the Polymer. Macromolecules **1995**, 28 (20), 6911–6914.

(11) Sanda, F.; Matsumoto, M. Degradation Behavior of Poly(2,3-Dihydrofuran). J. Appl. Polym. Sci. **1996**, 59 (2), 295–299.

(12) Yonezumi, M.; Kanaoka, S.; Aoshima, S. Living Cationic Polymerization of Dihydrofuran and Its Derivatives. J. Polym. Sci. Part A Polym. Chem. **2008**, 46 (13), 4495–4504.

(13) Feist, J. D.; Xia, Y. Enol Ethers Are Effective Monomers for Ring-Opening Metathesis Polymerization: Synthesis of Degradable and Depolymerizable Poly(2,3-Dihydrofuran). J. Am. Chem. Soc. **2020**, 142 (3), 1186–1189.

(14) Mita, F.; Sasaki, S.; Matsumoto, M. Heat-Resistant Furan Polymers as

Optical Substrates. JP02230201A, 1990.

(15) MITA, F.; MATSUMOTO, M. PRESERVATION OF DECOMPOSABLE POLYMER AND ITS COMPOSITION. JPH03277609A, 1991.

(16) Mita, F.; Sasaki, S.; Matsumoto, M. Preparation of Polymers Bearing Tetrahydrofuran Skeletons. JP02011622A, 1990.

(17) Mita, F.; Matsumoto, M.; Okazaki, M. Fibers from Polymers Containing Tetrahydrofurandiyl Units and Their Applications. JP03277609A, 1991.

(18) Mita, F.; Matsumoto, M. Air-Degradable Dihydrofuran Polymers and Their Stability under Nitrogen. JP03093847A, 1991.

(19) Mita, F.; Matsumoto, M. Resin Compositions and Their Moldings. EP434067A2, 1991.

(20) Mita, F.; Matsumoto, M. Furan Ring-Containing Polymers for Tapes and Similar Materials with Good Heat Resistance and Mechanical Properties. JP03206113A, 1991.

(21) Mita, F.; Matsumoto, M. Preparation of Polymers Containing Tetrahydrofuran Structure. JP03172307A, 1991.

(22) Matsumoto, M. Sanda, F. Disposable Molding Compositions Containing THF Skeleton-Containing Polymers and Phenolic Compounds and/or Plasticizers. JP03146509A, 1991.

(23) Mita, F.; Matsumoto, M. Heat-Resistant Transparent Tetrahydrofuran Ring-Containing Polymer Containers. JP03152107A, 1991.

(24) Mita, F.; Matsumoto, M. Transparent Heat-Resistant Polymer Sheets or

Films. JP03200856A, 1991.

(25) Mita, F.; Matsumoto, M. Dihydrofuran Polymer Compositions Containing Hindered Phenol Heat Stabilizers. JP03128227A, 1991.

(26) Ootake, Y.; Asabe, H. Biodegradable Polymer Compositions. JP06220333A, 1994.

(27) Matsumoto, M. Mita, F.; Takamatsu, H. Preparation of Polymers Containing Tetrahydrofuran Structure. JP06107721A, 1994.

(28) Yamanaka, M. Kodani, M.; Hayashibara, T. Watanabe, T. Iwasaki, H. Oxygen-Absorptive Resin Compositions and Molded Articles and Laminated Articles Produced Using Them. WO2006106780A1, 2006.

(29) Kottisch, V.; O'Leary, J.; Michaudel, Q.; Stache, E. E.; Lambert, T. H.; Fors, B. P. Controlled Cationic Polymerization: Single-Component Initiation under Ambient Conditions. J. Am. Chem. Soc. **2019**, 141 (27), 10605–10609.

(30) Watanabe, K.; Yamagiwa, N.; Torisawa, Y. Cyclopentyl Methyl Ether as a New and Alternative Process Solvent. Org. Process Res. Dev. **2007**, 11 (2), 251–258.

(31) de Gonzalo, G.; Alcántara, A. R.; Domínguez de María, P. Cyclopentyl Methyl Ether (CPME): A Versatile Eco-Friendly Solvent for Applications in Biotechnology and Biorefineries. ChemSusChem **2019**, 12 (10), 2083–2097.

(32) Watanabe, K. The Toxicological Assessment of Cyclopentyl Methyl Ether (CPME) as a Green Solvent. Molecules . 2013.

(33) Swallowe, G. M. Mechanical Properties and Testing of Polymers, Chapter 7:

Crazing; 1999.

(34) Sauer, J. A.; Chen, C. C. Crazing and Fatigue Behavior in One- and Two-Phase Glassy Polymers. Crazing Polym. **2005**, 169–224.

(35) Science, M. Microscopic and Molecular Fundamentals of Crazing. Kobunshi **1993**, 42 (5), 389–393.

(36) Ferry, J. D. Viscoelastic Properties of Polymers, 3rd Editio.; John Wiley & Sons, Ltd, 1980.

(37) Fetters, L. J.; Lohse, D. J.; Milner, S. T.; Graessley, W. W. Packing Length Influence in Linear Polymer Melts on the Entanglement, Critical, and Reptation Molecular Weights. Macromolecules **1999**, 32 (20), 6847–6851.

(38) León, S.; van der Vegt, N.; Delle Site, L.; Kremer, K. Bisphenol A Polycarbonate: Entanglement Analysis from Coarse-Grained MD Simulations. Macromolecules **2005**, 38 (19), 8078–8092.

(39) Aho, J.; Boetker, J. P.; Baldursdottir, S.; Rantanen, J. Rheology as a Tool for Evaluation of Melt Processability of Innovative Dosage Forms. Int. J. Pharm. **2015**, 494 (2), 623–642.

(40) Polychronopoulos, N. D.; Vlachopoulos, J. Polymer Processing and Rheology BT - Functional Polymers; Jafar Mazumder, M. A., Sheardown, H., Al-Ahmed, A., Eds.; Springer International Publishing: Cham, 2018; pp 1–47.

(41) Nadgorny, M.; Gentekos, D. T.; Xiao, Z.; Singleton, S. P.; Fors, B. P.; Connal, L. A. Manipulation of Molecular Weight Distribution Shape as a New Strategy to Control Processing Parameters. Macromol. Rapid Commun. **2017**, 38

(19), 1700352.

(42) Ha, H.; Park, J.; Ando, S.; Kim, C. Bin; Nagai, K.; Freeman, B. D.; Ellison, C. J. Gas Permeation and Selectivity of Poly(Dimethylsiloxane)/Graphene Oxide Composite Elastomer Membranes. J. Memb. Sci. **2016**, 518, 131–140.

(43) Ha, H.; Park, J.; Ha, K. R.; Freeman, B. D.; Ellison, C. J. Synthesis and Gas Permeability of Highly Elastic Poly(Dimethylsiloxane)/Graphene Oxide Composite Elastomers Using Telechelic Polymers. Polymer (Guildf). **2016**, 93, 53–60.

(44) Park, J.; Ha, H.; Yoon, H. W.; Noh, J.; Park, H. B.; Paul, D. R.; Ellison, C. J.; Freeman, B. D. Gas Sorption and Diffusion in Poly(Dimethylsiloxane) (PDMS)/Graphene Oxide (GO) Nanocomposite Membranes. Polymer (Guildf). **2021**, 212 (October 2020), 123185.

(45) Miguel, O.; Fernandez-Berridi, M. J.; Iruin, J. J. Survey on Transport Properties of Liquids, Vapors, and Gases in Biodegradable Poly(3-Hydroxybutyrate) (PHB). J. Appl. Polym. Sci. **1997**, 64 (9), 1849–1859.

(46) Sangroniz, A.; Chaos, A.; Iriarte, M.; del Río, J.; Sarasua, J.-R.; Etxeberria, A. Influence of the Rigid Amorphous Fraction and Crystallinity on Polylactide Transport Properties. Macromolecules **2018**, 51 (11), 3923–3931.

(47) Lizundia, E.; Vilas, J. L.; Sangroniz, A.; Etxeberria, A. Light and Gas Barrier Properties of PLLA/Metallic Nanoparticles Composite Films. Eur. Polym. J. **2017**, 91, 10–20.

(48) Sangroniz, A.; Zhu, J.-B.; Tang, X.; Etxeberria, A.; Chen, E. Y.-X.; Sardon, H.

Packaging Materials with Desired Mechanical and Barrier Properties and Full Chemical Recyclability. Nat. Commun. **2019**, 10 (1), 3559.

(49) Walling, C. Fenton's Reagent Revisited. Acc. Chem. Res. **1975**, 8 (4), 125–131.

4.7 Experimental Section

4.7.1 Materials

2,3-dihydrofuran (DHF) (99%, TCI) and cyclopentyl methyl ether (CPME) (99%, TCI) were dried over calcium hydride (CaH_2) (ACROS organics, 93% extra pure, 0–2 mm grain size) for 12 hours, distilled under vacuum, and degassed by three freeze-pump-thaw cycles. Dichloromethane (DCM), was purchased from J.T. Baker and was purified by purging with argon for 1 hour, followed by passing through two packed columns of neutral alumina under argon pressure. Poly(bisphenol A carbonate) (PC) (45 kg/mol, Sigma Aldrich) was used as received. Hydrogen peroxide (30 wt % in H_2O, Fisher Scientific), ammonium iron(II) sulfate hexahydrate (98%, Sigma Aldrich), and Irganox 1010® (BASF) were used as received. Benzene, ethyl acetate (EtOAc), methanol (MeOH), and triethylamine (NEt_3) were purchased from Fischer Scientific and used as received.Pentacarbomethoxycyclopentadiene (PCCP) was synthesized according to a reported literature procedure.[1] Hydrogen bond donor (HBD) tris(3,5-tris(trifluoromethyl)phenyl)thiophosphotriamide was synthesized according to a previous literature procedure.[2]

4.7.2 General Measurements

All polymer samples were analyzed using a Tosoh EcoSec HLC 8320 GPC system with two SuperHM-M columns in series at a flow rate of 0.350 mL/min. THF was used as the eluent and number-average molecular weights (M_n), weight-

average molecular weights (M_w), and dispersities ($Đ$) for PDHF were determined by light scattering using a Wyatt miniDawn Treos multi-angle light scattering detector and a calculated dn/dc value of 0.1116 mL g^{-1}. The reported M_ns for degradation of PDHF were calculated from refractive index chromatograms against TSKgel polystyrene standards. Nuclear magnetic resonance (NMR) spectra were recorded on a Varian 400 MHz, a Varian 600 MHz, or a Bruker 500 MHz instrument. Fourier Transform Infrared (FTIR) spectra were collected on a Bruker Tensor II IR spectrometer with a diamond Attenuated Total Reflectance (ATR) attachment. Ellipsometry was performed on a J.A. Woollam Co, Inc. M-2000 ellipsometer using wavelengths from 370 to 1000 nm with a 65° angle of incidence. The refractive index was predicted by the Cauchy dispersion equation. The transmittance index of PDHF film was measured by Thermo Scientific™ Evolution 220 UV-Vis spectrophotometers using wavelengths from 380 to 700 nm.

4.7.3 Procedure for Polymerization of DHF (250 kg/mol)

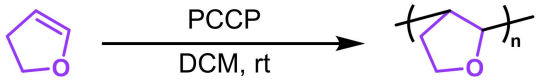

All polymerizations were set up in a nitrogen glovebox. A scintillation vial equipped with a magnetic stir bar was charged with PCCP (6.0 mg, 0.017 mmol, 1 equiv.). Distilled DHF (4.5 mL, 60 mmol, 3566 equiv.) was then added, promptly followed by DCM (4.5 mL). The reaction was sealed with a Teflon-lined cap, then removed from the glove box and placed in a 22 °C water bath for heat dissipation

and stirred for 26 hours. The reaction was terminated by the addition of 20 µL of 5% triethylamine/methanol. 89 µL (1 mmol) of benzene was added as an internal standard. Aliquots were taken for NMR and GPC and the sample was then precipitated twice into a 20% H_2O/methanol solution and dried under vacuum. ^{1}H and ^{13}C NMR of the polymer are shown in Figure 4.13 and Figure 4.14, respectively.

4.7.4 Procedure for Large Scale Polymerization of DHF (14 Gram Scale)

In a nitrogen filled glovebox, a 100 mL Schlenk flask was equipped with a magnetic stir bar and was charged with a 10.0 mg/mL stock solution of PCCP (2.0 mL, 0.056 mmol, 1 equiv.). DCM (15 mL) was added, followed promptly by DHF (15.0 mL, 198 mmol, 3460 equiv.). The reaction was then sealed, removed from the glove box, and placed in a 22 °C water bath for heat dissipation and stirred for 26 hours. The reaction was terminated by the addition of 0.50 mL of 5% triethylamine/methanol. 89 µL (1 mmol) of benzene was added as an internal standard. Aliquots were taken for NMR and GPC and the sample was then precipitated twice into a 20% H_2O/methanol solution and dried under vacuum.

4.7.5 Procedure for Polymerization of DHF in Cyclopentyl Methyl Ether

In a nitrogen glovebox, a scintillation vial equipped with a magnetic stir bar was

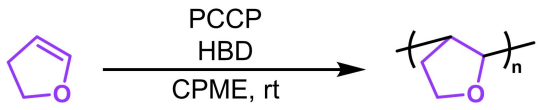

charged with PCCP (3 mg, 0.0084 mmol, 1 equiv.) and HBD (6.0 mg, 0.0084 mmol, 1 equiv.). DCM (2.3 mL) was added followed promptly by DHF (2.3 mL, 30 mmol,

3566 equiv.). The reaction was sealed with a Teflon-lined cap, then removed from the glove box and placed in a 22 °C water bath for heat dissipation and stirred for 26 hours. The reaction was terminated by the addition of 20 μL of 5% triethylamine/methanol. 89 μL (1 mmol) of benzene was added as an internal standard. Aliquots were taken for NMR and GPC.

4.8 Material Characterization

PDHF and poly(bisphenol A carbonate) (PC) were pressed into dog-bone-shaped tensile bars using a 4120 Hydraulic Unit Carver heated press. The polymer samples were placed in the mold between two sheets of Mylar protective lining. PDHF samples were held at 170 °C for 2 min. before pressing to 7,000 psi and holding for 2 min. The press was then water cooled to room temperature at an approximate rate of 10 °C/min before releasing pressure. Excess material was trimmed away with a hobby blade to obtain dog-bone-shaped tensile bars with approximate gauge dimensions of 16 x 2.5 x 0.9 mm.

Tensile properties of the prepared samples were examined using a Zwick/Roell Z010 testing system equipped a 500 N load cell and hand-tightened grips. Samples were stretched to break at an extension rate of 2 mm min^{-1}. Values reported are an average calculated from at least three samples.

For determination of thermal transitions, differential scanning calorimetry (DSC) was performed using a TA Instruments Q1000. Samples were placed in aluminum crucibles and heated to 200 °C at 20 °C min^{-1} to erase thermal history,

cooled to −70 °C and held at this temperature for 10 min to equilibrate. A second heat cycle was performed to 200 °C at 20 °C min^{-1} during which the thermal data was collected. Thermogravimetric analysis (TGA) was performed using a TA Instruments Q500 where samples were heated at a rate of 20 °C min^{-1} from 25 °C to 500 °C.

Rheological tests were performed on a TA Instruments DHR3 rheometer using an 8mm parallel plate in a temperature controlled environmental test chamber under a nitrogen atmosphere. The sample was loaded onto the bottom parallel plate at 180°C and the top plate was lowered to a trim gap of 1050µm. Excess polymer material was trimmed and then the plate was lowered to a gap of 1000µm. Strain sweeps (0.1–100%) at 180°C were first performed at 6.3 rad/s (1 Hz) to determine the linear viscoelastic region. A 0.1% strain was selected as it consistently lied within the linear viscoelastic region for the preceding range of frequencies. Before each frequency sweep, the sample was equilibrated at 180 °C for 5 min to ensure uniform sample temperature.

For gas permeation and water vapor transmission measurements, PDHF films were prepared by solvent casting. 400 mg of PDHF and 0.3 mg Irganox 1010® (0.07 wt%) were dissolved in 8 mL DCM to create a 50 mg/mL solution. 2 mL (each) of this solution was passed through a 13 mm, 0.45 µm pore size syringe filter into three separate glass casting dishes. Casting dishes were cleaned of debris with compressed air immediately before use. The dishes were then covered with glass petri dish covers and placed on a platform equipped with a

bubble leveler. The samples were left to evaporate solvent for 20 hours, then transferred to a vacuum oven and dried under vacuum at 70 °C for 18 hours. After allowing the films to cool, deionized water was added to the dishes and the films were cut around the edge with a hobby knife before delicate removal with blunt end forceps. The films were then individually placed between mylar protective sheets and stainless-steel sheets before pressing with a 4120 Hydraulic Unit Carver heated press. The films were held at 170 °C for 2 minutes before pressing to 5000 lbs for 2 minutes. Pressure was released, and the sample dwelled for 2 minutes at 170 °C, before pressure was increased again to 10,000 lbs and held for 2 minutes. This pressure was held while the press was cooled to room temperature at a rate of 10 °C/min. This procedure yielded clear PDHF films with a uniform thickness of 38 µm.

For ellipsometry, thin films of PDHF were spin-coated onto silicon wafers. PHDF was dissolved in DCM (6 mg/mL) and 0.2 mL of this solution was dropped onto a clean silicon wafer mounted in a spin coater. The spin coater was run at 5000 rpm for 30s, with an acceleration of 3000 rpm/s. This PDHF-coated wafer was then transferred to the ellipsometer for measurement of the refractive index.

Single gas permeabilities were measured by using constant volume, variable pressure method with ultra-high purity grade gases (O2, and CO2). PDHF film was placed in a 47 mm stainless steel HP Filter Holder, and the ultra-high purity grade gas was introduced from the upstream of the system. The gas permeability of the PDHF film was calculated by the increasing rate of the downstream pressure and

the thickness of the film. The upstream pressure was measured by using a 1000 psia pressure transducer (High-Pressure Baratron® Absolute Capacitance Manometer Model 750C13PFE2GA), and the upstream pressure was controlled by a pressure regulator. The downstream pressure was measured by using a 10 torr capacitance manometer (Absolute Capacitance Manometer, Model 626C11TBE). A vacuum pump (Welch, Model 1400B-01) was installed to remove gas molecules in the whole system and create partial vacuum (~0.001 torr). Upstream and downstream pressures were monitored and recorded by National Instruments Lab-VIEW software. The gas leak between the system and the environment was confirmed to be very low (< 10-7 torr/s). The average thickness of the PDHF films were measured by using a dial gauge and the testing area was calculated by image J software analysis.

4.9 PDHF Polymerization

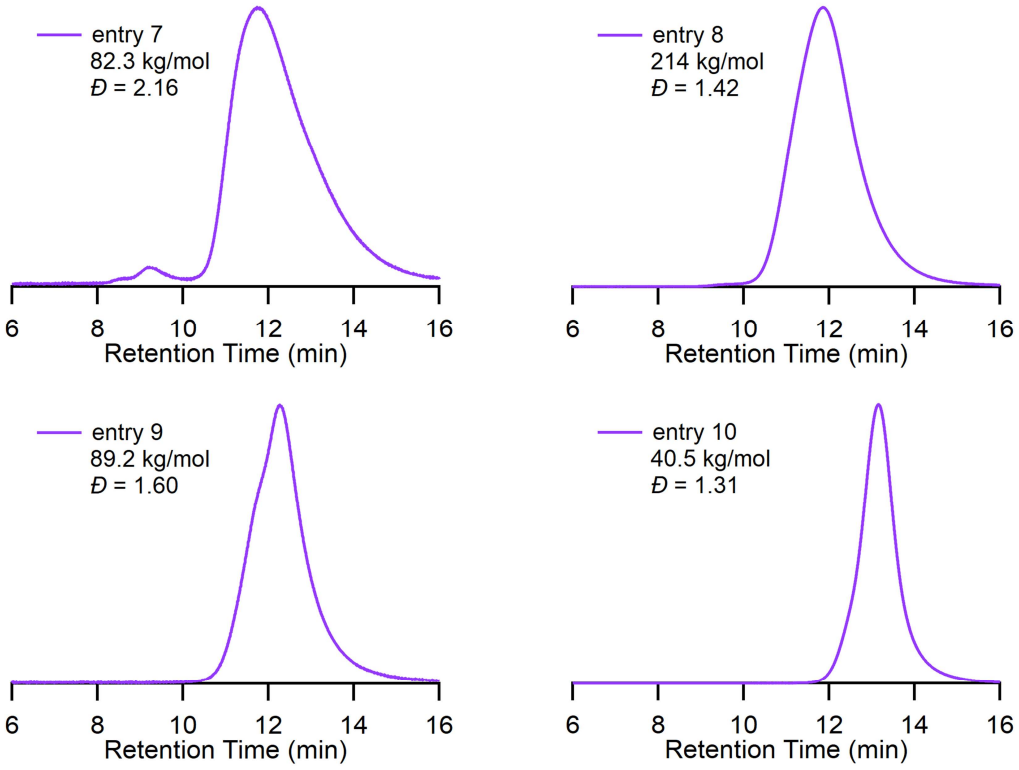

Figure 4.10: GPC traces of entries 7 – 10 from Table 1, polymerizations of PDHF in CPME

Table 4.3: PDHF polymerization monitored over time

Entry	Reaction time (h)	DHF Conversion[a] (%)	M_n^{theo} (kg/mol)	M_n^{b} (kg/mol)	$Đ$
1	0.5	18	18	16.5	1.38
2	1	28	28	17	1.46
3	2	39	39	27	1.38
4	3	47	47	32	1.41
5	4	57	57	44.9	1.37
6	5.5	70	70	58.3	1.37
7	6.5	78	78	65	1.42
8	7.5	84	84	77.5	1.34
9	8.5	89	89	77.9	1.43
10	9.25	91	91	84	1.43

[a] Conversion was calculated from quantitative ^{1}H NMR. [b] M_n and $Đ$ determined from light scattering

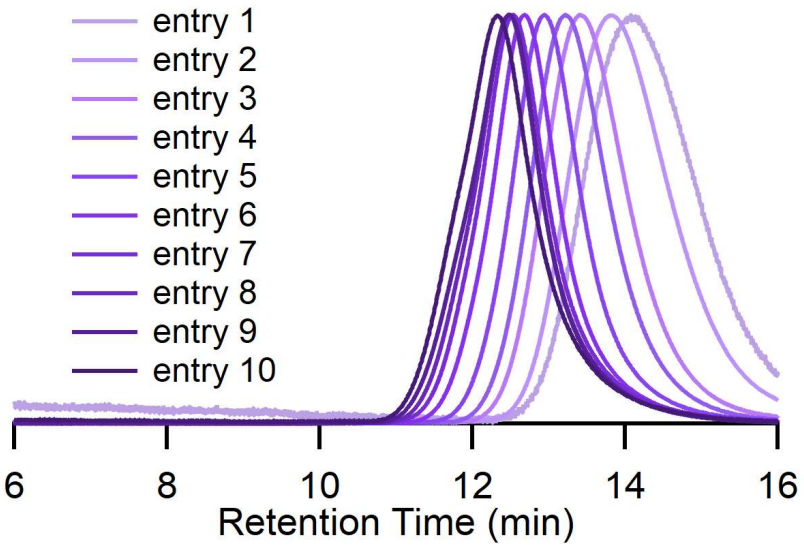

Figure 4.11: GPC traces of PDHF polymerization monitored over time.

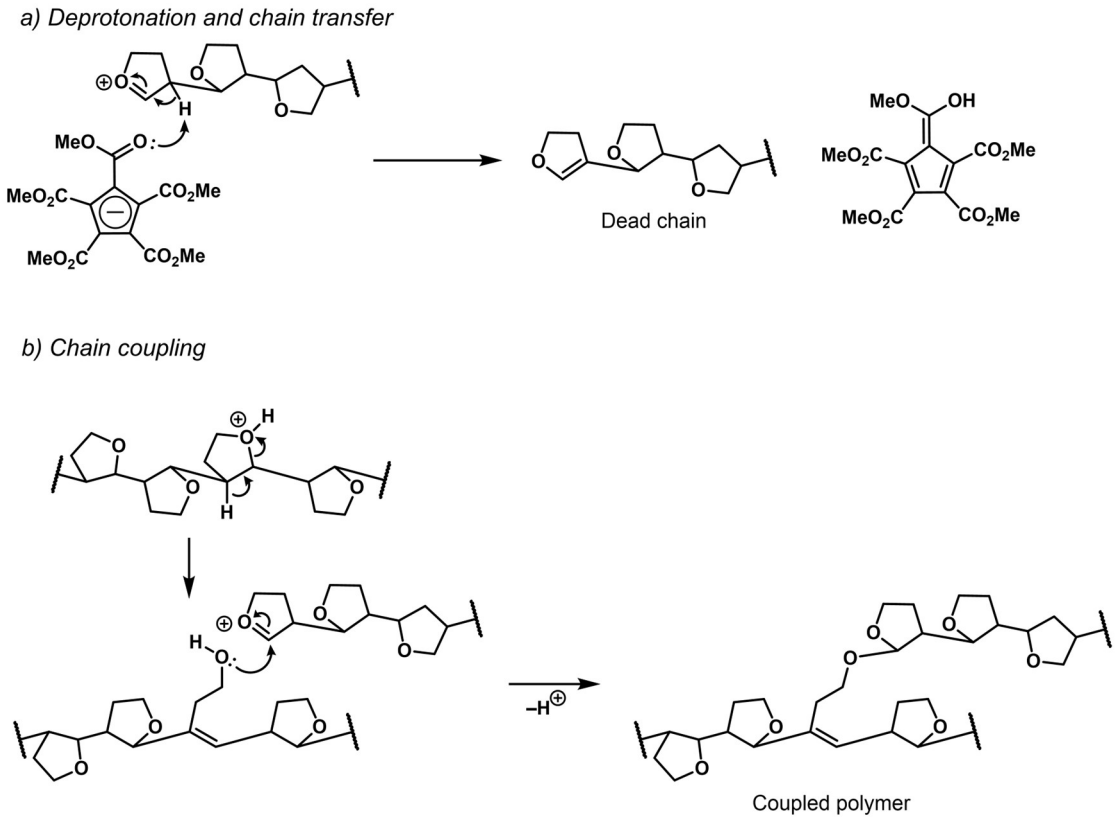

Figure 4.12: Proposed mechanism for chain transfer and coupling during PDHF polymerization.

The tailing to low molecular weight can be ascribed to chain transfer, while the high M_n shoulder could be from chain coupling (Figure 4.12). We hypothesize coupling could occur from protonation and subsequent ring opening of the cyclic ether in the polymer backbone, leading to a pendant alcohol (Figure 4.12b). This alcohol side chain could then perform nucleophilic attack on the oxocarbenium atom of a growing chain, resulting in a coupled polymer. Thus, while the polymerization could not be classified as living, we hypothesize the chain transfer and chain coupling mechanisms have opposing effects on M_n, broadening the dispersity, but still attaining the M_n calculated from [PCCP]:[DHF].

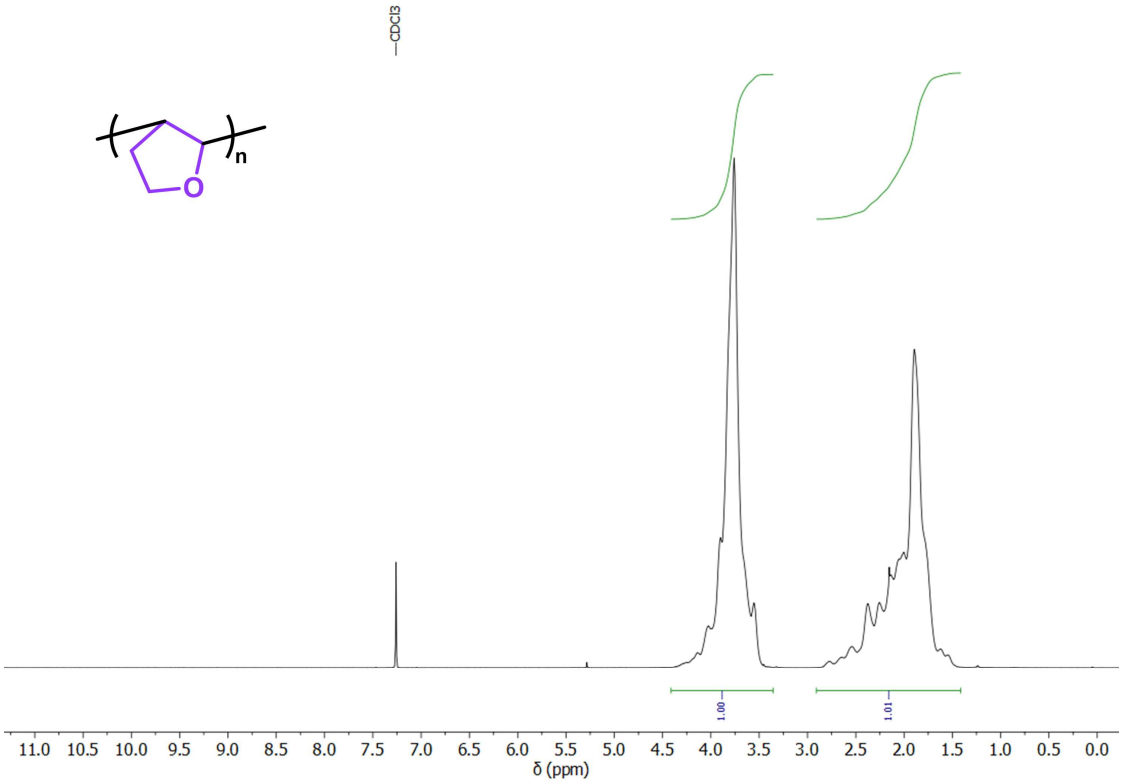

Figure 4.13: Quantitative ^{1}H NMR in $CDCl_3$ of PDHF.

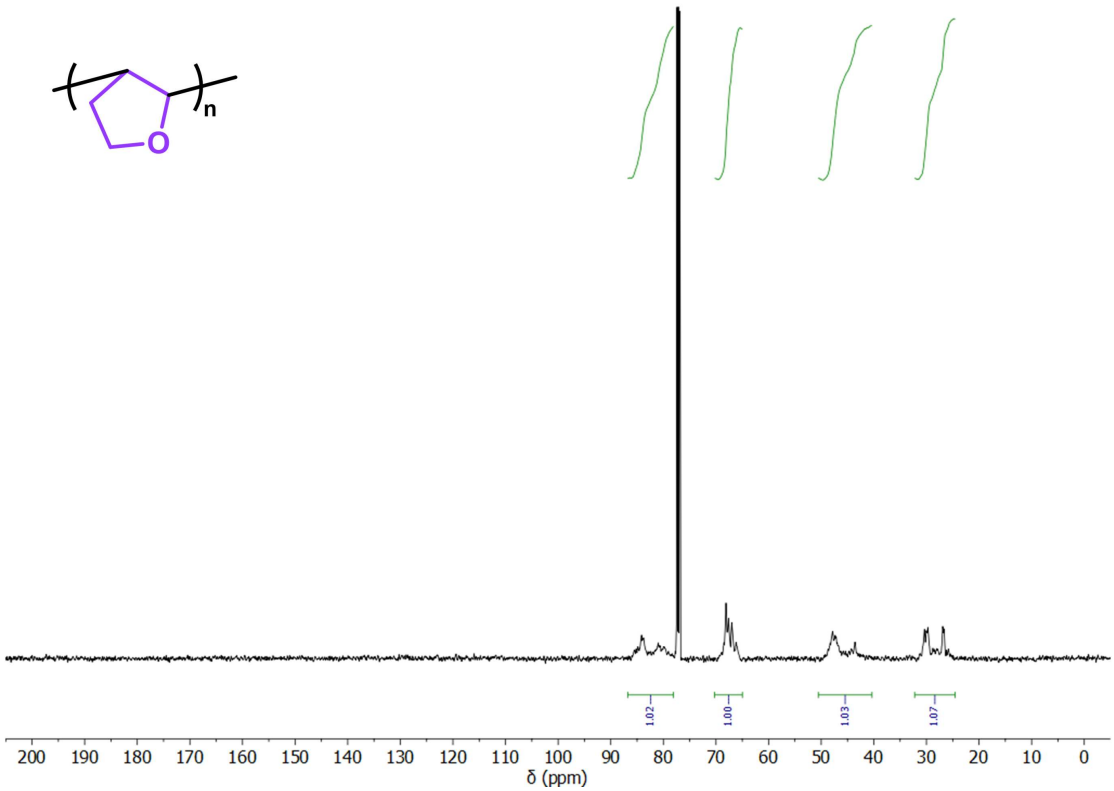

Figure 4.14: ^{13}C NMR in $CDCl_3$ of PDHF.

4.9.1 Distereoselectivity of PDHF and the Effect on Glass Transition Temperature

Previous work by Sanda and coworkers has assigned the peaks at 40-45 ppm and 76-82 ppm to the *cis* isomer of PDHF, while the peaks at 45-50 ppm and 82-87 ppm were assigned to the *trans* isomer.[3] The ratio of peaks 40-45 ppm and 45-50 ppm were then used to calculate the ratio of *trans* to *cis* for a given polymer. We examined our polymers in a consistent manner using ^{13}C spectra of PDHF samples obtained in 1,1,2,2-tetrachloroethane-d2 (Figure 4.15-Figure 4.17).

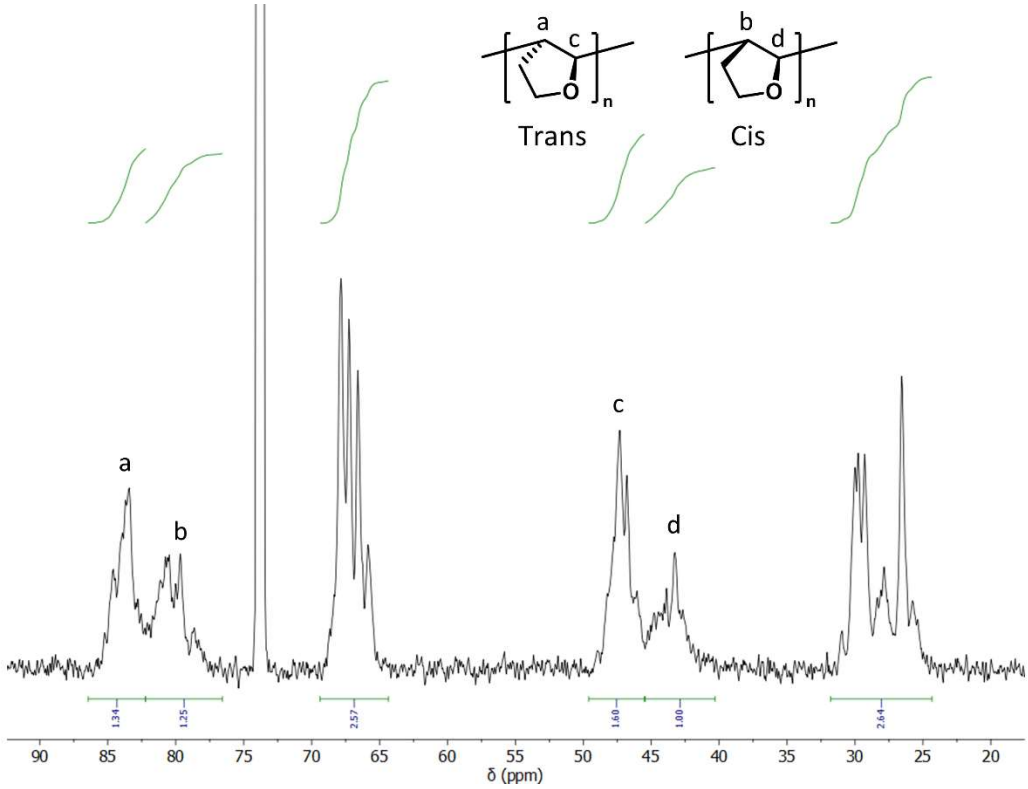

Figure 4.15: Quantitative ^{13}C NMR in 1,1,2,2-tetrachloroethane-d2 of PDHF, 15 kg/mol.

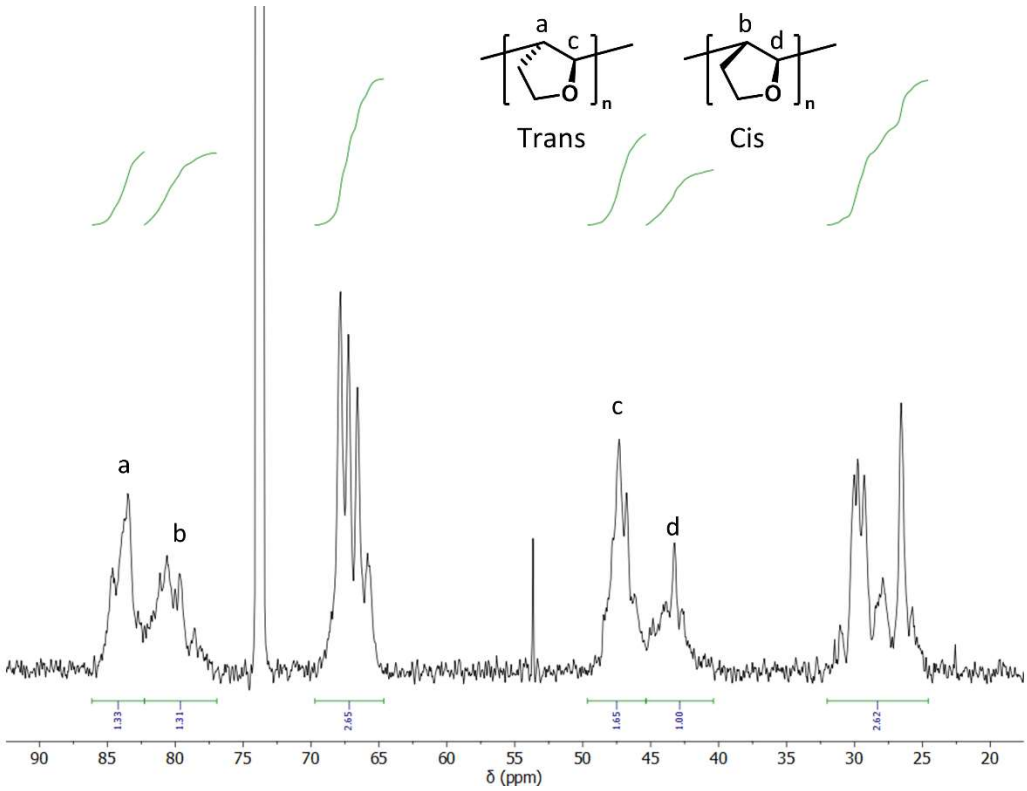

Figure 4.16: Quantitative ^{13}C NMR in 1,1,2,2-tetrachloroethane-d2 of PDHF, 30 kg/mol.

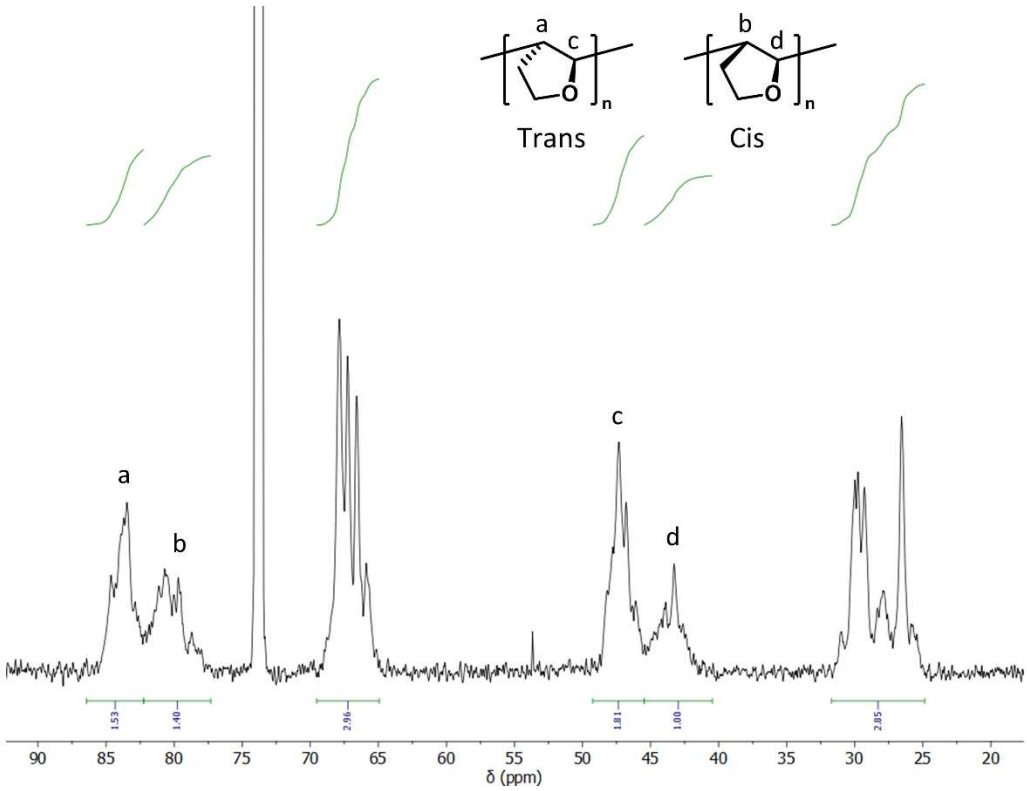

Figure 4.17: Quantitative ^{13}C NMR in 1,1,2,2-tetrachloroethane-d2 of PDHF, 47 kg/mol.

For all PDHF samples evaluated, the *trans*-content was similar, ranging from 50-64% (Table 4.4). Our method's higher reaction temperature (22 °C) favors the *trans*-isomer. Interestingly, our samples maintained T_gs of around 131 °C, higher than what was observed for previous high *trans*-PDHF (<120 °C). We attribute this discrepancy to the previous paper reporting T_gs for uncontrolled polymerizations, with $Đ$ > 2. In addition, we observe inconsistent ratios of a:b and c:d for our integrations in the ^{13}C NMRs, indicating the assigned *trans*- and *cis*- peaks overlap to different extents, making this an inaccurate method for determining isomer content. We believe a more rigorous study would have to be performed to determine the relationship between distereoselectivity and T_g.

Table 4.4: Trans-content of PDHF Samples and the Effect on T_g.

Entry	PDHF (kg/mol) [a]	$Đ$	Reaction Temperature (°C)	Solvent	*Trans*-content [b]	T_g [c]
1	14.9	1.38	20	DCM	52-62%	131
2	30.1	1.38	20	DCM	50-62%	131
3	47.0	1.30	20	DCM	52-64%	130

[a] M_n and $Đ$ determined from light scattering data. [b] *Threo*-content estimated from ^{13}C NMR. [c] T_gs determined with DSC.

4.10 Characterization of Physical Properties

4.10.1 Stress-Strain Curves of PDHF and PC

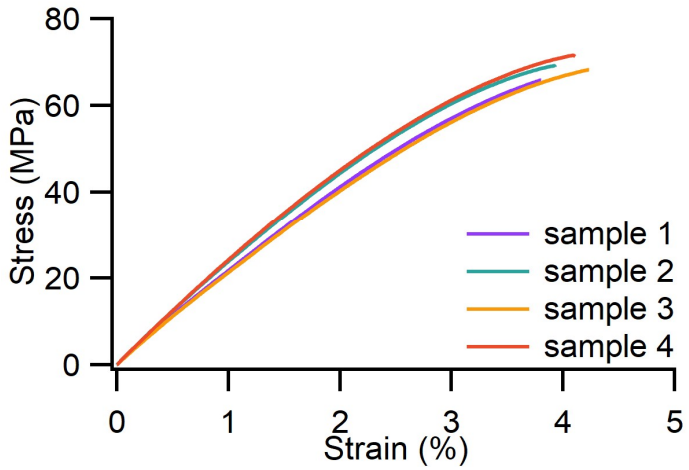

Figure 4.18: Stress-strain curves for PDHF-53.

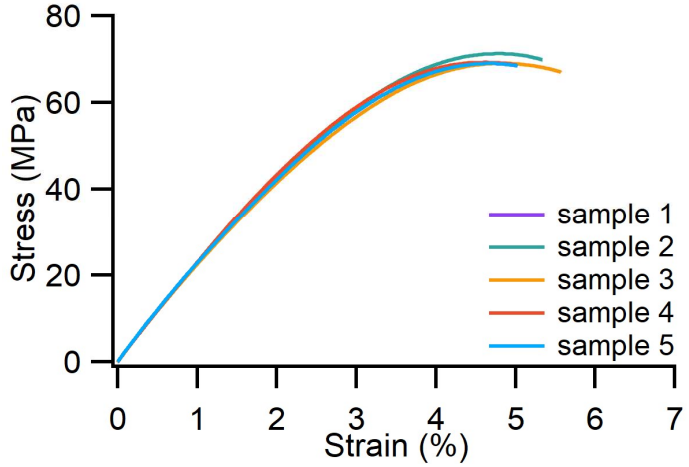

Figure 4.19: Stress-strain curves for PDHF-78.

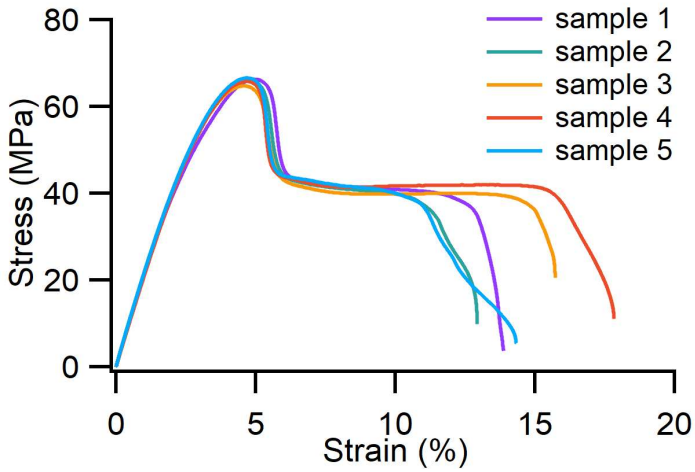

Figure 4.20: Stress-strain curves for PDHF-140.

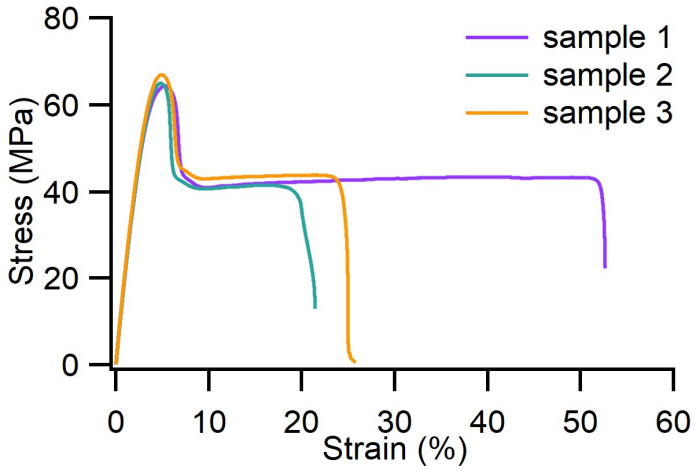

Figure 4.21: Stress-strain curves for PDHF-198.

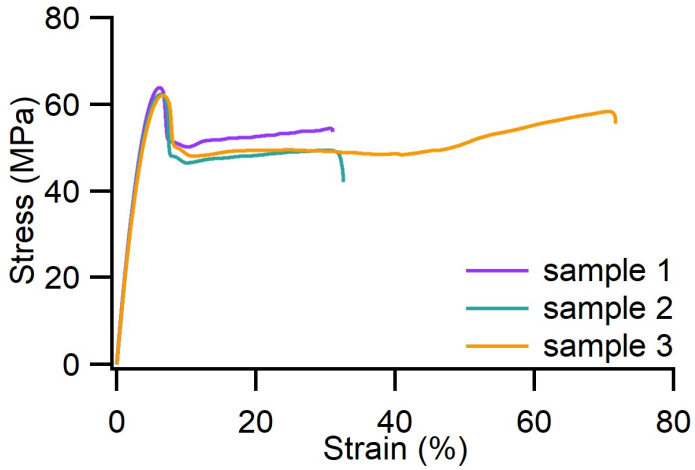

Figure 4.22: Stress-strain curves for PC-45.

4.10.2 Rheology

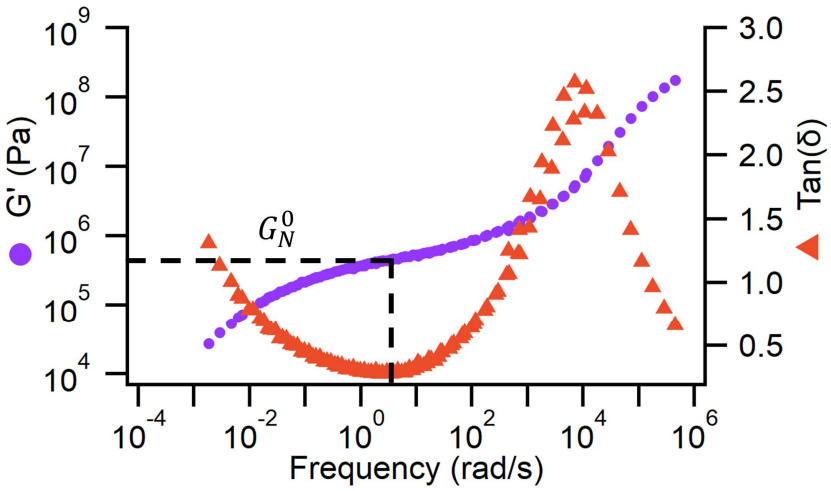

Figure 4.23: Master curve for PDHF generated at a reference temperature of 170 °C.

The master curve was generated using time-temperature superposition from frequency sweeps (0.1–100 rad/s, 1 Hz) at temperatures 140, 150, 160, 170 (reference), 180, 190, and 200 °C. The minimum of tan(δ) was found at 3.5 rad/s and this was used to find the plateau modulus (G_N^0), as indicated by the dashed line in Figure 4.23. G_N^0 was then used in Equation S1 to calculate entanglement MW (M_e), in accordance with the equation derived by Ferry.[4,5]

Equation S1:

$$M_e = \frac{\rho RT}{3G_N^0} = \frac{1040\left[\frac{kg}{m^3}\right] \cdot 8.314\left[m^3 \cdot \frac{Pa}{K \cdot mol}\right] \cdot (170+273)[K]}{(3) \cdot 486{,}826\,[Pa]} = 2.8\,\frac{kg}{mol}$$

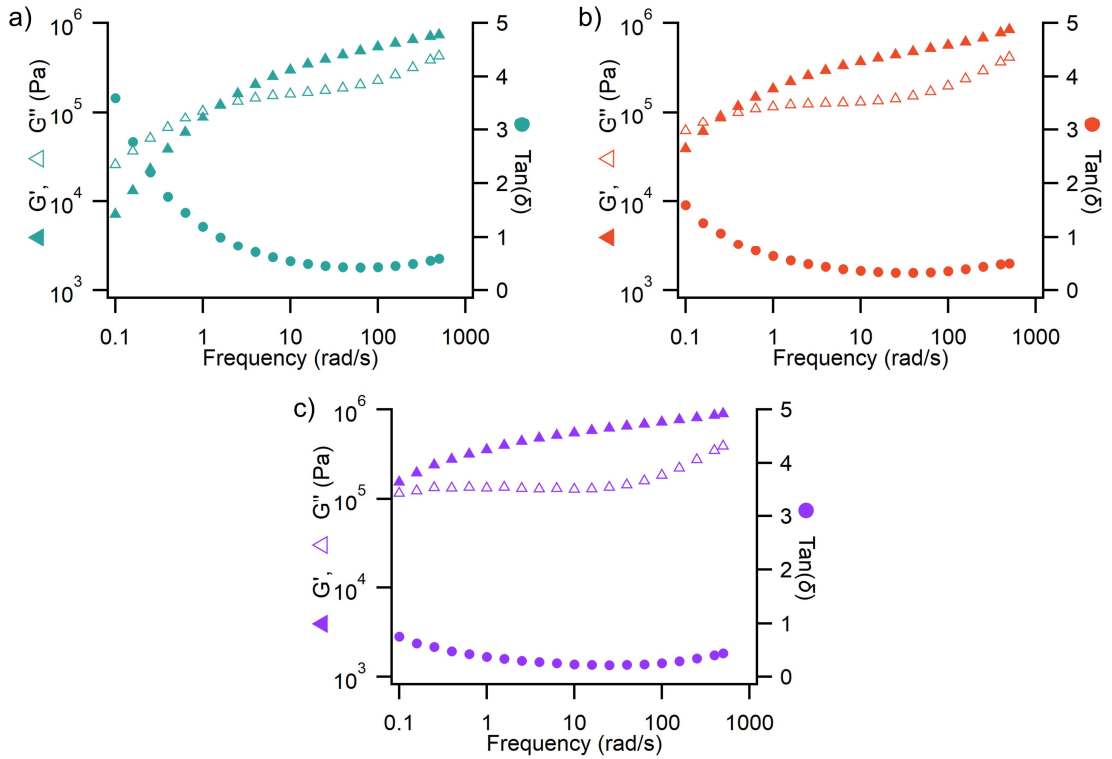

Figure 4.24: Frequency sweeps of PDHF-53 (a), PDHF-78 (b), and PDHF-198 (c) with G' (filled triangles), G" (open triangles), and Tan(δ) (circles) performed at 180 °C.

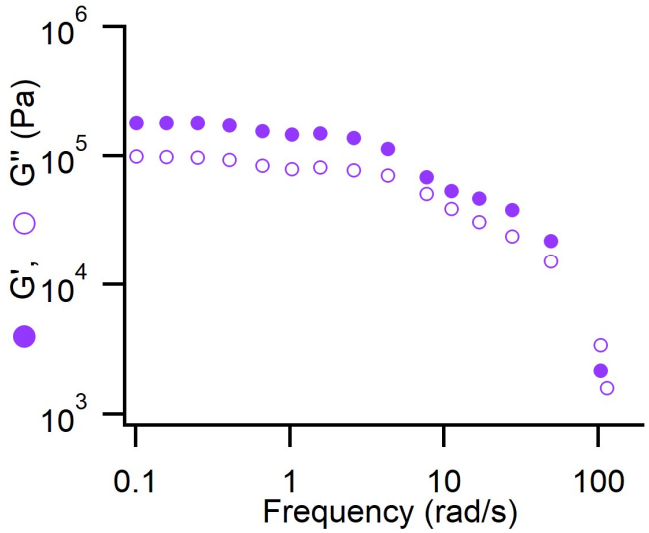

Figure 4.25: Strain sweep of PDHF performed from 0.1 to 100% strain, at 1 Hz, 180 °C.

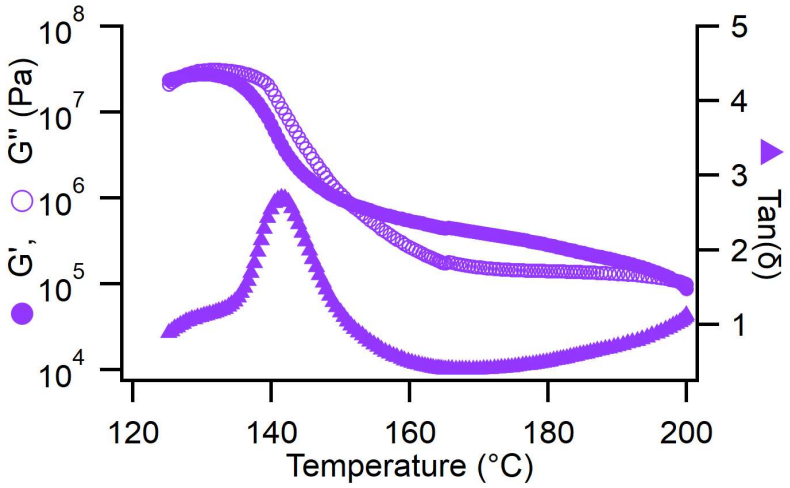

Figure 4.26: Temperature sweep of PDHF performed from 125 to 200 °C at 0.1% strain, 1 Hz.

4.10.3 Thermal Properties

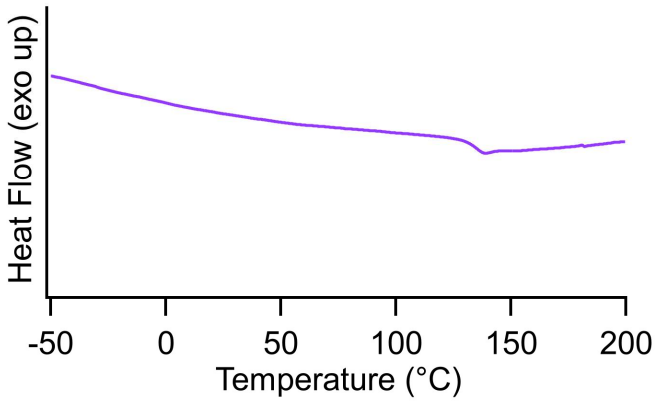

Figure 4.27: Differential Scanning Calorimetry (DSC) of a 126 kg/mol PDHF sample. The T_g was observed at 135 °C.

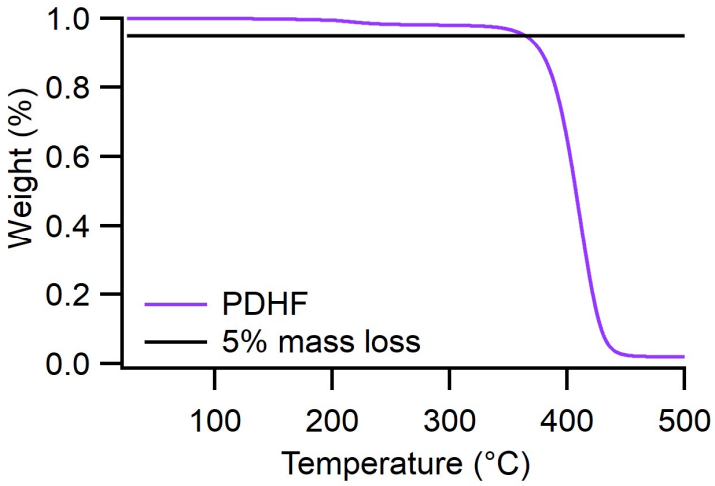

Figure 4.28: Thermal Gravimetric Analysis of PDHF. 95% weight loss reported at 364 °C.

4.10.4 Film Optical and Barrier Properties

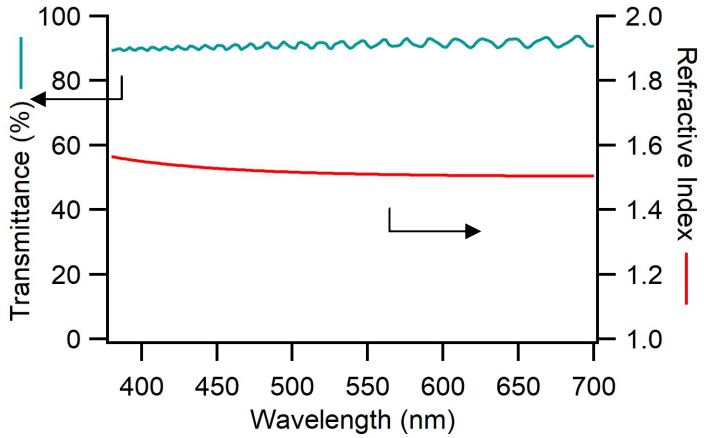

Figure 4.29: Transmittance and refractive index of PDHF film measured across visible wavelengths (380 – 700 nm).

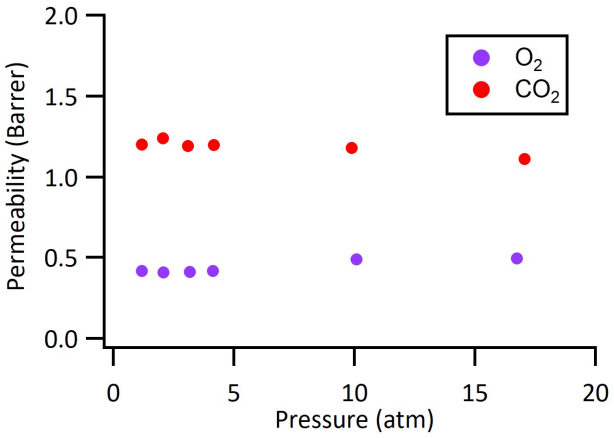

Figure 4.30: O_2 and CO_2 permeability of PDHF film.

Water vapor transmission rate (WVTR) was tested on PDHF ~38 µm films prepared through the solvent casting procedure described previously. The films were tested in accordance with ASTM E-96, using a film diameter of 28 mm. The films were sealed with a 1:1 mixture of beeswax:rosin to a glass dish filled with activated desiccant ($CaCl_2$). This fixture was then placed in a 49% relative humidity chamber. The dish was removed, and the mass recorded each day at the

same time for 8 days. WVTR was then calculated using the following equation:

Equation S2:

$$WVTR = \frac{thickness\ [mm] \cdot transmission\ rate\left[\frac{g}{day}\right]}{area[m^2] \cdot (rel.humidity_{out} - rel.humidity_{in})}$$

Permeation of O_2 and CO_2 (PO_2, PCO_2) was measured in accordance with a method previously described by the Ellison group.[6–8] The values obtained were compared to values reported in a recent article on barrier properties of bio-based food packaging materials.[9]

4.11 PDHF Degradation

4.11.1 Procedure for the Accelerated Oxidative Degradation of PDHF

A 50 mL round bottom flask equipped with a magnetic stir bar was charged with PDHF (0.120 g, 1.71 mmol of DHF subunits, 1 equiv.) followed by DCM (12.0 mL). Once the polymer was completely dissolved, H_2O_2 (30 wt % in water) was added (12.0 mL, 118 mmol, 68.7 equiv.) followed by $(NH_4)_2Fe(SO_4)_2 \bullet 6H_2O$ (0.134 g, 0.343 mmol, 0.2 equiv.). The flask was fit with a rubber septum which was pierced with a needle and stirred at room temperature for 48 h. The reaction appeared red at first but faded in color over the course of the reaction. Aliquots were taken from the organic layer for GPC analysis.

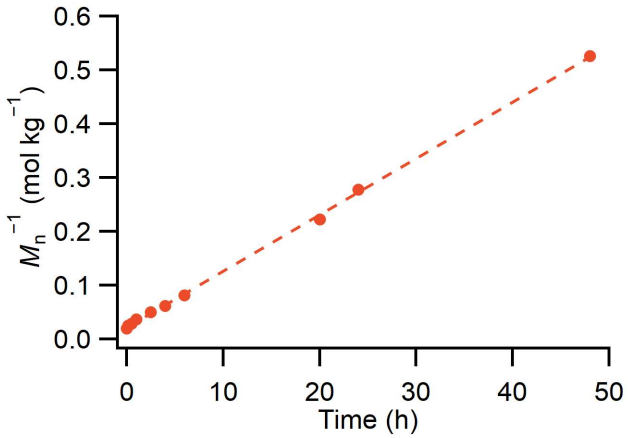

Figure 4.31: Inverse plot of M_n vs. time for PDHF degradation

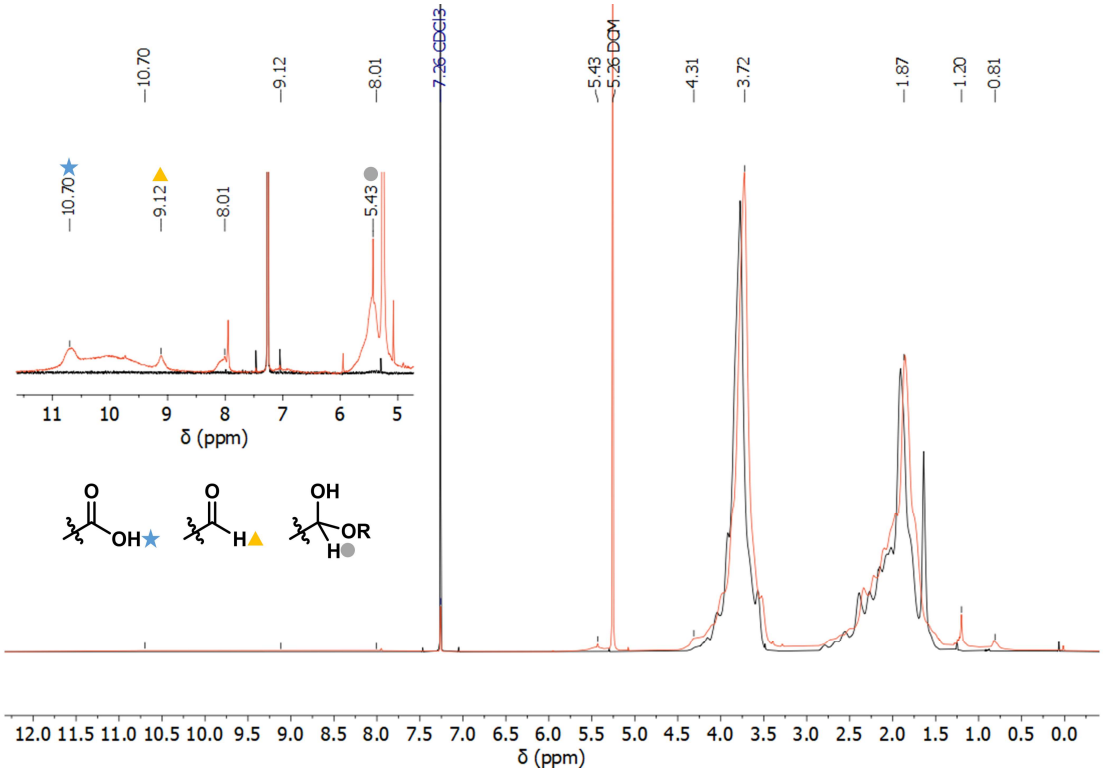

Figure 4.32: ^{1}H NMR spectra of PDHF (black) and degradation product (red).

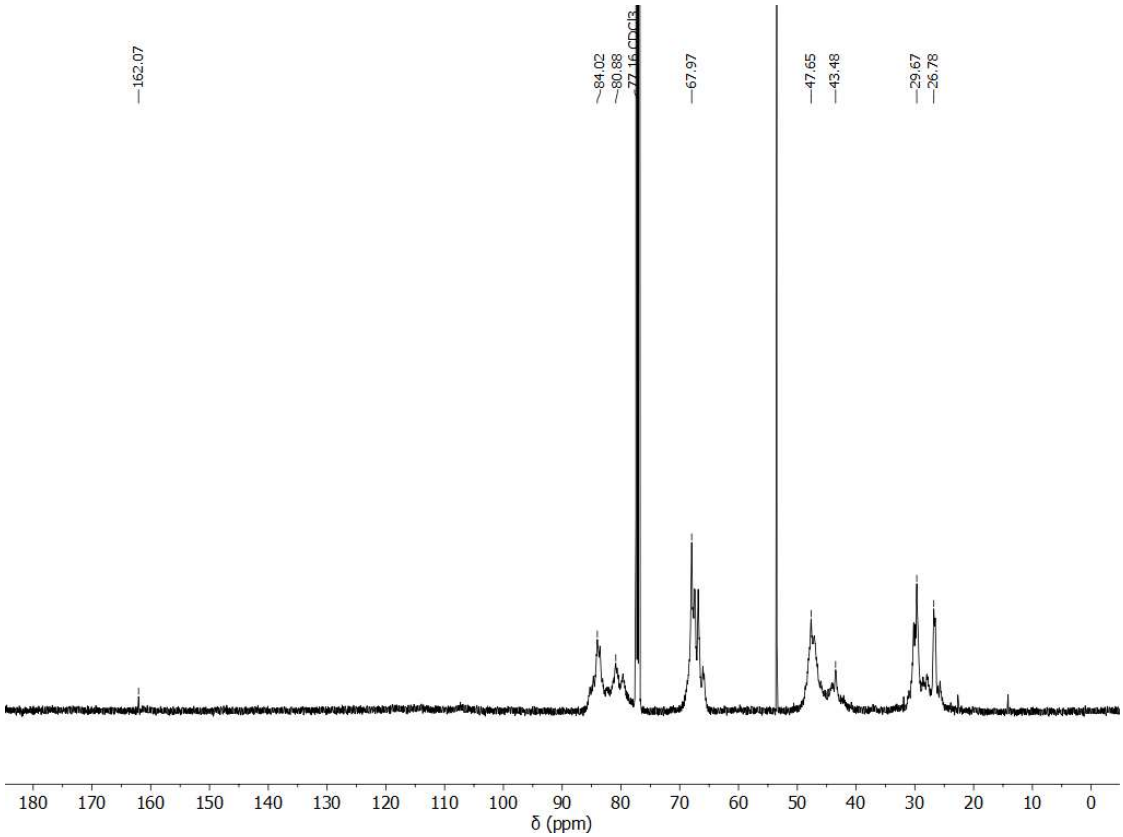

Figure 4.33: ^{13}C NMR spectra of PDHF degradation product.

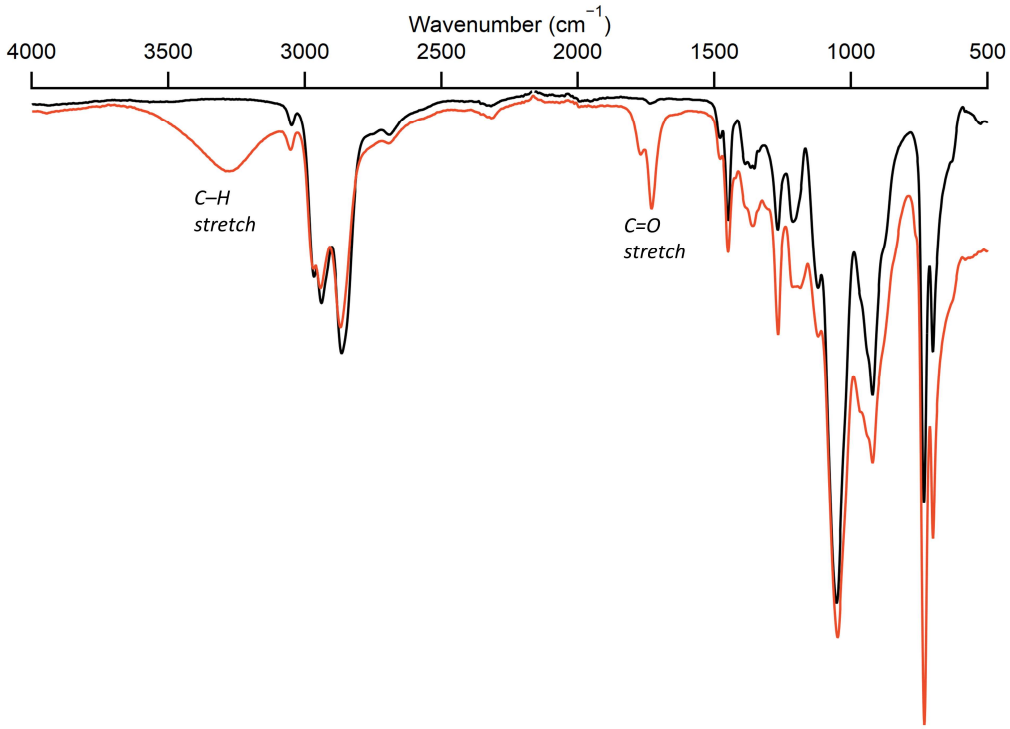

Figure 4.34: FTIR spectra of PDHF (black trace) and degradation product (red trace).

4.12 References

(1) Kottisch, V.; O'Leary, J.; Michaudel, Q.; Stache, E. E.; Lambert, T. H.; Fors, B. P. Controlled Cationic Polymerization: Single-Component Initiation under Ambient Conditions. *J. Am. Chem. Soc.* **2019**, *141* (27), 10605–10609.

(2) Kottisch, V.; Jermaks, J.; Mak, J.-Y.; Woltornist, R. A.; Lambert, T. H.; Fors, B. P. Hydrogen Bond Donor Catalyzed Cationic Polymerization of Vinyl Ethers. *Angew. Chemie Int. Ed.* **2021**, *60* (9), 4535–4539.

(3) Sanda, F.; Matsumoto, M. Cationic Polymerization of 2,3-Dihydrofuran. Study on the Relationship between Glass Transition Temperature and Tacticity of the Polymer. *Macromolecules* **1995**, *28* (20), 6911–6914.

(4) Ferry, J. D. *Viscoelastic Properties of Polymers*, 3rd Editio.; John Wiley & Sons, Ltd, 1980.

(5) Fetters, L. J.; Lohse, D. J.; Milner, S. T.; Graessley, W. W. Packing Length Influence in Linear Polymer Melts on the Entanglement, Critical, and Reptation Molecular Weights. *Macromolecules* **1999**, *32* (20), 6847–6851.

(6) Park, J.; Ha, H.; Yoon, H. W.; Noh, J.; Park, H. B.; Paul, D. R.; Ellison, C. J.; Freeman, B. D. Gas Sorption and Diffusion in Poly(Dimethylsiloxane) (PDMS)/Graphene Oxide (GO) Nanocomposite Membranes. *Polymer (Guildf)*. **2021**, *212* (October 2020), 123185.

(7) Ha, H.; Park, J.; Ando, S.; Kim, C. Bin; Nagai, K.; Freeman, B. D.; Ellison, C. J. Gas Permeation and Selectivity of Poly(Dimethylsiloxane)/Graphene Oxide Composite Elastomer Membranes. *J. Memb. Sci.* **2016**, *518*, 131–140.

(8) Ha, H.; Park, J.; Ha, K. R.; Freeman, B. D.; Ellison, C. J. Synthesis and Gas Permeability of Highly Elastic Poly(Dimethylsiloxane)/Graphene Oxide Composite Elastomers Using Telechelic Polymers. *Polymer (Guildf)*. **2016**, *93*, 53–60.

(9) Sangroniz, A.; Zhu, J.-B.; Tang, X.; Etxeberria, A.; Chen, E. Y.-X.; Sardon, H. Packaging Materials with Desired Mechanical and Barrier Properties and Full Chemical Recyclability. *Nat. Commun.* **2019**, *10* (1), 3559.